論文 / 著書情報
Article / Book Information

題目(和文)	
Title(English)	Study of Miniaturization and High Functionalization of Radiating Elements for Array Antennas on Moving Platforms
著者(和文)	後藤準
Author(English)	Jun Goto
出典(和文)	学位:博士（工学）, 学位授与機関:東京工業大学, 報告番号:甲第11936号, 授与年月日:2021年3月26日, 学位の種別:課程博士, 審査員:廣川 二郎,阪口 啓,西方 敦博,青柳 貴洋,TRAN GIA KHANH
Citation(English)	Degree:Doctor (Engineering), Conferring organization: Tokyo Institute of Technology, Report number:甲第11936号, Conferred date:2021/3/26, Degree Type:Course doctor, Examiner:,,,,
学位種別(和文)	博士論文
Type(English)	Doctoral Thesis

Doctoral Dissertation

Study of Miniaturization and High Functionalization of Radiating Elements for Array Antennas on Moving Platforms

February 2021

Jun Goto

Under the supervision of

Professor Jiro Hirokawa

Department of Electrical and Electronic Engineering

Tokyo Institute of Technology

Acknowledgements

I would like to express my sincerest appreciation and respect to Professor Jiro Hirokawa for his guidance and stimulating supervision in the present work.

I also wish to express my deep gratitude to Dr. Makoto Ando for his supervision for my bachelor and master's degrees. I owe him my present career as a researcher of electromagnetic wave engineering.

I am greatly indebted to Associate Professor Tran Gia Khanh, Professor Kei Sakaguchi, Professor Takahiro Aoyagi, Professor Hiroyuki Uenohara, and Professor Atsuhiro Nishikata for their kind guidance and fruitful advice.

I also wish to express my devout thanks to Professor Yoshihiko Konishi and Professor Shigeru Makino during their careers in Mitsubishi Electric Corporation.

I would like also to show my sincere gratitude to Dr. Fukasawa for his insightful advice and for giving me a chance to complete this dissertation.

I would like to express my deep gratitude to Dr. Satoshi Yamaguchi for his guidance with essential suggestions, and his big-brotherly encouragement.

I would like to show my special thanks to Dr. Takashi Maruyama for his tremendous insightful suggestions and advices.

I am greatly indebted to Dr. Kazunari Kihira, Dr. Toru Takahashi, Dr. Yoshio Inasawa, Dr. Kazufumi Hirata, Dr. Naofumi Yoneda, Dr. Masataka Otsuka, and Dr. Hiroaki Miyashita for their continuous encouragements and technical instructions. The studies in this dissertation could not have been completed

without the technical supports and discussions with Dr. Makoto Matsuki, Dr. Akimichi Hirota, Mr. Kyosuke Mochizuki, Ms. Miyuki Tanaka, Mr. Hideo Sumiyoshi, and Dr. Shigeo Udagawa. I also wish to express my thanks to elder and younger fellows in Antenna. Technology Dept.

I would like also to thank the staff and colleagues of Hirokawa-Laboratories in Tokyo Institute of Technology. I also wish to my thanks and affection to all the students in the Laboratories, especially to Dr. Testu Shijo for his supervision for my bachelor and master's degrees, and Dr. Masafumi Nagasaka and Dr. Akira Kuriyama for their supports as colleagues in doctorial course.

Finally, I would like to express thanks to my wife Yoko, my daughter Hiroko, and my son Kei, and sincerely devote this dissertation to my father and mother.

Jun Goto

Tokyo, February 2021

Abstract

The target of the study in this dissertation is the realization of miniaturization and high functionalization of radiating elements for array antennas on moving platforms. There are three issues in these antennas: first, miniaturizing antennas reduces their degree of freedom and increases the input impedance, which makes it difficult to obtain the impedance matching; second, since array antenna performances are often degraded when scanned to a wide angle, design technology to realized high performances over the wide coverage is required; third, because the size of wideband antennas tends to become large, the antenna type and the material used must be selected appropriately. In order to design antennas that suit for moving platforms, this dissertation deals with newly proposed design methods for three types of antennas, as shown below.

Firstly, a novel traveling-wave series-fed microstrip antenna array is discussed. A conventional series-fed microstrip antenna array is lack of the degree of freedom, and only way to control radiation power from each element is changing the width of each element. In addition, a meander line is used to compensate the phase distortion because the transmission phase varies with the radiation power from each element. Although the length of the meander line can be arbitrarily selected and makes array design easy, the meander line increases insertion loss and spurious radiation. In the proposed antenna, additional slits placed on the output side of the antenna element are introduced as a new degree of freedom to control the radiation power from each element. Also, the unequal element spacing is applied to compensate passing phases of each antenna element; meander lines that would increase the insertion loss and

spurious radiation are not used. Because the phase distribution is adjusted by the element position and the excitation amplitude distribution required to realize a desired radiation pattern changes according to the element position, the amplitude distribution is designed by using a genetic algorithm. A 9-element linear array is designed and tested, and the simulated and measured results agree, thus validating the proposed design.

Secondly, a novel circularly polarized ring microstrip antenna and its design. A conventional ring microstrip antenna maintains good radiation characteristics with a smaller dimension than circular microstrip antennas. But, since the minimum input impedance of ring microstrip antennas quickly increases when the inner/outer diameter ratio increases, an additional matching circuit needs to be embedded, which prevents the inner area from being used for other purposes. In the proposed antenna, the shorting pins, which are discretely disposed on the inner edge of the ring microstrip antenna, are introduced as a new degree of freedom to improve the resonance frequency control. The number and diameter of the shorting pins control the resonance frequency; the resonance frequency can be made almost constant with respect to the inner/outer diameter ratio, thereby expanding the use of the ring microstrip antenna. As an example of a use for the proposed antenna, a dual-band antenna where the proposed antenna includes another ring microstrip antenna is designed and measured, and these results agree well with measurement. Furthermore, the electrical performance for a proto flight model of a satellite positioning system using the proposed antenna is demonstrated. The measurement and designed results agreed well, which proves that the antenna can be put into practical use.

Lastly, a light-weight horn antenna that covers up to 45 degrees is proposed. A conventional metal horn array antenna is low loss but has large weight as well as large element spacing, which prevents wide-angle beam scanning. To solve this problem, an injection-molded horn array antenna, which is compact, low-loss and highly manufacturable, has been proposed. However, the axial ratio was deteriorated during wide-angle beam scanning, because the antenna was designed to be impedance-matched in the front direction, without considering the axial ratio at all. In this dissertation, the mechanism that the axial ratio degrades in the injection-molded horn array antenna is clarified. Besides, the reflection wave that degrades the axial ratio is extracted by converting the expression of the reflection wave from the liner polarization to the circular one. The circular component of the reflection wave can be controlled by the position and depth of the iris placed near the horn array antenna's aperture. By suppressing this component over the wide coverage, the beam scanning characteristics are guaranteed. The proposed method enables a definitive and efficient design of the injection-molded horn array antenna, by utilizing the same degree of freedom as conventional one. A prototype antenna has been fabricated in the millimeter-wave band, and the validity of the design method has been confirmed by measurement.

The antennas and design methods developed in this dissertation contribute to the realization of miniaturization and high functionalization of radiating elements for array antennas on moving platforms and are considered to have wide applicability for communications and radar systems.

Contents

1. Introduction 14
1.1. Background of the study 14
1.2. Requirements for sensors in moving platforms 15
1.3. Outline of the dissertation 16
2. Technical issues and approaches 19
2.1. Miniaturization and functionality of sensors in moving platforms 19
2.2. Target of the study 23
2.3. Technical issues dealing with the thesis 26
2.4. References 30
3. Traveling-Wave Series-Fed Microstrip Array Antenna with Unequal Inter-Element Spacing 33
3.1. Introductory remarks 33
3.2. Electric al design 35
3.3. Measurement Results 56
3.4. Versatility 60
3.5. Summary 62
3.6. References 63
4. Design of the Circularly Polarized Ring Microstrip Antenna with Shorting Pins 66
4.1. Introductory remarks 66
4.2. Proposed antenna 69
4.3. Dual-band circularly polarized antenna 84
4.4. The test results of the array 99
4.4.1. Aperture design 99
4.4.2. Proto flight model test results 104
4.5. Versatility 109
4.6. Summary 114
4.7. References 115
5. Two-Dimensional Injection-Molded Horn Array Antenna for Millimeter-Wave Active Phased Array Antenna 118
5.1. Introductory remarks 118

5.2. APAA system overview 120
5.2.1. Configuration of APAA 120
5.2.2. Configuration of radiating part 122
5.3. Design of radiating part 125
5.3.1. Principle 125
5.3.2. Design procedure 129
5.4. Measurement results 134
5.4.1. Antenna measurement 134
5.4.2. APAA measurement results 137
5.5. Versatility 142
5.6. Summary 144
5.7. References 145
6. Conclusions 147
6.1. Summary 147
6.2. Future works 150

List of figures

Fig. 1.3-1 Structure of the dissertation 18
Fig. 2.1-1 Comparison of typical antennas for moving platforms 22
Fig. 2.2-1 Objectives, approaches, and technical issues in the dissertation. 25
Fig. 2.3-1 Comparison of conventional microstrip array antennas 27
Fig. 2.3-2 Comparison of conventional dual-band microstrip array antennas (λLow indicates the wavelength at the center frequency of the low band) 28
Fig. 2.3-3 Comparison of conventional horn array antennas 29
Fig. 3.2-1 Proposed traveling-wave series-fed microstrip arrays 38
Fig. 3.2-2 Equivalent circuit of microstrip array antenna 38
Fig. 3.2-3 Current path on microstrip antenna 39
Fig. 3.2-4 Reference model for verifying the output slit. 39
Fig. 3.2-5 Characteristics when the length of the output slit is changed by ± 0.005λ: (a) transmission coefficient, (b) reflection coefficient, and (c) transmission phase. 41
Fig. 3.2-6 Chebyshev distribution 44
Fig. 3.2-7 Radiation pattern of Chebyshev distribution 44
Fig. 3.2-8 Proposed antenna design flow chart. 48
Fig. 3.2-9 Comparison of element positions for each trial number. 51
Fig. 3.2-10 Comparison of the excitation amplitude distribution for each trial number. 51
Fig. 3.2-11 Comparison of the array factor for each trial. 52
Fig. 3.2-12 Comparison of the reflection coefficient for each trial. 52
Fig. 3.2-13 Designed model of the proposed traveling-wave series-fed microstrip array antenna 53
Fig. 3.2-14 Comparison of the radiation pattern of the proposed traveling-wave antenna in the horizontal direction at the center frequency, with and without mutual coupling. 54
Fig. 3.2-15 Comparison of excitation amplitude distributions 55
Fig. 3.2-16 Comparison of radiation patterns 55
Fig. 3.3-1 Microstrip array antenna of (a) designed model, (b) manufactured antenna.

.....57
Fig. 3.3-2 Simulated and measured reflection coefficient versus the frequency. 58
Fig. 3.3-3 Simulated and measured array pattern in the horizontal cut plane at the center frequency. 58
Fig. 3.4-1 Simulated reflection coefficient versus the frequency.....61
Fig. 3.4-2 Simulated array pattern in the horizontal cut plane at the center frequency in each band. 61
Fig. 4.2-1 Geometry of the proposed antenna. (top and cross-sectional views along the A-A' line) 70
Fig. 4.2-2 Resonance frequency versus inner/outer diameter ratio. In the proposed antenna, the number and diameter of the shorting pins are 4 and 4 mm, respectively. All resonance frequencies are normalized by that of the circular microstrip antenna.....76
Fig. 4.2-3 Eigenvalue analysis model for the proposed antenna. (Top and cross-sectional views along the B-B' line).....77
Fig. 4.2-4 Electromagnetic field analysis results for the surface current vectors of three types of antennas for various inner/outer diameter ratios: black lines indicate currents between the outer and inner circles, whereas white lines indicate currents along the radiating conductor.....78
Fig. 4.2-5 The analytical results of the surface current magnitude of the proposed antenna. The number of shorting pins is four, and the inner/outer diameter ratio is 0.5. All resonance frequencies are normalized by the resonance frequency of the circular microstrip antenna. 82
Fig. 4.2-6 The analytical surface-current-magnitude results for the proposed antenna. The number of shorting pins is two, and the inner/outer diameter ratio is 0.5. All resonance frequencies are normalized by the resonance frequency of the circular microstrip antenna. 82
Fig. 4.2-7 Simulated resonance frequency of Case 9 and 9' in Fig. 4.2-6 : the number of shorting pins is two, the inner/outer diameter ratio is 0.5, and the installation angle of shorting pins is 50°. All resonance frequencies are normalized by the resonance frequency of the circular microstrip antenna.....83
Fig. 4.3-1 A dual-band circular polarized antenna using the proposed antenna as a low-band element (top and cross-section view along C-C' line.....86
Fig. 4.3-2 Design flow for a dual-band circularly polarized antenna using the proposed antenna as a low-band element. 89
Fig. 4.3-3 Manufactured antenna element.....91

Fig. 4.3-4. Simulated and measurement reflection coefficient: 93
Fig. 4.3-5 Element pattern in the xz cut plane at the center frequency of (a) L5 (b) L2 94
Fig. 4.3-6 Element pattern in the xz cut plane at the center frequency of (a) L6 (b) L1. 95
Fig. 4.3-7 Axial ratio versus frequency: (a) low band and (b) high band. 96
Fig. 4.3-8 Actual gain versus frequency: (a) low band (b) high band. 97
Fig. 4.4.1-1 Mask pattern 101
Fig. 4.4.1-2 Excitation distribution required for rectangular beam 101
Fig. 4.4.1-3 Initial excitation distribution 102
Fig. 4.4.1-4 Array arrangement 102
Fig. 4.4.2-1 Measurement setup for proto flight model test. 105
Fig. 4.4.2-2 Simulated and measured reflection coefficients in low band. 106
Fig. 4.4.2-3 Simulated and measured reflection coefficients in high band. 106
Fig. 4.4.2-4 Relative radiation patterns in the azimuth cut plane at the center frequency of (a) L5 (b) L2 107
Fig. 4.4.2-5 Relative radiation patterns in the azimuth cut plane at the center frequency of (a) L6 (b) L1. 108
Fig. 4.5-1. Simulated reflection coefficient in each band: 110
Fig. 4.5-2. Element pattern in the xz cut plane at the center frequency: 111
Fig. 4.5-3 Axial ratio versus frequency: (a) low band and (b) high band. 112
Fig. 5.2.1-1 Photos of the prototype APAA 121
Fig. 5.2.2-1 Two dimensional circular polarized horn array antenna 124
Fig. 5.2.2-2 Principle of the inverse polarized wave radiations 124
Fig. 5.3.1-1 Iris design model 127
Fig. 5.3.1-2 Equivalent circuit model of Fig. 5.3.1-1 128
Fig. 5.3.1-3 Equivalent circuit model of the iris. 128
Fig. 5.3.2-1 Reflection Properties without the iris with respect to the component of the linear polarization on azimuth cut plane 130
Fig. 5.3.2-2 Reflection properties without the iris with respect to the component of the circular polarization on azimuth cut plane 131
Fig. 5.3.2-3 Reflection properties with the iris with respect to the component of the circular polarization on azimuth cut plane 131
Fig. 5.3.2-4 Unit cell model (proposed method) 132
Fig. 5.3.2-5 Active reflection characteristic on azimuth cut plane 132
Fig. 5.3.2-6 Axial ratio with respect to the component of the RHCP 133

Fig. 5.4.1-1 Measurement configurations for array antenna 135
Fig. 5.4.1-2 Average array element pattern (azimuth cut plane)..... 135
Fig. 5.4.1-3 Axial ratio pattern (azimuth cut plane)..... 136
Fig. 5.4.2-1 Measurement configurations for APAA 138
Fig. 5.4.2-2 Elevation radiation pattern (broadside beam) 139
Fig. 5.4.2-3 Azimuth radiation pattern at the edge of coverage..... 139
Fig. 5.4.2-4 Elevation axis ratio..... 140
Fig. 5.5-1 Axial ratio versus frequency in each band..... 143
Fig. 5.5-2. Simulated reflection coefficient in each band..... 143

List of Tables

Table 3.2-1 Dimensions of the reference model for verifying output slit 40
Table 3.2-2 The designed lengths of output slits and the transmission amplitude of each element 53
Table 3.3-1 Benchmark of microstrip array antennas 59
Table 3.4-1 Comparison of gains and losses for each antenna 61
Table 4.2-1 Normalized resonance frequencies with respect to the inner/outer diameter ratio in the proposed antenna. The numbers of cases correspond to those in Fig. 4.2-5 and Fig. 4.2-6. 83
Table 4.3-1 Parameters normalized by the central-frequency wavelength of the whole band (1.377 GHz) 92
Table 4.3-2 Benchmark of dual band microstrip antennas 98
Table 4.4.1-1 Ideal excitation distribution for the low band 103
Table 4.4.1-2 Ideal excitation distribution for the high band 103
Table 4.5-1 Comparison of gains and losses for each antenna for low band 113
Table 4.5-2 Comparison of gains and losses for each antenna for high band 113
Table 5.4.2-1 Error analysis with respect to the sidelobe level 140
Table 5.4.2-2 Benchmark of horn array antennas 141
Table 5.5-1 Comparison of gains and losses for each antenna 144

1. Introduction

1.1. Background of the study

It is no exaggeration to say that the history of human is the history of mobility. People who had no choice but to move around on their own eventually acquired a "vehicle" and went farther and faster. Around 3000 BC, people began riding horses. Riding a horse allowed them to travel much faster and farther than they had ever been able to before. Cars were invented in the late 19th century. The development of industrial technology made "mass production" possible, and people could no longer dream of owning a car.

In 1903, the Wright brothers made the world's first manned flight. Since then, improvements have been made to enable people to fly faster, higher and farther. In World War I, it was used as a reconnaissance aircraft, and soon after, the fighter was born. In World War II, airplanes became a major part of combat, with the side that gained control of the airplane winning the battle; from the mid-20th century onwards, a series of large, high-speed vehicles were developed for civilian use, including large, jet-powered passenger aircraft. In addition to performance, the specifications required for airplanes have also become more important to reduce operating costs and ease of maintenance.

In the space field, the world's first satellite "Sputnik" was launched in 1957. In 1961, Astronaut Gagarin of "Vostok 1" made a round of the earth. Furthermore,

Apollo 11 succeeded in landing on the moon for the first time in 1969. The International Space Station was developed as a multipurpose manned space facility. Besides, satellites for various purposes such as communication, broadcasting, positioning, and earth observation have been launched, and recently private companies have begun to launch space rockets.

1.2. Requirements for sensors in moving platforms

Communication / radar systems are widely used in moving platform, including cars, airplanes and satellites which is described in the previous section. Various sensors are equipped with the moving platforms in order to accomplish each mission.

The installation space for sensors on moving vehicles is limited for reasons of appearance and fuel efficiency. Therefore, miniaturization is a must for sensors that use a moving object as a platform. On the other hand, it is necessary to expand the detection range. In automotive applications, improvement of safety by expanding the detection range is needed. For aircraft applications, tracking satellites by scanning to low elevation angles are often required. Furthermore, antennas mounted on low earth orbit satellites need to obtain communication capacity by scanning, since the target direction changes as the satellite moves. Furthermore, wideband and multiband antennas are required because of the increasing capacity in the communication field and the need for higher resolution in the radar field.

From the above background, the objective of this thesis is set to achieve miniaturization and high performance of antennas in moving platforms.

1.3. Outline of the dissertation

This dissertation is organized with the following chapters.

Chapter 2 shows the technical issues and approaches dealing in the thesis, whreas previous researches and their issues are organized.

Chapter 3-5 describes the studies on miniaturization and high functionalization of array antennas that suit for moving platforms. Structure of the dissertation is shown in Fig. 1.3-1. Chapter 3 focuses on the techniques for reducing the width of the microstrip array antenna. A novel traveling-wave series-fed microstrip array antenna and its design are presented. The proposed antenna has two features: additional slits placed on the output side of the antenna element are introduced as a new degree of freedom to control the radiation power from each element. Also, the unequal element spacing is applied to compensate passing phases of each antenna element; meander lines that would increase the insertion loss are not used. A 9-element linear array is designed and tested, and the simulated and measured results agree, thus validating the proposed design.

Chapter 4 discusses the electrically small dual-band circularly polarized microstrip antenna. A novel circularly polarized ring microstrip antenna and its design are presented. The shorting pins, which are discretely disposed on the inner edge of the ring microstrip antenna, are introduced as a new degree of freedom to improve the resonance frequency control. The number and diameter of the shorting pins control the resonance frequency; the resonance frequency can be made almost constant with respect to the inner/outer diameter ratio, thereby expanding the use of the ring

microstrip antenna. A dual-band antenna where the proposed antenna includes another ring microstrip antenna is designed and measured, and these results agree well with measurement.

Chapter 5 is devoted to the two-dimensional scanning injection-molded horn array antenna. A conventional metal horn antenna has the advantage of low loss. However, it has large weight and is difficult to realize wide-angle beam scanning because of large element spacing. The array antenna made by injection molding and metal coating has light weight and can avoid grating lobes thanks to the wavelength shortening effect. In the conventional method, the input impedance was designed in the front direction, and the axial ratio characteristics deteriorated during wide-angle beam scanning. In this dissertation, a design method to obtain low axial ratio characteristics even in wide-angle beam scanning has been described.

In chapter 6, summaries and conclusions are described.

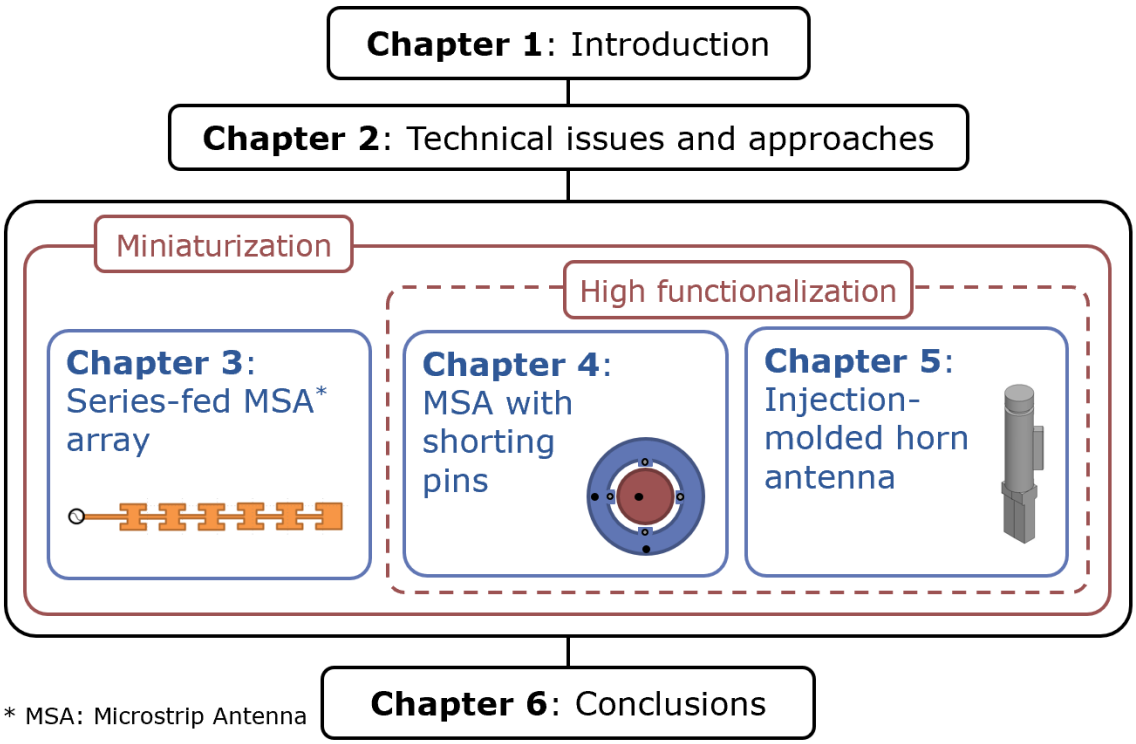

Fig. 1.3-1 Structure of the dissertation

2. Technical issues and approaches

In the previous chapter, the introduction of the thesis is presented. In this chapter, the technical issues dealing in the thesis and approaches to these issues are discussed.

2.1. Miniaturization and functionality of sensors in moving platforms

Various sensors, including radars, lidars and optical cameras are equipped with the moving platforms. Among these sensors, radars have the following characteristics compared to other sensors: it has superior detection capability at night and in adverse weather conditions such as rainfall and fog; it is not affected by sunlight (backlighting); it can easily obtain a long-range detection; and it can directly detect the relative speed of the target of observation. Commercialization of automotive radars began in the 1990s and has enabled many safety systems such as adaptive cruise control (ACC), autonomous emergency braking (AEB), and blind-spot monitoring (BSM). From 2017, Federal Communications Commission (FCC) lifted the ban on 77-81 GHz to improve distance resolution. This has led to the development of target detection for pedestrians, bicycles and other non-vehicle targets [1].

On the other hand, internet services were only available in places where there was a ground network, but in recent years, mobile phones and smartphones have become popular, and internet services that is realized by the communication devices mounted on the airplanes have become widespread [2]. It was necessary to turn off all electronic devices in the cabin, but now we can enjoy e-mail, internet searches and social networking through in-flight Wi-Fi.

Furthermore, car navigation systems have become a part of the daily lives of ordinary citizens and have become an important infrastructure that contributes to the realization of a safe and secure society through the sophistication and efficiency of industry and living. In the United States and Russia, satellite positioning systems have been originally developed for military purposes and have historically been utilized mainly for needs from the military field. In recent years, positioning satellites have been used for the purpose of complementing and reinforcing Global Positioning System (GPS), and antennas for positioning missions and other purposes are mounted on the satellites.[3]

As shown in the previous chapter, the needs of radar and communication devices based on moving platforms such as automobiles, airplanes, and satellites are expected to increase in the future. In these systems, antennas are one of the main components that converts energy between radio waves and electric devices.

Herein, some examples of antennas mounted on moving platforms from the viewpoint of such miniaturization and high functionality are introduced. First, microstrip antennas (MSA) [4]-[8] and waveguide slot antennas [9]-[13] are representative of planar antennas. Microstrip antennas are widely used as antennas for moving platforms because of their small size and light weight. However, they are

not applicable to all applications due to their narrow bandwidth and loss. Waveguide slot antennas have the advantage of low loss but require a little more height than microstrip antennas which may not be applicable to some systems in terms of weight and bandwidth.

By contrast, aperture antennas such as horn antennas [14]-[16] and reflector antennas [17]-[21] have the advantage of wide bandwidth and low loss, compared to planar antennas. However, these antennas are generally large and weight, which poses a problem when they are mounted on moving platforms.

Fig. 2.1-1 summarizes typical antennas used for moving platforms. There is a trade-off between mechanical and electrical properties. However, not only miniaturization but also performance (wideband, multi-frequency and wide coverage) is required in antennas in moving platforms. Herein, microstrip and horn antennas are complementary in terms of mechanical and electrical properties, as can be seen from Fig. 2.1-1. Therefore, this dissertation discusses these two types of antennas to meet the various needs for moving platforms.

In many radar / communications systems, array antennas are often used. Array antennas, which are composed of many antenna elements, realize beam scanning and flexible beam shape by controlling the phase of each antenna. Phase control enables beam control without mechanical movement of the antenna, which is suitable for moving platforms. In this thesis, miniaturization and high functionalization of radiating elements for array antennas are discussed.

Items		Planer		Aperture	
		Microstrip	Waveguide slot	Horn	Reflector
Mechanical properties	Size	○	○	△	△
	Weight	○	△	△	△
Electrical properties	Bandwidth	△	△	○	○
	Loss	△	○	○	○

Fig. 2.1-1 Comparison of typical antennas for moving platforms

2.2. Target of the study

Fig. 2.2-1 summarizes the objectives, approach and technical issues of this thesis. To achieve miniaturization, an approach from impedance matching and wide / multi band is effective. On the other hand, for high functionalization, techniques of wideband, multi-band, and wide coverage are crucial. Since impedance matching is also necessary for high functionalization, they are connected by a dotted line in the figure. In addition, the number of antennas used in some systems may be reduced by increasing the coverage area, therefore the miniaturization and the wide coverage are connected by a dotted line in the same manner.

(1) Impedance matching

Miniaturizing antennas reduce their degree of freedom and increases the input impedance, which makes it difficult to obtain the impedance matching. The effective use of existing parameters and creation of a new degree of freedom is mandatory.

If the design cannot be accomplished with existing parameters, new degrees of freedom are required to create a new impedance matching technique within a limited area. Therefore, design technology that makes effective use of existing parameters is needed.

(2) Wideband/Multiband

The selection of the antenna type and material used should be selected appropriately. The type of antenna determines the approximate bandwidth and the physical size: wider bandwidths generally tend to increase in size and weight, which design technology is required to avoid.

Because the conventional methods require a large antenna size to obtain the required bandwidth, technologies that cover the required bandwidth with minimum antenna size is investigated in this dissertation.

(3) Enhancement of the coverage

Since array antenna performances are generally degraded when scanned to a wide angle due to the mutual coupling, design technology to realized high performances over the wide coverage is desired. Miniaturization technology is also needed to closely arrange the antennas so that they can scan a beam to a wide angle. In the cases that the element spacing cannot be shortened, utilizing a dielectric substrate reduces the wavelength inside the antenna. In these cases, the selection of a low-loss material become important issue especially in high frequency because the insertion loss becomes large.

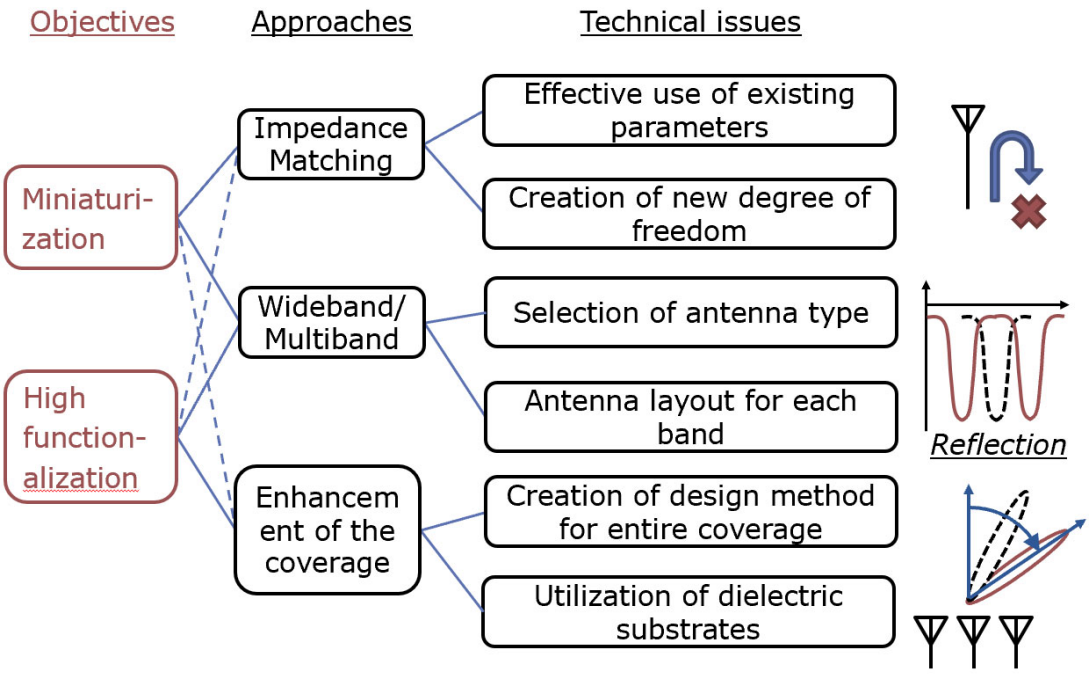

Fig. 2.2-1 Objectives, approaches, and technical issues in the dissertation.

2.3. Technical issues dealing with the thesis

In this section, technical issues for three topics dealing with the thesis are discussed.

(1) Technical issues in microstrip array antennas

The configuration of microstrip array antennas can be divided into two main categories, shown in Fig. 2.3-1.

In [4], an array antenna with a branch line is proposed. It has the advantage that it can be designed easily by installing power adjustment components and matching circuits before and after the bifurcation. However, since the radiating element and the feed line are placed separately, the overall width of the array antenna becomes larger. In addition, because each radiating elements and the feed line separate each other, the total length of the feed line tends to be large, which increases the feed loss. To compensate the large insertion loss, a larger aperture is required to obtain the specified antenna gain, which makes an antenna size larger.

On the other hand, an antenna in which the radiating element and the feed line are arranged in a straight line is proposed [5]. Compared to the antenna proposed in [4], the width of the antenna is narrower, but the excitation amplitude is adjusted by the width of the radiating element to reduce the degree of freedom of the branch line. For the array with tapered excitation distribution, the width of elements near the center in the array must be wide to radiate more power than the rest, which causes to increase the whole

size of the array. In addition, the standing-wave array causes the electromagnetic waves to travel back and forth across the feed line, resulting in a large loss. Therefore, a low-loss, wideband antenna with a narrow width is required.

Items	Branch [4]	Series-fed w/o slits [5]
Width(<0.5λ_{eff})	△ (0.9λ_{eff})	△ (0.7λ_{eff})
Bandwidth(>2%)	○ (>2%)	△ (<2%)
Loss	△ (Long feed line)	△ (Standing-wave, 2 way)

Fig. 2.3-1 Comparison of conventional microstrip array antennas

(2) Technical issues in dual-band MSAs

Next, another type of microstrip antenna, that is the dual-frequency shared antenna, is discussed. Fig. 2.3-2 shows the Comparison of conventional dual-band microstrip array antennas. An antenna that obtains dual-frequency shared characteristics by stacking patch antennas is proposed in [6][7]. The antenna's footprint is small but has the problem its height. By contrast, the antenna in [8] obtains dual-frequency characteristics by arranging the antennas in concentric circles. Compared to the antenna in [6][7], this antenna can be lower profile, but its footprint becomes larger.

Therefore, a dual-frequency shared antenna with a low profile and a small footprint is required.

Items	Ring grounded at the inner edge [6][7]	Ring antenna with a parasitic element[8]
Height (< 2-layer)	△ (3-layer)	○ (2-layer)
Footprint (<0.6λ_{Low})	○ (0.5λ_{Low})	△ (1.0λ_{Low})
Bandwidth (dual-band)	○	○

Fig. 2.3-2 Comparison of conventional dual-band microstrip array antennas

(λ_{Low} indicates the wavelength at the center frequency of the low band)

(3) Technical issues in horn antennas

Finally, the study for horn antennas is discussed. Horn antennas are larger in size than microstrip antennas but have the advantage of providing broadband characteristics. Fig. 2.3-3 shows the comparison of conventional horn array antennas.

In [15], a waveguide horn array antenna has been proposed. Although it shows low-loss characteristics because it is composed only of aluminum, it is large and weight, and the beam can only be directed in boresight due to the wide element spacing. In [22], an injection-molded waveguide horn array antenna is proposed. After the resin is molded, metal plating is applied to make it work as an antenna. The features of this antenna include small size, light weight, low cost, and ease of manufacturing. However, the design method studied in [22] has a narrow coverage area.

Therefore, a low-loss light-weight horn antenna that can scan the beam to a wider angle is needed.

Chapters 3 through 5 describe the design techniques to address these issues.

Items	Metal horn array [15]	Injection-molded horn array[22]
Size/Weight	△ (using metal)	○ (using dielectric material)
Scan range (>45deg.)	× (only boresight)	△ <30deg.
Loss	◎	○

Fig. 2.3-3 Comparison of conventional horn array antennas

2.4. References

[1] https://www.jstage.jst.go.jp/article/bplus/12/3/12_234/_pdf

[2] http://ieice-hbkb.org/files/05/05gun_07hen_01.pdf

[3] https://www.researchgate.net/profile/Chris_Rizos/publication/267254924_Trends_in_GPS_Technology_Applications/links/548f43830cf214269f263925/Trends-in-GPS-Technology-Applications.pdf

[4] F. Kuo and R. Hwang, "High-isolation X-Band marine radar antenna design, " *IEEE trans. and propagat.* vol. 62, no. 5, pp. 2331-2337, May 2014.

[5] J. Yin, Q. Wu, C. Yu, H. Wang, and W. Hong, "Low-sidelobe-level series-fed microstrip antenna array of unequal interelement spacing," *IEEE Trans. Antennas Wireless Propag. Lett.*, vol. 16, pp. 1695-1698, Feb. 2017.

[6] A. Montesano, C. Montesano, R. Caballero, M. Naranjo, F. Monjas, L. E. Cuesta, P. Zorrilla, and L. Martinez, "Galileo system navigation antenna for global positioning," *in Proc. 2nd Eur. Conf. Antennas Propag. (EUCAP)*, Edinburgh, UK, 2007, pp.1-6.

[7] J. Rubio, M. A. Gonzalez, J. Zapata, A. Montesano, F. Monjas, L. E. Cuesta, "Full-wave analysis of the galileo system navigation antenna by means of the generalized scattering matrix of a finite array," *in Proc. 1st Eur. Conf. Antennas Propag. (EUCAP)*, Nice, France, 2006, pp.1-6.

[8] A. Al-Zoubi, F. Yang, and A. Kishk, "An efficient center-fed circular patch antenna loaded with an annular ring," *in Proc. 2008 IEEE Antennas and Propag. Society Int. Symp.*, San Diego, CA, USA, 2008, pp.1-4.

[9] Y. Konishi, H. Mizudamari, S. Sato, S. Mano, and T. Katagi, "Analysis and design

methods of planar array antennas with slotted waveguides taking into account mutual coupling," *IEICE Trans.on Commun*. vol. J71-B, no. 11, pp. 1325-1331, Nov. 1988.

[10] J. Hirokawa, L. Manholm, and P. Kildal, "Analysis of an untilted wire-excited slot in the narrow wall of a rectangular waveguide by including the actual external structure," *IEEE Trans. Antennas Propag.*, vol.45, no.6, pp.1038-1044, June 1997.

[11] Y. Miura, J. Hirokawa, M. Ando, Y. Shibuya, and G. Yoshida, "Double-layer full-corporate-feed hollow-waveguide slot array antenna in the 60-GHz Band," *IEEE Trans. Antennas Propag.*, vol.59, no.8, pp.2844-2851, Aug. 2011.

[12] S. Yamaguchi, Toru Takahashi, Y. Aramaki, M. Ohtsuka, Y. Konishi, and K. Sawaya, "A series-slotted waveguide array antenna covered by a dielectric slab with a post-wall cavity," *IEICE Trans.on Commun*. vol. J96-B, no. 6, pp. 631-640, June 2013.

[13] H. Kirino and H. Kamo, "A 76.5GHz Planar antenna using waffle-iron ridge waveguides," *IEICE Tech. Report*, AP2017-51, SAT2017-7, 2017.

[14] H. Deguchi, T. Goto, M. Tsuji, H. Shigesawa,and S. Matsumoto, "Multimode horn with low cross polarization optimized for dual-band use", *IEICE Trans.on Commun*. vol. E87-B, no. 9, Sept. 2004.

[15] R. Shen, X. Ye, J. Xie, Z. Chen and C. Jin, "A W-band circular box-horn antenna array radiating sum and difference beams with suppressed sidelobe," *IEEE trans. and propagat.* vol. 67, iss. 9, Sept. 2019.

[16] https://www.rfspin.cz/en/antennas/pyramidal-horn-antennas/ha50

[17] S. Makino, Y. Kobayashi, and T. Katagi, "Design of offset dual reflector type multibeam antenna composed of parabolic reflector and shaped subreflector,"

IEICE Trans.on Commun. vol. J69-B, no. 9, pp. 993-940, Sept. 1986.

[18] M. Takikawa, Y. Inasawa, H. Miyashita, and I. Naito, "Novel beam-scanning center-fed imaging reflector antenna with elliptical aperture for wide area observation," *IEICE Trans.on Commun.*, vol. E99–C, no.9, Sept. 2016.

[19] T. Tomura, M. Takikawa, Y. Inasawa, and H. Miyashita, "Simultaneous optimal design method of primary radiator and main reflector for shaped beam antennas," *IEICE Trans.on Commun.*, vol.E100–B, no.2, Feb. 2017.

[20] M. Nagasaka, S. Nakazawa,and S. Tanaka, "Dual-circularly polarized offset parabolic reflector antenna with microstrip antenna array for 12-GHz band satellite broadcasting reception," *IEICE Trans.on Commun.*, vol.E101–B, no.2, Feb. 2018.

[21] https://www.nict.go.jp/data/presentation/open-house2016/nict-open-house-2016-presentation-2-2.pdf

[22] Y. Aramaki, H. Uchida, T. Nishino, N. Yoneda, I. Naito, H. Miyashita, Y. Konishi, "Molded dielectric waveguide horn array antenna," *Technical Report of IEICE*, AP2008-178, pp.163-167, Jun. 2009.

3. Traveling-Wave Series-Fed Microstrip Array Antenna with Unequal Inter-Element Spacing

3.1. Introductory remarks

Microstrip antennas are low-cost, small, and light, and are widely used in mobile communication and radar systems. A branched-type array where each element is connected to the common feed line has been proposed as a microstrip configuration [24]- [26]. The power divider and the matching circuit placed near the branch points can be designed independent of the antenna element geometry. However, the insertion loss increases because of the bend line between the feed line and antenna element. In comparison, series-fed arrays [27]-[32] are highly efficiency because their short feedline length results in minimized spurious radiation and dissipation losses. Considering insertion loss, the traveling-wave series-fed microstrip arrays [29]-[32] are more advantageous than standing-wave arrays [27][28] where the electromagnetic wave travels back and forth inside the feed line.

However, due to the lack of the degree of freedom (DOF) in antenna elements, adequate geometry and design for traveling-wave series-fed microstrip array antenna have not been achieved. In the phase distribution, a meander line is used to compensate the phase distortion because the transmission phase varies with the radiation power from each element [29][30]. Since the length of the meander line can be arbitrarily selected, it enables easy array design. However, the meander line

increases insertion loss, the frequency dependency, and spurious radiation [33]. The only way to control radiation power from each element is changing the width of each element in the standing-wave array [27][28]. A slot-coupled microstrip array antenna has been proposed [31][32] for a high DOF feed line to control the radiation power from each element. Nonetheless, since this type of antenna requires two-layered dielectric substrates, it is sensitive to manufacturing errors and is more costly.

Herein, a single-layer microstrip array antenna and its design to overcome the aforementioned limitations of the traveling-wave array is proposed[34]. The slit on the output side of the antenna element is introduced as a new DOF to control the radiation power from each element. To remove meander lines that increase insertion loss and spurious radiation, the excitation phase distribution is adjusted by each element position.

This chapter is organized as follows: Section 3.2 discusses the electrical design procedure of the proposed array antenna, and Section 3.3 discusses the electrical performance of the proposed antenna array. Concluding remarks are given in Section 3.5.

3.2. Electric al design

Fig. 3.2-1 shows the proposed antenna. An electromagnetic wave is emitted by individual elements from the feeding point. The electromagnetic power transmitted through the feed line is large near the feed point and becomes smaller as the distance from the feed point increases. As a result, the radiation power is small for elements closer to the feeding point and large for elements closer to the end of the antenna. All the remaining power is radiated at the terminating element.

Since the microstrip antenna is described as a parallel resonant circuit, the equivalent circuit of the microstrip array antenna can be written as shown in the figure. Assuming that the radiation power from each element is A_i, the admittance of each element Y_i is expressed by the following equation[35].

$$\boldsymbol{Y_i} = \frac{\boldsymbol{A_i}}{\sum_{k=1}^{N} \boldsymbol{A_k}} \tag{3.2-1}$$

The power radiated by each element must be controlled to obtain the desired excitation distribution. In the proposed antenna, this is realized by the antenna element itself. The emphasis is on the output slit as a new DOF. In this section, the electrical design of the proposed antenna is described.

A. Design of the Antenna Element with an Output Slit

In this section, the behavior of the microstrip antenna with the output slit is described.

Herein, the principle of the output slit is described. Fig. 3.2-3 shows that adding slits or slots to the radiating conductor changes the path of the current. Some of the current path in Fig. 3.2-3 (b) are enlarged, resulting in a wider bandwidth. The current path of the proposed antenna changes due to the output slit. The current along the edge increases and the radiation power also increases.

Next, Numerical simulations were conducted to confirm the influence the output slit has on the antenna performance, as shown in Fig. 3.2-4. The electromagnetic field simulator HFSS was used for the analysis. A microstrip feed line and antenna element were arranged on the surface of a dielectric substrate, and an infinite ground plane was attached to the backside. The relative permittivity and dielectric loss tangent of the dielectric substrate were 3.0 and 0.0016, respectively. The thickness of the substrate was chosen to be 0.026 λ (λ is the wavelength at the center frequency), and the feed line width was 0.041 λ (The input impedance was 61.8 Ω). The phase reference point of this model was located at the center of the antenna element. The dimensions of the reference model are listed in Table 3.2-1. The dashed line and the dot-dash line in Fig. 3.2-5correlate to a ± 0.005 λ change in the length of the output slit. As shown in Fig. 3.2-5 (a), the transmission amplitude varies within approximately 1 dB at the center frequency. A large radiation power can be obtained by increasing the length of the output slit. As shown in Fig. 3.2-5 (b),

the reflection coefficient degrades slightly as the length of the output slit changes. However, this can be easily compensated by adjusting the length of the antenna element p_a and the length of the input slit s_i, because p_a and s_i mainly affect the resonance frequency and the input resistance, respectively, in a manner similar to that in an ordinary microstrip antenna. Fig. 3.2-5 (b) and (c) indicate that when the transmission coefficient of the proposed antenna decreases (i.e., radiation power increases), the transmission phase is delayed. This is because the electric field is confined inside the microstrip antenna and the phase delay increases when the amplitude of currents increases, and the antenna resonates. In this chapter, the deviation of the transmission phase is compensated by the position of the element in such a way that the entire array can be excited in-phase without meander lines that would otherwise increase insertion loss and spurious radiation. The element spacing is adjusted by Δd_i, when increasing the radiation power causes a phase delay $\Delta\varphi_i$.

Note that the dimensions of output slits for realizing the array in this chapter are shown in Table 3.2-2 in Section 3.2-C. The resonant frequency is determined by the length of the antenna, independent of the length of the slit. The resonant frequency is defined in the same way as for a normal microstrip antenna by the following equation[38].

$$f_{res} = \frac{c}{2\lambda_0\sqrt{\varepsilon_{eff}}} \tag{3.2-2}$$

$$a_e = a\left\{1 + 0.824\frac{t}{a}\frac{\left(\varepsilon_{eff} + 0.3\right)(a/t + 0.264)}{\left(\varepsilon_{eff} - 0.258\right)(a/t + 0.813)}\right\} \tag{3.2-3}$$

$$\varepsilon_{eff} = \frac{\varepsilon_r + 1}{2} + \frac{\varepsilon_r - 1}{2}\left\{1 + 12\frac{t}{a}\right\}^{-1/2} \tag{3.2-4}$$

,where c is the velocity of light, λ_0 is the wavelength in free space, a is the length of the microstrip antenna, t is the thickness of the microstrip antenna, ε_r is the relative permittivity of the dielectric substrate used.

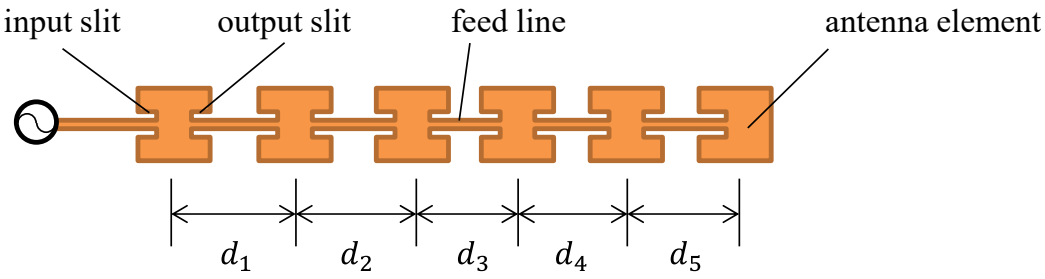

Fig. 3.2-1 Proposed traveling-wave series-fed microstrip arrays.

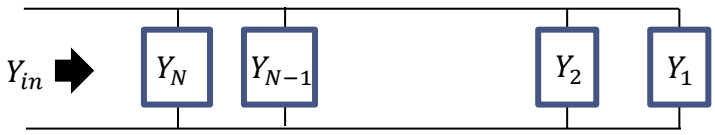

Fig. 3.2-2 Equivalent circuit of microstrip array antenna

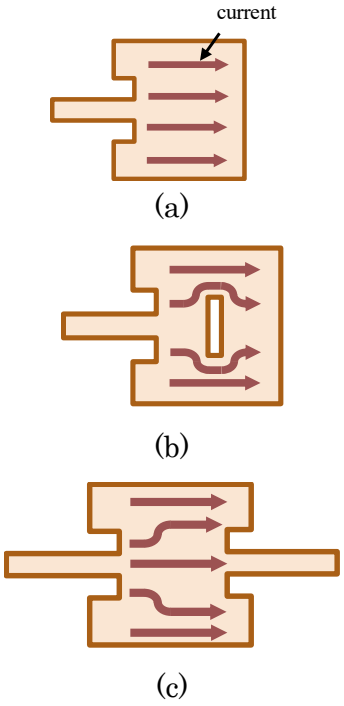

Fig. 3.2-3 Current path on microstrip antenna

(a) ordinary microstrip antenna, (b) microstrip antenna w/ slot, (c) proposed antenna

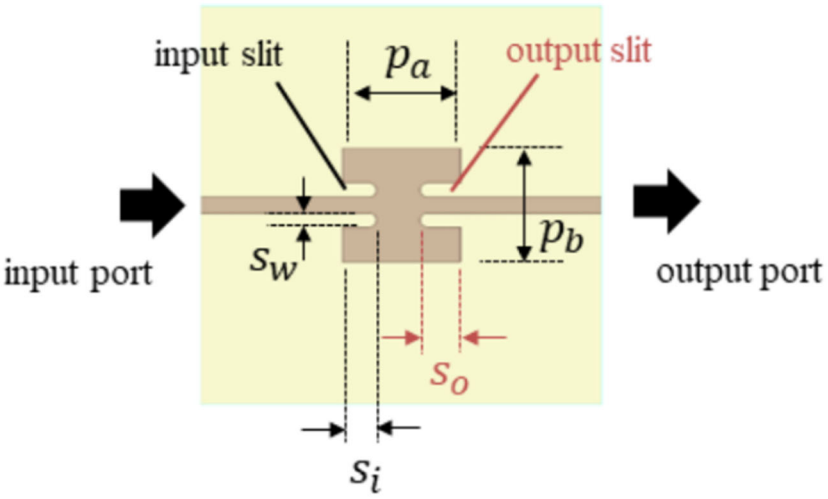

Fig. 3.2-4 Reference model for verifying the output slit.

Table 3.2-1 Dimensions of the reference model for verifying output slit

Symbol	Quantity	Value (λ)
p_a	Length of the antenna element	0.291
p_b	Width of the antenna element	0.302
s_i	Length of the input slit	0.0867
s_o	Length of the output slit	0.102
s_w	Width of the input & output slit	0.0357

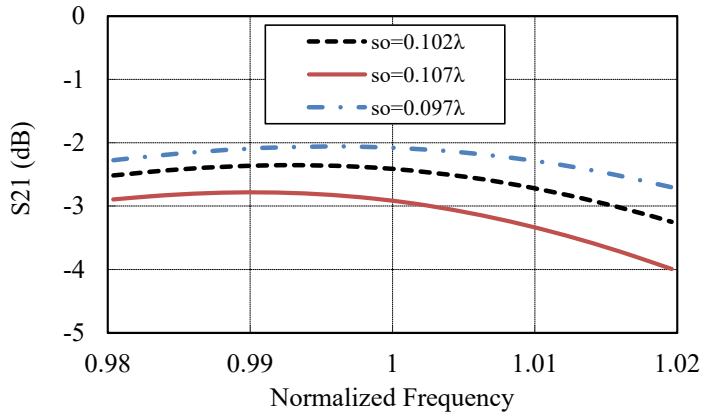

(a)

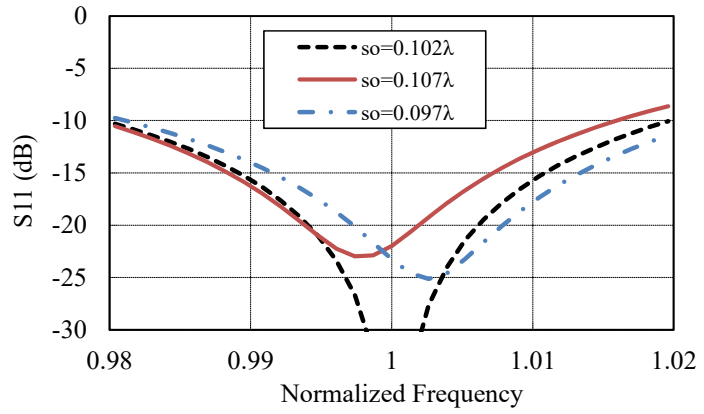

(b)

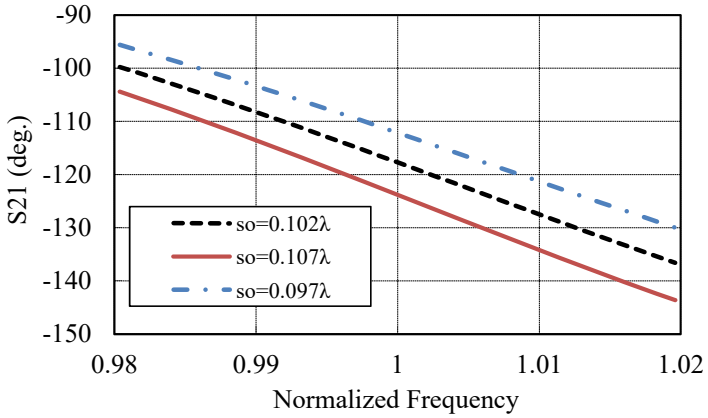

(c)

Fig. 3.2-5 Characteristics when the length of the output slit is changed by ± 0.005λ: (a) transmission coefficient, (b) reflection coefficient, and (c) transmission phase.

B. Prediction of the excitation distribution

As described below, the design under the condition that sidelobe level (SLL) < -20 dB or less in this thesis. Here, the Chebyshev distribution, which is known to give a constant SLL radiation pattern is described.

The Chebyshev distribution is known as a side-lobe constant excitation distribution [39]. The synthesized pattern for an array of N_T elements spaced d_x apart is

$$F(z) = T_M(z) \qquad for\ \ M = N_T - 1 \tag{3.2-5}$$

where $T_M(z)$ is the Chebyshev polynomial of order M:

$$T_M(z) = \cos(M \cos^{-1} z) \qquad for\ |z| \le 1 \tag{3.2-6}$$

$$T_M(z) = \cosh(M \cosh^{-1} z) \qquad for\ |z| \ge 1 \tag{3.2-7}$$

and

$$z = z_0 \cos[(\pi d_x/\lambda_0) \sin\theta] \tag{3.2-8}$$

$$z_0 = \cosh\left\{\frac{cosh^{-1}(r)}{M}\right\} \tag{3.2-9}$$

$$SLL_{dB} = 20 \log_{10} r \tag{3.2-10}$$

The currents required to produce the Chebyshev pattern are given as

$$I_m = \frac{2}{N_T}\left[r + 2\sum_{s=1}^{(N_T-1)/2} T_m\{z_0 \cos(s\pi/N_T)\}\cos((2m-1)s\pi/N_T)\right] \quad for\ N_T\ odd$$

$$m = 0,1,2,\cdots,(N_T-1)/2$$

(3.2-11)

$$I_m = \frac{2}{N_T}\left[r + 2\sum_{s=1}^{N_T/2-1} T_m\{z_0 \cos(s\pi/N_T)\}\cos(2s\pi m/N_T)\right] \quad for\ N_T\ even$$

$$m = 0,1,2,\cdots,(N_T/2-1)$$

(3.2-12)

Fig. 3.2-6 and Fig. 3.2-7 show an example of the excitation distribution and radiation pattern for varying sidelobe levels, respectively.

The excitation coefficients to realize the Chebyshev distribution satisfying SLL<-20dB are focused in the thesis. For equally spaced arrays, the excitation distribution is symmetrical. Unequal spacing to compensate for the passing phase of each element results in a density taper. To maintain the original distribution, the amplitude near the feeding point is to be dense, while the amplitude near the terminating elements is to be sparse. The comparison between the expectation and the design result will be shown in Section 3.2-D.

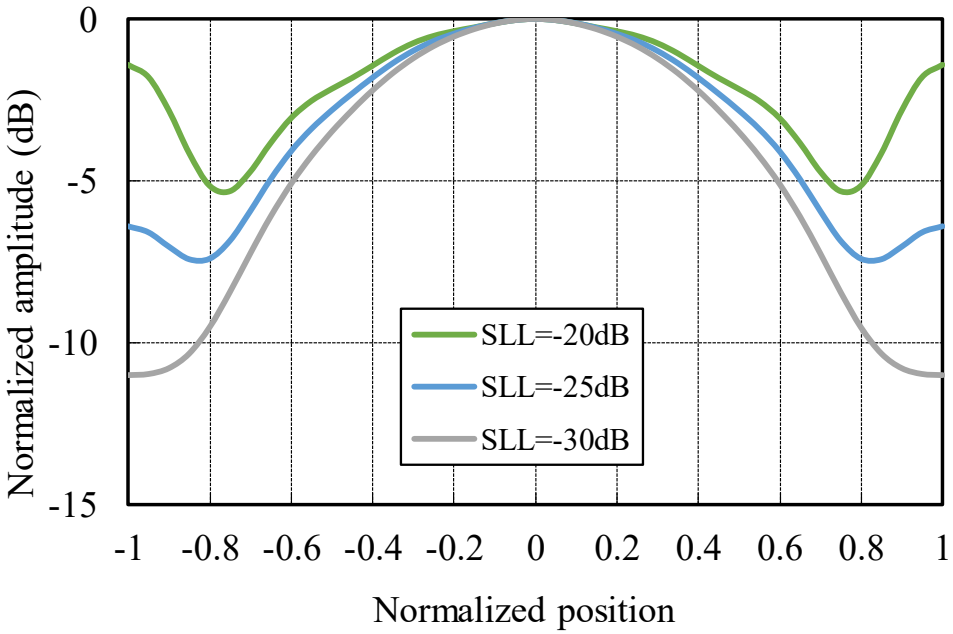

Fig. 3.2-6 Chebyshev distribution

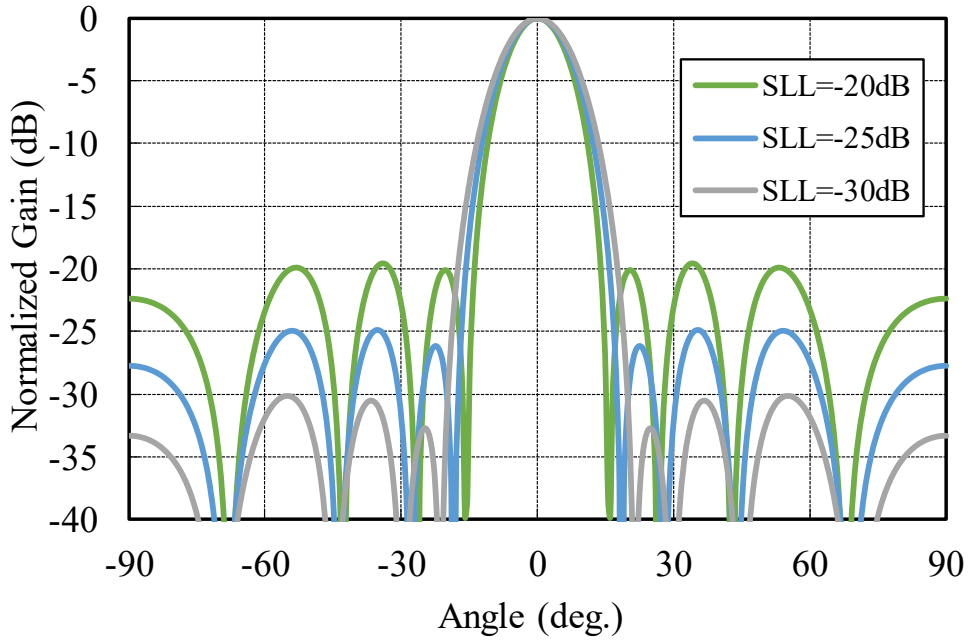

Fig. 3.2-7 Radiation pattern of Chebyshev distribution

C. Procedure for Designing Proposed Antenna

This section describes the detailed design procedure. The flow chart for the design is shown in Fig. 3.2-8. First, the element position is tentatively determined, and the excitation distribution is designed. Next, the input power is distributed to each antenna element. Then, the element design is performed, and the information of the transmission phase is fed back. This operation is repeated until each element satisfies the target of the reflection coefficient and power division to each antenna element. Finally, fine adjustment including mutual coupling in the array is performed.

1) Element position setting

Since the antenna element has a lag phase (the transmission phase is negative), the element interval must be shorter than the wavelength λ_g of the feed line to achieve in-phase excitation.

2) Excitation distribution design

When the required excitation amplitude distribution is uniform, the radiation power from each element is the same. However, if the excitation distribution is non-uniform, the radiation power differs from element to element. As described in Step 1, since the phase distribution is adjusted by the element position, the excitation amplitude distribution required to realize a desired radiation pattern changes according to the element position. Herein, the amplitude distribution is designed by

using a genetic algorithm (GA) [40][41] for the element position determined in Step 1, because it is difficult to derive a theoretical excitation distribution for discrete sources placed at unequal inter-element spacing.

3) Power division

The input power is distributed to each element such that the excitation distribution obtained in Step 2 is realized [42][43]. Because the feed line loss between elements affects the power distribution, it must be considered in this step by solving the following simultaneous equations:

$$\begin{cases} A_i = b_i - a_i \\ L_i = a_{i+1} - b_i \end{cases} \tag{3.2-13}$$

where A_i (dB) is the excitation amplitude of the i-th element, a_i (dB) and b_i (dB) are the input and output power to the i-th element, respectively, and L_i (dB) is the line loss between the i-th element and the $(i+1)$-th element. $A_i(i = 1,2,\cdots,N)$ is already obtained in Step 2. L_i can be calculated from the electromagnetic field analysis using the element position information provisionally determined in Step 1. By solving the simultaneous equations in Eq. (3-2.-13), a_i and b_i are obtained. Therefore, the power distribution to each element is uniquely determined.

4) Antenna element design

To realize the excitation distribution in Step 3, the element design is performed to reduce reflection while obtaining the desired radiation power. The goal of element design is to obtain a reflection characteristic S_{11}^e of each element that is less than

−20 dB; also, the difference between the calculated S_{21}^{e} and the target value S_{21}^{t} should be less than 0.1 dB. The excitation distribution design and element design are repeated until both converge, i.e., using the information of the transmission phase obtained by the element design, the element spacing is updated to obtain a desired excitation phase distribution. The excitation distribution is redesigned using a genetic algorithm.

5) Array design

Based on the element design results obtained in Steps 1–4, array design is implemented by considering the influence of inter-element coupling. In the process of adjusting the reflection characteristics, it is better to vary the length of the input slit s_i and the length of the antenna element p_a than to vary the length of the output slit s_o and the width of the antenna element p_b because p_a and s_o have little effect on the excitation distribution. When the influence of the mutual coupling cannot be canceled out by changing the length of the input slit s_i and the length of the antenna element p_a, a square hole is carved in the microstrip element to obtain high input impedance[44].

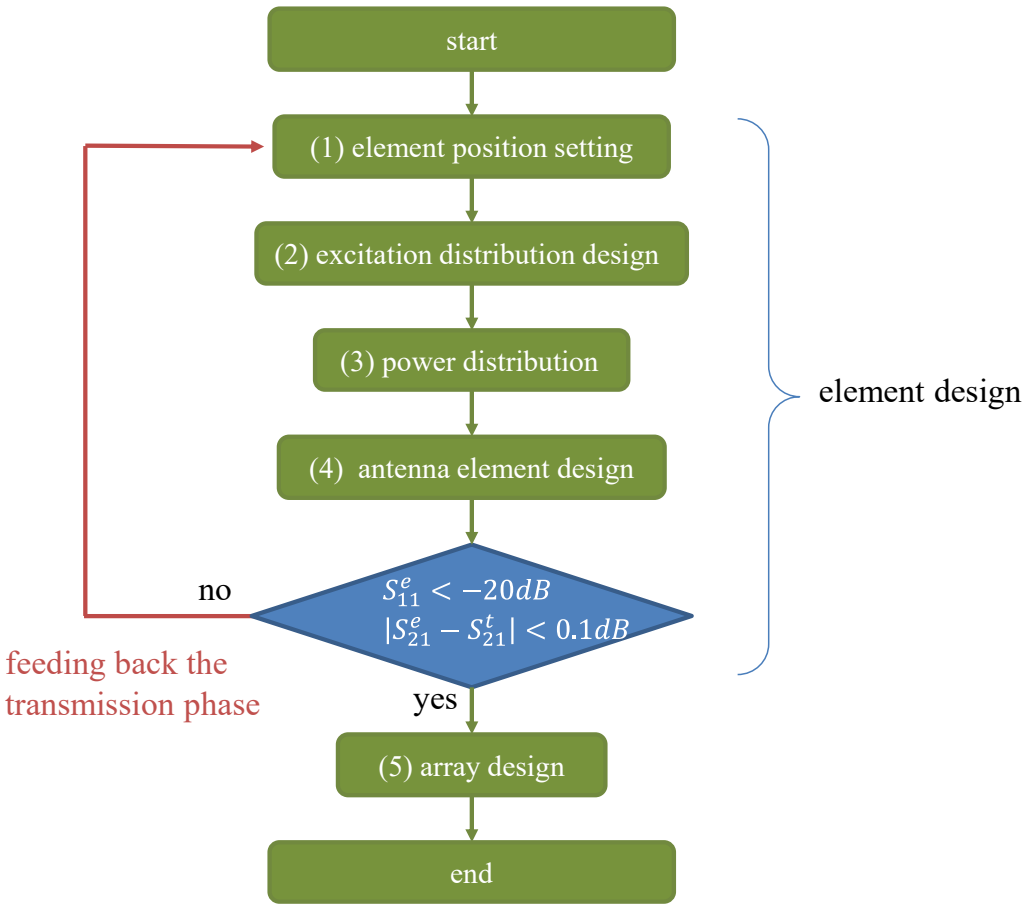

Fig. 3.2-8 Proposed antenna design flow chart.

D. Design Results

In this section, results for designing a 9-element array are presented. The design goals are to realize (i) S11 <−20 dB and (ii) a sidelobe level less than −20 dB. The dielectric substrate used in this part is the same as that in Section 3.2-A.

First, an initial element position is set up at which the element spacing becomes gradually narrow as shown by the dashed line in Fig. 3.2-9. The dot-dashed chain line and the solid line are the element design results of second and third trials, respectively. The element number 1 indicates the element closer to the feed point, whereas the number 9 indicates the termination element.

Next, the excitation distribution is determined. If there is an element with an extremely small amplitude, the robustness of the array decreases. Therefore, the minimum value of the relative amplitude in the genetic algorithm is set according to the following procedure. Assuming a 9-element array of equal inter-element spacing with the Taylor distribution that satisfies the desired sidelobe level, the minimum relative amplitude becomes approximately -7 dB. In this dissertation, the threshold to −8 dB, including the margin is set.

The solid line in Fig. 3.2-10 shows the designed excitation distribution. A symmetrical excitation distribution is obtained for the equally spaced array. However, since the obtained element positions are not equally spaced, the obtained distributions are asymmetric. Note that the trial #3 distribution shown in Fig. 3.2-10 looks like a Chebyshev polynomial distribution, which is caused by the design of the excitation distribution such that the sidelobe level is less than the specified value.

Fig. 3.2-11 shows the normalized array factor for each trial. Fig. 3.2-9-Fig. 3.2-11 show that the solution converged in the third trial. Fig. 3.2-12 shows the reflection coefficients for each trial, which indicates that all amplitudes are below the threshold of −20 dB. The designed lengths of output slits and transmission amplitude for realizing the desired excitation distribution shown in Fig. 3.2-10 are presented in Table 3.2-2. The transmission of each element is properly controlled by the length of the output slit s_o. Finally, the array is subjected to fine adjustment. A square hole of side of 0.0766λ inside the rectangular element #1 and #2 is carved to obtain a high input impedance.

Fig. 3.2-13 shows the designed traveling-wave series-fed microstrip array antenna. In Fig. 3.2-14, the normalized radiation patterns are shown in which a sidelobe level less than −20dB can be achieved. The radiation pattern without mutual coupling is also shown as a reference. The difference between the patterns with and without mutual coupling is considered to be acceptable. Note that the insertion loss of the proposed traveling-wave array is 0.82 dB in the W band, whereas that of the standing-wave array is 1.10 dB, i.e., the former is lower by 0.28 dB.

Lastly, Fig. 3.2-15 shows the comparison of the excitation amplitude distributions between the expectation and the design result. As expected, in the GA-designed results, the amplitude near the feeding point becomes strong, while the amplitude near the terminating elements becomes weak. Fig. 3.2-16 shows the comparison of the radiation patterns, which indicates that the designed and the original pattern correspond well.

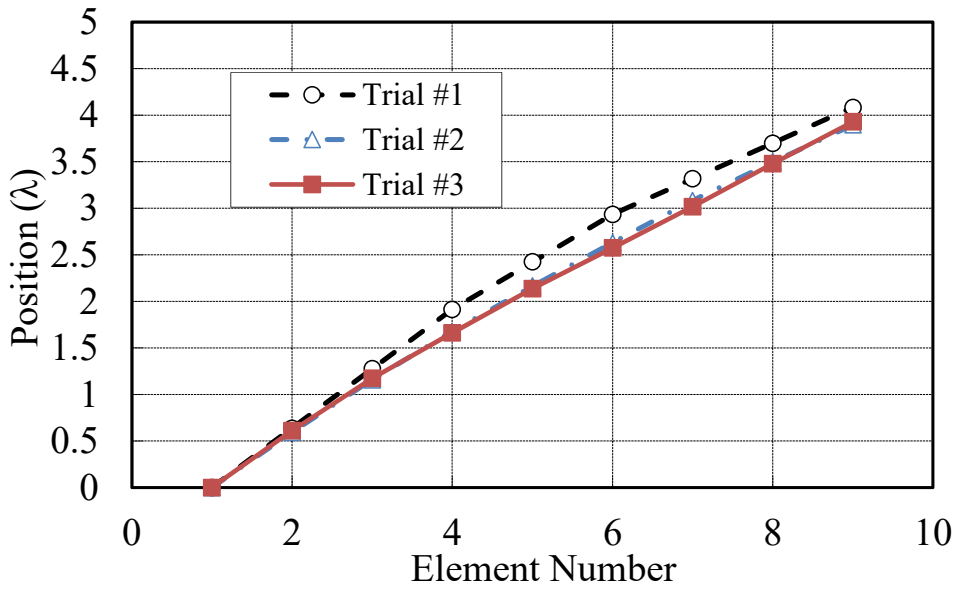

Fig. 3.2-9 Comparison of element positions for each trial number.

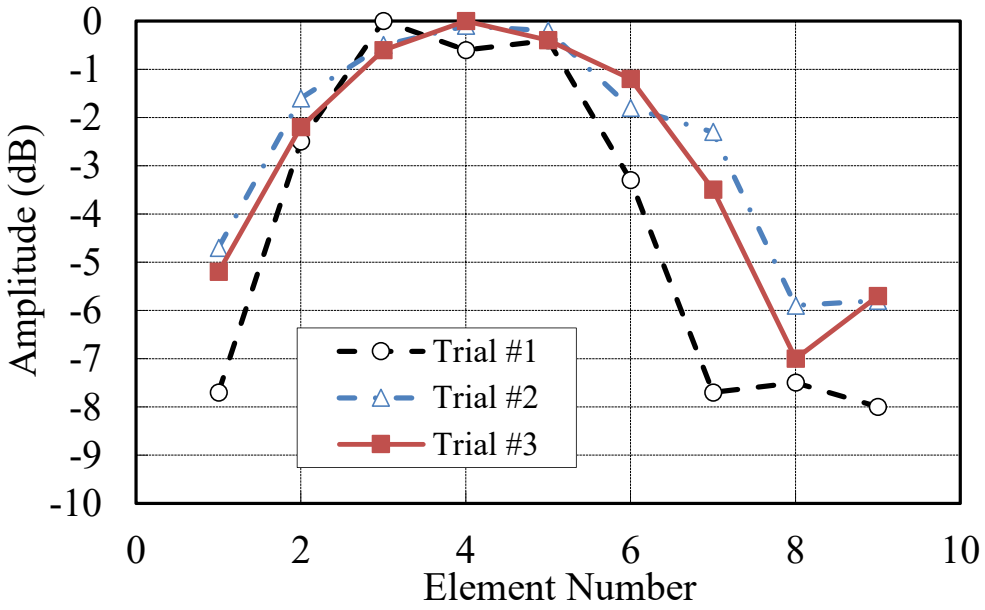

Fig. 3.2-10 Comparison of the excitation amplitude distribution for each trial number.

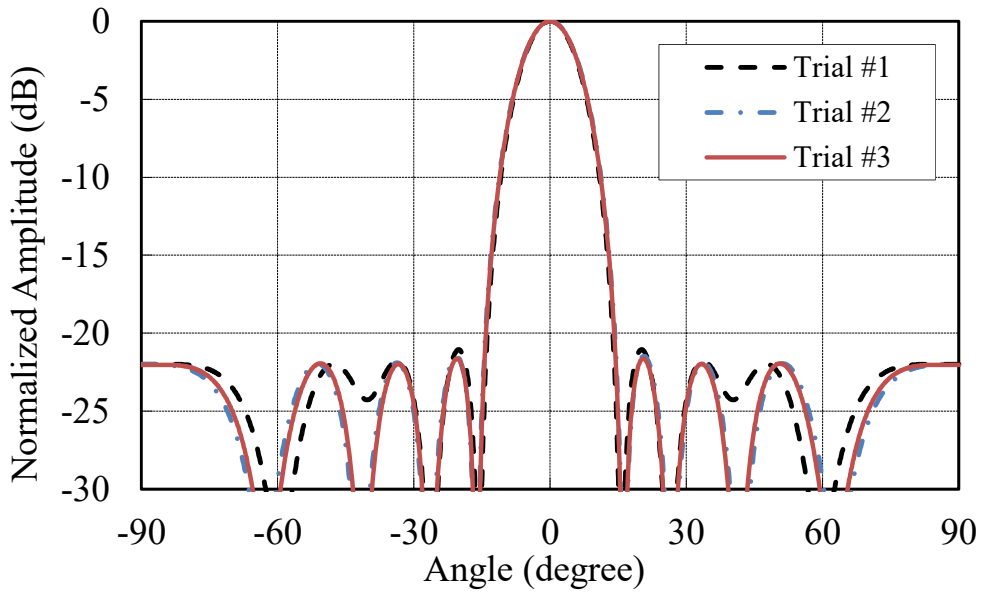

Fig. 3.2-11 Comparison of the array factor for each trial.

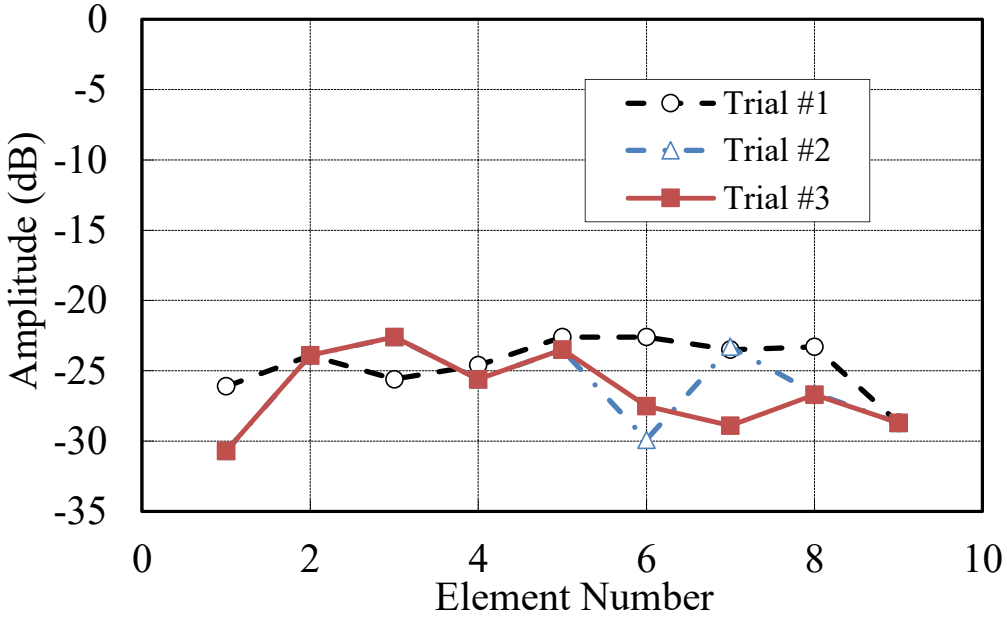

Fig. 3.2-12 Comparison of the reflection coefficient for each trial.

Table 3.2-2 The designed lengths of output slits and the transmission amplitude of each element

Element Number	Length of the output slit s_o (λ)	S21 (dB)
1	0.000	−0.24
2	0.0153	−0.51
3	0.0587	−0.85
4	0.0818	−1.33
5	0.0919	−1.86
6	0.103	−2.52
7	0.105	−2.77
8	0.102	−2.41

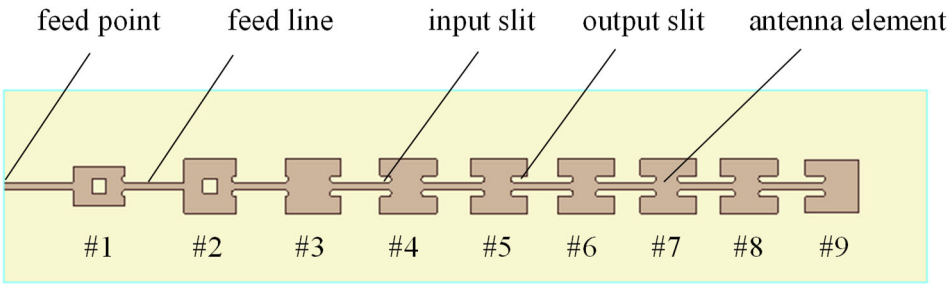

Fig. 3.2-13 Designed model of the proposed traveling-wave series-fed microstrip array antenna.

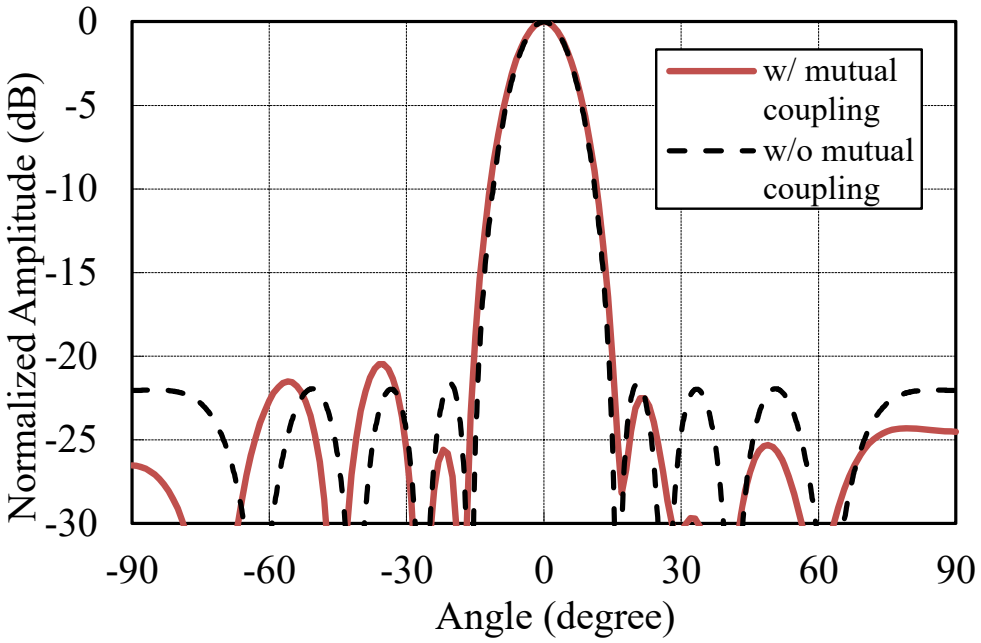

Fig. 3.2-14 Comparison of the radiation pattern of the proposed traveling-wave antenna in the horizontal direction at the center frequency, with and without mutual coupling.

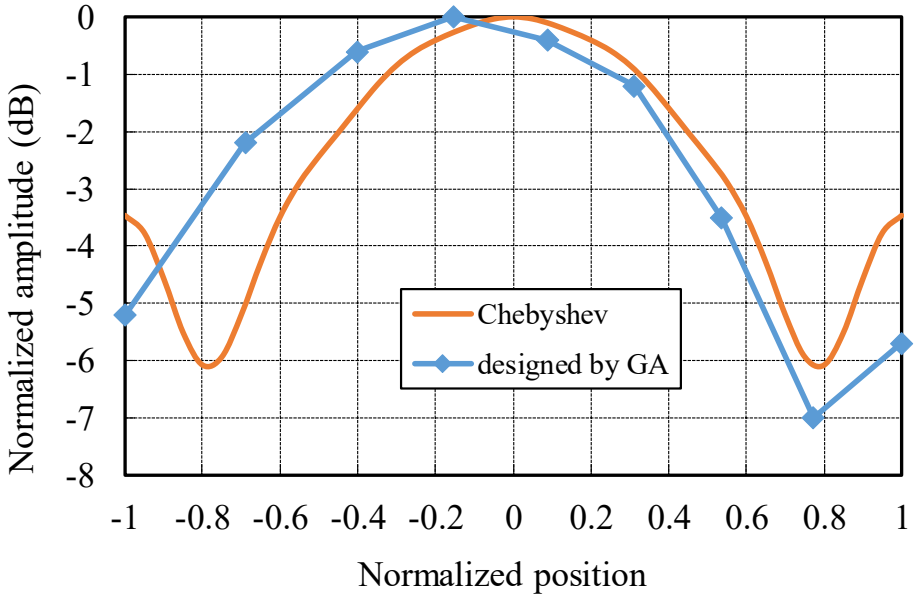

Fig. 3.2-15 Comparison of excitation amplitude distributions

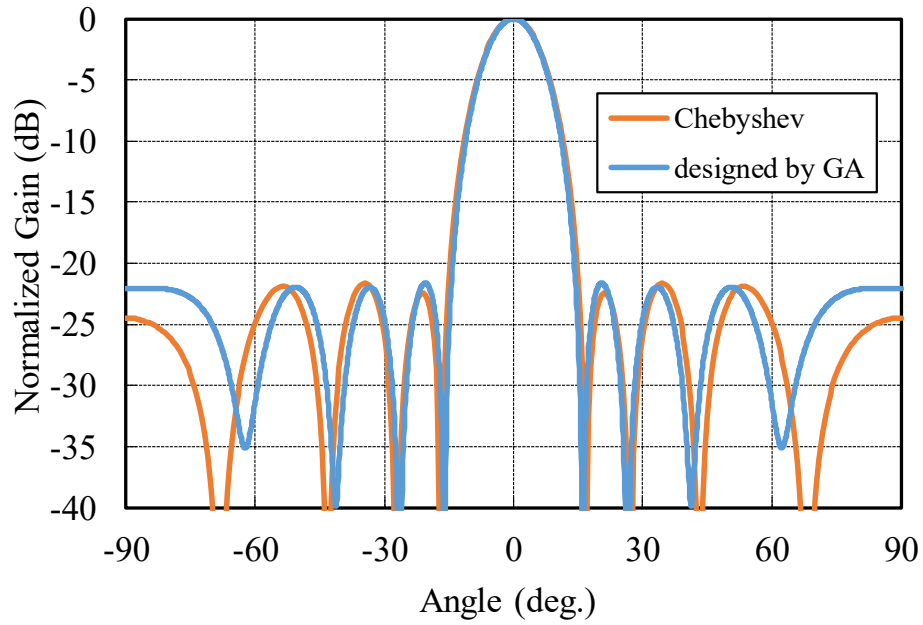

Fig. 3.2-16 Comparison of radiation patterns

3.3. Measurement Results

In this section, the results of the manufactured array antenna are presented. Note that the simulated and measured results in this section contain the waveguide to the microstrip line transition [45], and the design result in Section 3.2 corresponds to the antenna elements and microstrip feed line only. The design model and the manufactured antenna are shown in Fig. 3.3-1, and the simulated and measured results of the reflection coefficient are presented in Fig. 3.3-3. The measured result is −10 dB or less with a relative bandwidth of 2% which agrees with the simulated result. As shown in Fig. 3.3-3, the simulated and measured radiation patterns at the center frequency agree well, meaning that the desired sidelobe level (<−20 dB) is achieved. The actual measured gain, including the feed network in the boresight, is 13.4 dBi (14.1 dBi, designed). The overall efficiency of the antenna is 70.5% (calculated value: 82.8%). These results show that the design method discussed in the Section 3.2 is valid.

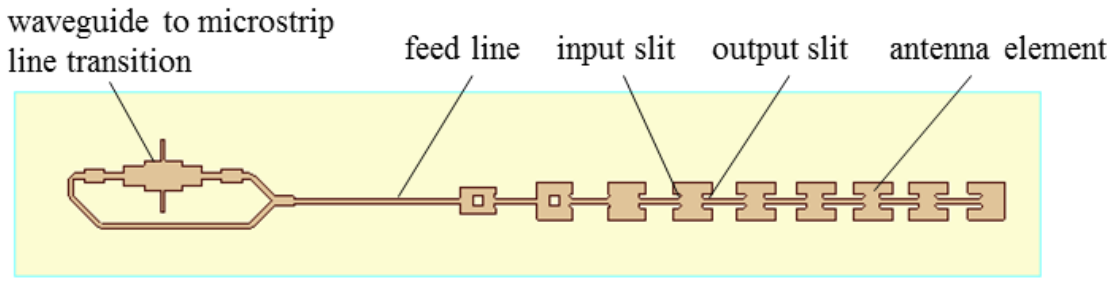

(a)

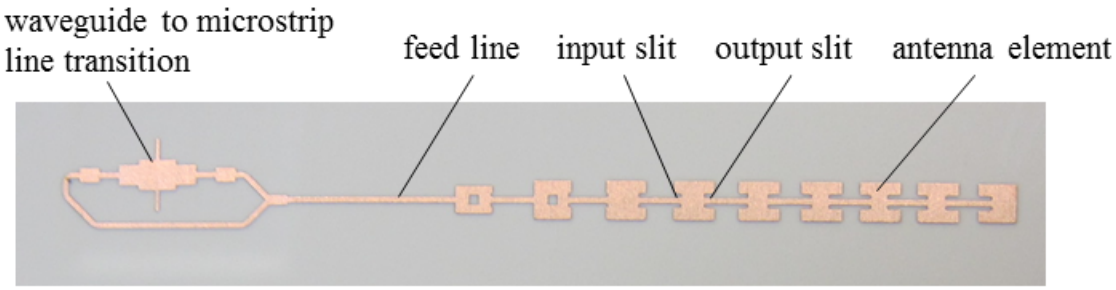

(b)

Fig. 3.3-1 Microstrip array antenna of (a) designed model, (b) manufactured antenna.

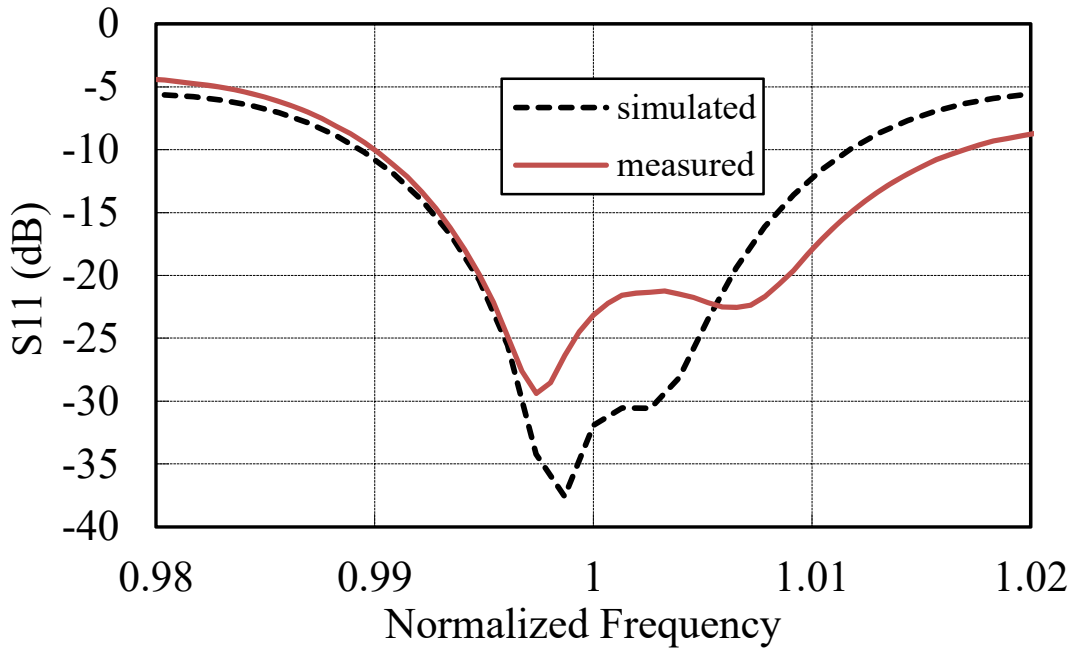

Fig. 3.3-2 Simulated and measured reflection coefficient versus the frequency.

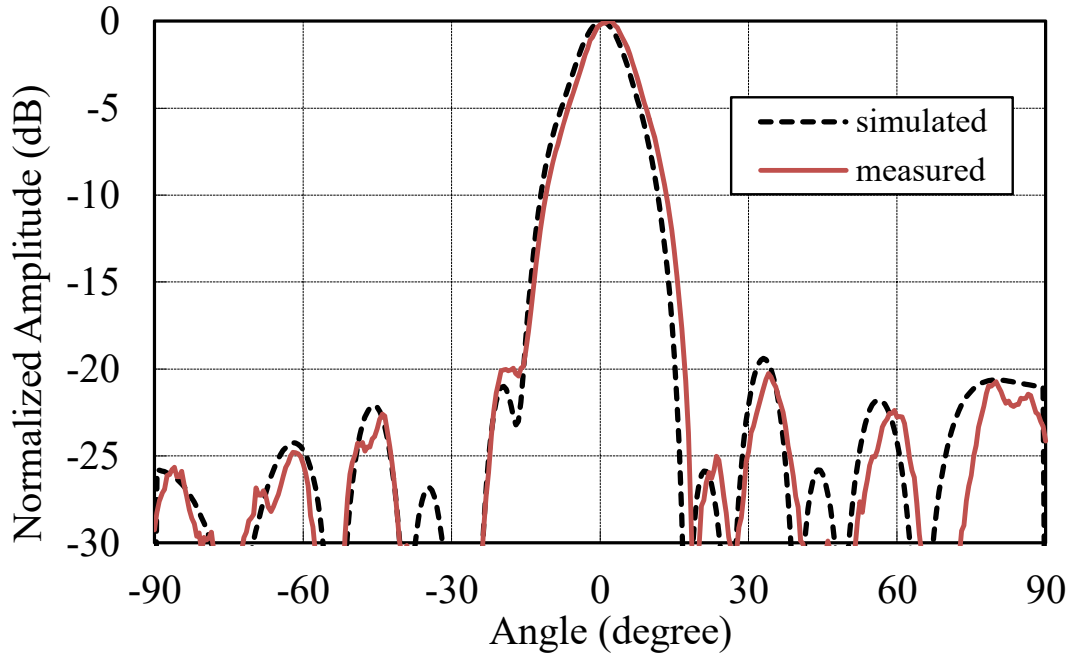

Fig. 3.3-3 Simulated and measured array pattern in the horizontal cut plane at the center frequency.

Table 3.3-1 shows the benchmark of microstrip array antennas. It was confirmed that the proposed antenna has a narrow width of about 0.5 wavelengths and a wide bandwidth. Besides, the proposed antenna has high efficiency even though it uses a higher frequency band than other methods.

Table 3.3-1 Benchmark of microstrip array antennas

Ref.	Width	Band width (%) (*1)	Efficiency	Frequency band
[4]	$0.7\,\lambda_{eff}$	2.2	63%	X
[26]	$1.3\,\lambda_{eff}$	1.9	60%	X
[28]	$0.5\,\lambda_{eff}$	1.9	61%	K
Proposed	$0.5\,\lambda_{eff}$	2.2	71%	W

*1 BW is bandwidths for -10 dB of reflection coefficient.

3.4. Versatility

Finally, the versatility of the proposed antenna is demonstrated. The antennas shown so far have been designed in the W band. Here, the characteristics of the design at 60GHz, 90GHz, and 120GHz are shown.

Fig. 3.4-1 shows the reflection characteristics, and Fig. 3.4-2 shows the radiation pattern. The same performance can be obtained even if the frequency band changes. Table 3.4-1 shows that the realized gain decreases as the frequency increases, because of the increase of dielectric loss.

From the above, it was found that this antenna and the design method operate effectively even if the frequency changes.

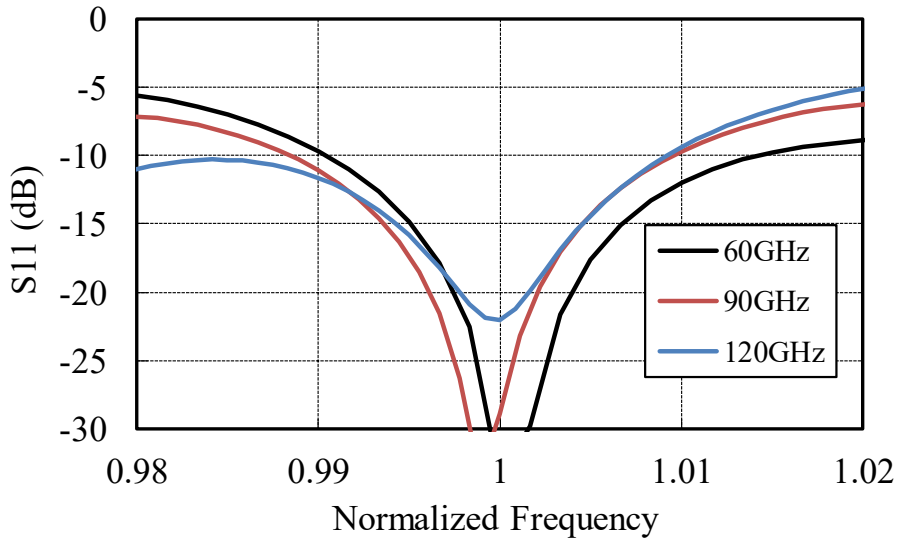

Fig. 3.4-1 Simulated reflection coefficient versus the frequency.

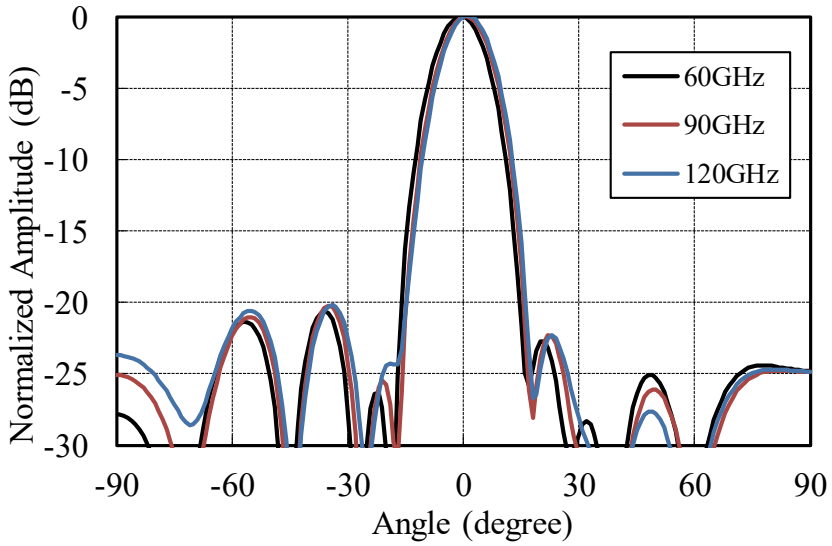

Fig. 3.4-2 Simulated array pattern in the horizontal cut plane at the center frequency in each band.

Table 3.4-1 Comparison of gains and losses for each antenna

	60 GHz	90 GHz	120 GHz
Realized Gain (dBi)	14.9	13.0	11.1
Dielectric Loss (dB)	1.0	1.9	3.6
Conductor Loss (dB)	0.4	0.4	0.4

3.5. Summary

In this chapter, the design method to create a novel traveling-wave series-fed microstrip array antenna was proposed. The power control slits and unequal inter-element spacing control amplitude and phase in the array, respectively. These bring a new DOF, which enables a single-layer microstrip array exhibiting low-loss and low spurious radiation. The measured and simulated results agree well.

3.6. References

[24] D. M. Pozar, and D.H. Schaubert, "Comparison of three series fed microstrip array geometries," in *Proc. of Antennas and Propag. Society Int. Symp.*, Ann Arbor, MI, USA, 1993, pp. 728-731.

[25] R. Bayderkhani, and H. R. Hassani, "Wideband and low sidelobe slot antenna fed by series-fed printed array," *IEEE Trans. on Antennas and Propagat.*, vol. 58, no. 12, Dec. 2010.

[26] I. Slomian, K. Wincza, and S. Gruszczynski, "Series-fed microstrip antenna array with inclined-slot couplers as three-way power dividers," *IEEE Trans. Antennas Wireless Propag. Lett.*, vol. 12, pp. 62-54, May 2013.

[27] D. G. Babas, and J. N. Sahalos, "Synthesis method of series-fed microstrip antenna arrays" *Electron. Lett.*, vol. 43, iss. 2, pp. 78-80, Jan. 2007.

[28] H. Khalili, K. Mohammadpour-Aghdam, S. Alamdar, and M. Mohammad-Taheri, "Low-cost series-fed microstrip antenna arrays with extremely low sidelobe levels," *IEEE Trans. on Antennas and Propagat.*, vol. 66, no. 9, pp. 4606-4612, Sept. 2018.

[29] C. G. Christodoulou, P. F. Wahid, M. Riad Mahbub, and M. C. Bailey, "Design of a minimum-loss series-fed foldable microstrip," *IEEE Trans. on Antennas and Propagat.*, vol. 48, no. 8, pp. 1264-1267, Aug. 2000.

[30] J. Yin, Q. Wu, C. Yu, H. Wang, and W. Hong, "Low-sidelobe-level series-fed microstrip antenna array of unequal interelement spacing," *IEEE Trans. Antennas Wireless Propag. Lett.*, vol. 16, pp. 1695-1698, Feb. 2017.

[31] A. Vallecchi and G. B. Gentili, "Design of dual-polarized series-fed microstrip

arrays with low losses and high polarization purity," *IEEE Trans. on Antennas and Propagat.*, vol. 53, no. 5, pp. 1791-1798, May 2005.

[32] S. Karimkashi, and G. Zhang, "A dual-polarized series-fed microstrip antenna array with very high polarization purity for weather measurements," *IEEE Trans. on Antennas and Propagat.*, vol. 61, no. 10, pp. 5315-5319, Oct. 2013.

[33] J. Wang and O. Fujiwara, "TDR analysis of electromagnetic radiation from a bend of micro-strip line," *IEICE Trans.on Commun*. vol. E88-B, no. 8, Aug. 2005.

[34] J. Goto, M. Matsuki, T. Maruyama, T. Fukasawa, N. Yoneda, and J. Hirokawa, "Design of the Traveling-Wave Series-Fed Microstrip Antenna Array with Power Control Slits of Unequal Inter-Element Spacing," *IEICE Trans. Commun,* vol. E104-B, no.6, Jun. 2021.

[35] W. Stutzman, G. Thiele, *Antenna theory and design*, 3rd Edition, 2012.

[36] S. Weigand, G. Huff, K. Pan, and J. Bernhard, "Analysis and design of broad-band single-layer rectangular U-slot microstrip patch antennas," *IEEE Trans. on Antennas and Propagat.*, vol. 51, no. 3, pp. 457-468, March 2003.

[37] Y. Chen, S Yang, and Z. Nie, "Bandwidth enhancement method for low profile E-shaped microstrip patch antennas," *IEEE Trans. on Antennas and Propagat.*, vol. 58, no. 7, pp. 2442-2447, July 2010.

[38] J. James and P. Hall. *Handbook of microstrip antennas*, Peter Peregrinus, 1989.

[39] R. Mailloux, *Phased array antenna handbook*, 2nd Edition, Artech House, pp. 116-121, 2005.

[40] B. Aljibouri, A.J. Sambell, and B.S. Sharif, "Application of genetic algorithm to design of sequentially rotated circularly polarised dual-feed microstrip patch antenna array," *Electron. Lett.*, vol. 44, no. 12, pp. 708-709, June 2008.

[41] Y. Wen, B. Wang, and X. Ding, “A wide-angle scanning and low sidelobe level microstrip phased array based on genetic algorithm optimization,” *IEEE Trans. on Antennas and Propagat.*, vol. 64, no. 2, pp. 805-810, Feb. 2016.

[42] J. P. Daniel, E. Penard and C. Terret, “Design and technology of low-cost printed antennas,” in *Handbook of Microstrip Antennas,* vol. 1, J. R. James and P. S. Hall, London, UK: Peter Peregrinus, 1989, pp. 645–655.

[43] R. Garg, P. Bhartia, I. Bahl, and A. Ittipiboon, “Design and analysis of microstrip antenna arrays,” in *Microstrip Antenna Design Handbook*, Norwood, MA, USA: Artech House, 2001, pp. 726–727.

[44] J. S. Dahele, K. F. Lee, and D. P. Wong, “Dual-frequency stacked annular-ring microstrip antenna,” *IEEE Trans. Antennas Propagat.*, vol.AP-35, no. 11, pp. 1281–1285, Nov. 1987.

[45] T. Maruyama and S. Udagawa, “Via-less and small-radiation waveguide to microstrip line transition for millimeter wave radar modules,” *IEICE Comm. Express*, vol.6, no. 8, pp. 548–553, June 2017.

[46] M. Haneishi, S. Yoshida, “A design method of circularly polarized microstrip antenna by one-point feed,” *IEICE Trans. Commun.*, vol. J64-B, pp.225-231, April 1981. (in Japanese)

4. Design of the Circularly Polarized Ring Microstrip Antenna with Shorting Pins

4.1. Introductory remarks

Microstrip antennas are low-cost, small, and light, and are therefore widely used. Ring microstrip antennas have become good candidates [47], because they can maintain good radiation characteristics with a smaller dimension than circular microstrip antennas. Utilization of the inner areas of such ring microstrip antennas has been proposed, and some improvements have been obtained without increasing their size.

The input impedance of the ring microstrip antenna has a lower limit, since there is no radiation conductor near the center and the feeding pin cannot be moved there. Furthermore, because the minimum input impedance of ring microstrip antennas quickly increases under TM11 mode excitation when the inner radius of the ring microstrip antenna increases, it has been proposed to embed a matching circuit in the antenna without increasing its size [48]. However, this prevents the inner area from being used for other purposes.

Another way to utilize the inner area is to place another smaller antenna inside the ring microstrip antenna to operate as a dual-band antenna [49] [50]. In [50], an aperture-shared ring microstrip antenna was proposed. This can be used for Global Positioning System (GPS) and satellite digital audio radio. However, the frequency

ratio of the two antennas is large because the radiating elements must not overlap, meaning that this technology cannot be readily applied to other systems dealing with closer frequencies. In[50], to address this problem, two kinds of substrate are used to obtain the extra degree of freedom (DOF), reducing productivity and increasing costs.

In comparison, ring microstrip antennas grounded at the inner edge have been proposed [51]-[55]. These are often utilized as the lower layer of a dual-band share-aperture stacked microstritp antenna. As the inner diameter becomes increased, the outer diameter must be large to maintain the resonance frequency. Because small antennas are generally required, the inner diameter of a ring microstrip antenna grounded at the inner edge needs to be small. Therefore, the internal space is only used to incorporate the feed line to the upper-layer element of the shared-aperture microstrip antenna. Note that the ring microstrip antenna grounded at the inner edge and the ring microstrip antenna without any shorting pins are called “the ring patch antenna” and “the annular patch antenna” in [51]-[54], respectively. In this dissertation, I call the former “the ring microstrip antenna grounded at the inner edge”, and the latter “the ring microstrip antenna”.

As described above, the usage of the inner area of the ring antenna has been limited for three reasons: first, ring antennas with a large inner/outer ratio have high input impedance and requires the additional matching circuit; second, ring antennas cannot include other ring antennas with similar operating frequencies; third, the ring microstrip antenna grounded at the inner edge has a large size. In this dissertation, shorting pins discretely placed on the inner edge are introduced as a new degree of freedom to solve the above issues [56]-[58]. By changing the distance

between the shorting and feeding pins, moderate input impedance can be obtained without adding a matching circuit. Moreover, the number and diameter of the shorting pins can control the resonance frequency, such that the proposed antenna can expand its inner area and include another antenna with a similar resonance frequency. Moreover, the outer diameter can remain almost unchanged, even when the inner diameter increases.

This chapter is organized as follows: the principles and analytical results of the proposed antenna are explained in Section4.2. In Section4.3, the design procedures and measurement results of the dual-frequency circularly polarized antenna using the proposed antenna are presented. In Section 4.4, the electrical performance for a proto flight model of a satellite positioning system using the proposed circularly polarized ring microstrip antenna with shorting pins is demonstrated. The concluding remarks are presented in Section4.6.

4.2. Proposed antenna

In this section, the operational principle of the proposed antenna and its eigenvalue analysis results are presented.

A. Principles

First, the differences between the ring microstrip antenna and the ring microstrip antenna grounded at the inner edge are presented.

In the ring microstrip antenna in which both the inner and outer circles are in an open-circuit state, the outer diameter decreases as the inner diameter increases to maintain the desired resonance frequency. This is because the ring antenna has an open inner circle, and the current is diverted along the radiating conductor.

By contrast, a ring microstrip antenna grounded at the inner edge is considered as an antenna in which the center of a circular microstrip antenna is enlarged because the outer circle is electrically in an open-circuit state, while the inner circle is in a short-circuit state. Therefore, to maintain a resonance frequency, the outer diameter increases as the inner diameter increases.

As shown in Fig. 4.2-1, the proposed antenna has the shorting pins discretely placed on the inner edge which improve to control the resonance frequency: the resonance frequency of the proposed antenna remains almost unchanged, even when the inner diameter is increased.

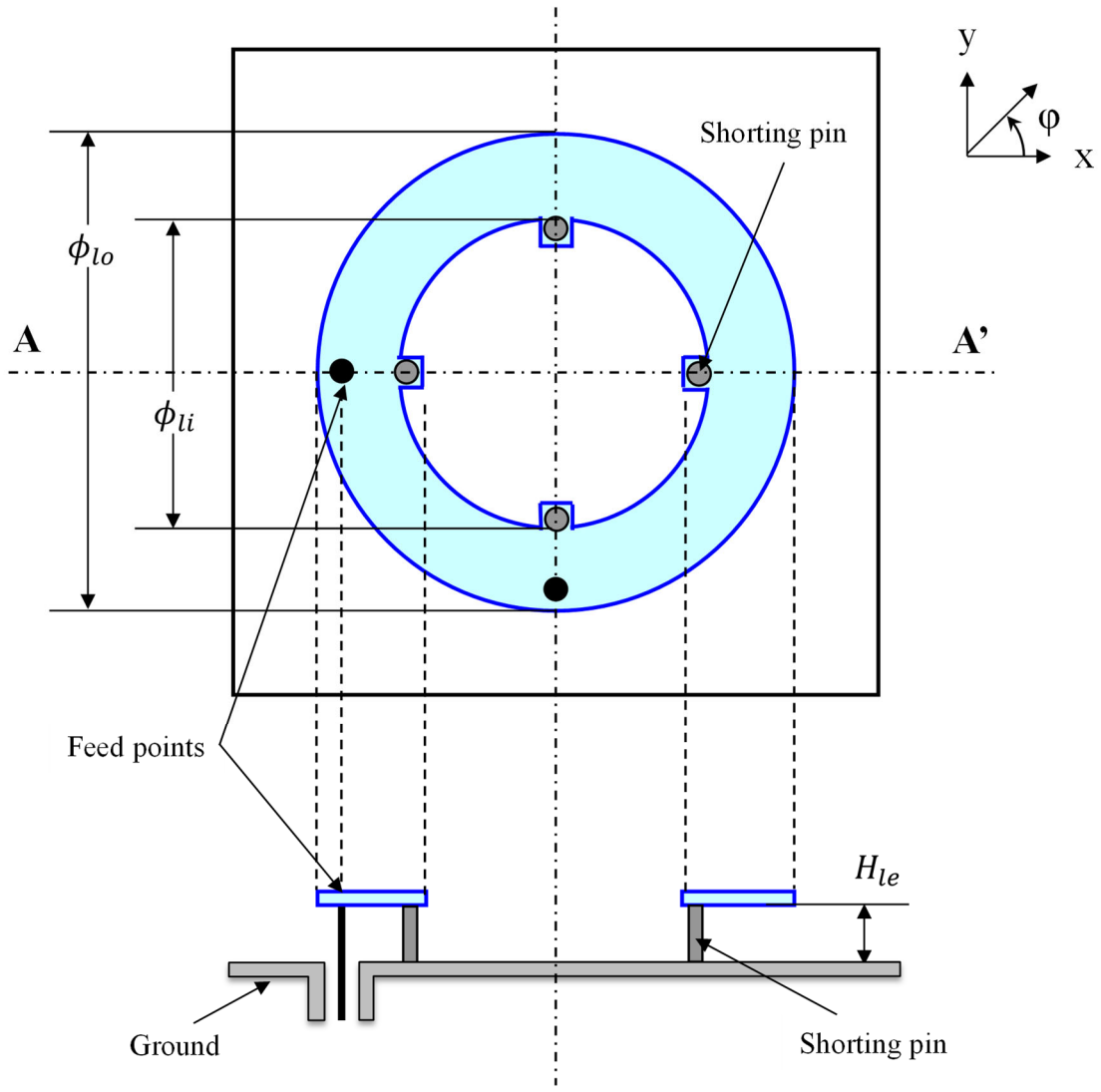

Fig. 4.2-1 Geometry of the proposed antenna.

(top and cross-sectional views along the A-A' line)

Herein, the internal electromagnetic field of microstrip antenna is written as follows[59]:

$$E_z = \sum_{n=0}^{\infty} f_n(k_1 r)\cos n\phi \tag{4.2-1}$$

$$H_\phi = \frac{-jk}{\omega\mu}\sum_{n=0}^{\infty} f'_n(k_1 r)\cos n\phi \tag{4.2-2}$$

$$f_n = \begin{cases} A_n J_n(k_1 r) + B_n Y_n(k_1 r) & (\phi_{li}/2 < r < d) \\ C_n J_n(k_1 r) + D_n Y_n(k_1 r) & (d < r < \phi_{lo}/2) \end{cases} \tag{4.2-3}$$

where d is the distance between the center and the feed point, k is the wave number, ω is the angular frequency, μ is the permeability in the air.

The field of the feeding pin can be expressed using the delta function as follows;

$$H_{\phi 1} - H_{\phi 2} = \frac{I_0 \delta(\phi)}{d} \tag{4.2-4}$$

subscripts 1 and 2 denote the two regions separated by the cylinder containing the feed probe at $r = d$. Since the outer edge is open state,

$$H_\phi = 0 \quad (r = \phi_{lo}/2) \tag{4.2-5}$$

The boundary conditions vary depending on the antenna type;

1) Ring antenna grounded at the inner edge

$$E_z = 0 \quad (r = \phi_{li}/2) \tag{4.2-6}$$

2) Ring antenna

$$H_\phi = 0 \tag{4.2-7}$$

3) Proposed antenna

The electromagnetic field including the shorting pins have not be derived. In this thesis, analysis and design was performed using an electromagnetic field simulator. In the future, the expression of the inner field will be derived from the theoretical equation for the shorting pin, which is described as follows [60] :

$$Z_p = \frac{\eta kd}{4}\left[1 - J_0^2(kl) + j\left\{\frac{2}{\pi}\ln\left(\frac{2}{\gamma k\delta}\right) + J_0(kl)N_0(kl)\right\}\right] \tag{4.2-8}$$

B. Eigenvalue and Electromagnetic Analysis Results

Here, the eigenvalue analysis results to confirm the aforementioned principle for the proposed antenna are presented. The commercial simulator HFSS based on the finite element method was used for this analysis.

In Fig. 4.2-2, three lines show the eigenvalue-based simulation results for the resonance frequency in the TM11 mode of the proposed antenna, the ring microstrip antenna, and the ring microstrip antenna grounded at the inner edge. After performing the eigenvalue analysis assuming the cavity model [61], the resonance frequency including the fringing effect was calculated [62]. The radiating element and the ground plane were assumed to be perfect conductor walls (short-circuit condition) and the outer edge was defined as a complete magnetic wall (open-circuit condition). The boundary conditions for the inner periphery were determined according to the type of antenna. For the inner edge of the ring microstrip antenna and of the ring microstrip antenna grounded at the inner edge, the perfect magnetic wall and the perfect conductor wall were applied, respectively. For the proposed antenna, the perfect conductor walls for the shorting pins and the perfect magnetic walls for the other parts are assigned to the inner edge, as depicted in Fig. 4.2-3.

As shown in Fig. 4.2-2, when the inner/outer diameter ratio increases, the resonance frequency of the ring microstrip antenna grounded at the inner edge increases sharply, whereas that of the ring microstrip antenna decreases.

Conversely, the resonance frequency of the proposed antenna remains almost constant even if the inner/outer diameter ratio changes, when the number and diameter of the shorting pins are 4 and 4 mm, respectively. In other words, the

resonance frequency of the proposed antenna does not increase, even when the inner diameter increases. Therefore, the overall size remains almost unchanged, even if other antennas or feeding networks are placed inside. This expands the usability of the ring microctrip antenna.

To validate the eigenvalue analysis models and their results, an electromagnetic analysis was performed for a single feed, single band, and the same condition (i.e., substrate, thickness, outer size) for three types of antennas that have no substrates, 1 mm height, and fed by a coaxial connector. The inner diameters were varied while the outer diameters were fixed. The resonance frequencies in the electromagnetic analysis were defined as the frequencies crossing the real axis in the Smith chart. The phase reference is located at the ground plane, and the effect of the feed pins is also considered. As shown in Fig. 4.2-2, the results of the eigenvalue and the electromagnetic analyses agree well, and the eigenvalue analysis models proved appropriate for each antenna. The difference between the two types of analyses is considered to result from the fact that the eigenvalue analysis does not consider the influence of the fringing effect of the inner circle and the reactance of the feed pins. Further, since the inner/outer diameter ratio of the proposed antenna increases and the feed pin approaches the shorting pin, the interaction between the two increases, which is difficult to include in the eigenvalue analysis.

Here, the electromagnetic field analysis results are shown for three inner/outer diameter ratio (0.2, 0.5, and 0.8). In Fig. 4.2-4, the surface current vectors are summarized to discuss the resonance frequencies of the ring antenna grounded at the inner edge, the ring antenna, and the proposed antenna. The black line indicates the current between the outer and inner edges, whereas the white line indicates the

current on the radiating conductor along the circumferential direction.

1) Ring antenna grounded at the inner edge

Since the inner circle is all short-circuited, the current flows between the outer and inner circles along the x-axis. As shown in Fig. 4.2-4, when the inner/outer diameter ratio is increased, the length of the current decreases, such that the resonance frequency increases. Note that weak currents on the right side of the antenna are observed due to poor antenna reflection characteristics with the inner/outer diameter ratio being 0.8.

2) Ring antenna

The ring antenna has an open inner circle, and the current is diverted along the radiating conductor, resulting in a low resonance frequency. As shown in Fig. 4.2-4, if the inner/outer diameter ratio is increased, the length of the current increases. Therefore, the resonance frequency decreases. Note that the amplitude of the surface current becomes strong near the short-circuited surface.

3) Proposed antenna

Due to the presence of the shorting pin near the feeding point, currents flow between the outer and inner circles, increasing the resonance frequency as in the ring grounded at the inner edge. However, because the shorting pins are discretely placed (unlike the ring antenna grounded at the inner edge), a surface current can be generated along the radiating conductor. The shorting pins that are orthogonal to the feeding point are located on the short-circuit plane of the microstrip antenna,

such that the surface current can exist along the radiation conductor, as in the ring antenna. This surface current contributes to a decrease in the resonance frequency. Therefore, the resonance frequency of the proposed antenna remains almost constant even when the inner/outer diameter ratio changes, as shown in Fig. 4.2-2.

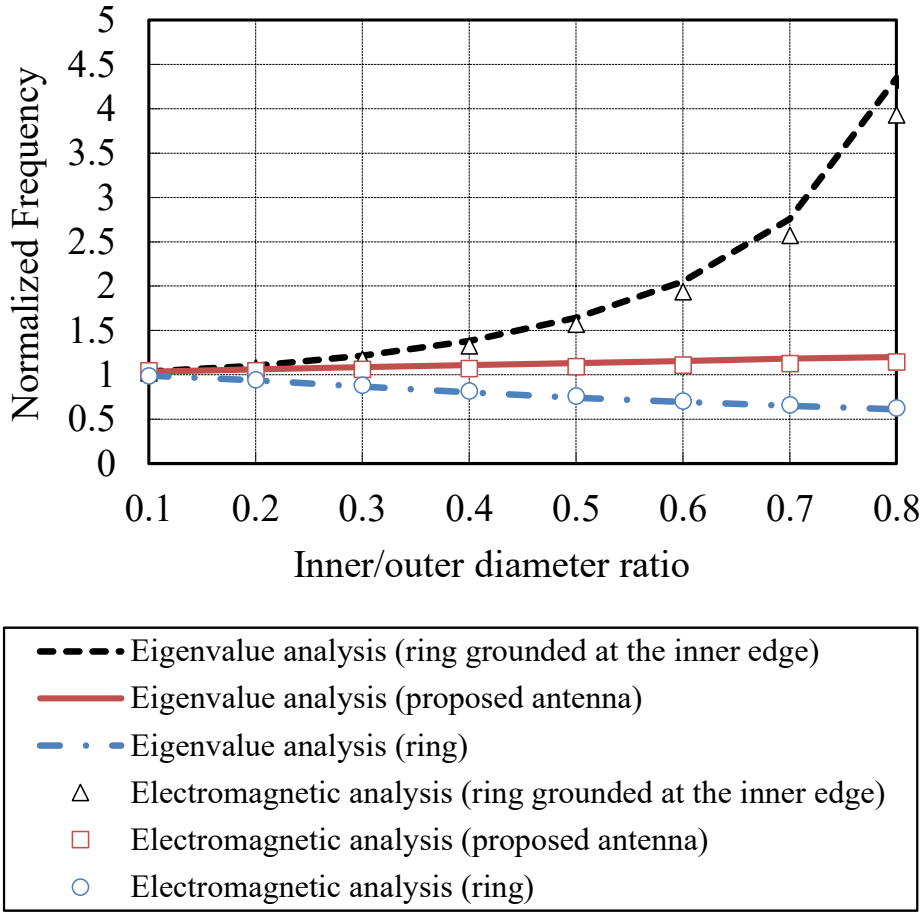

Fig. 4.2-2 Resonance frequency versus inner/outer diameter ratio. In the proposed antenna, the number and diameter of the shorting pins are 4 and 4 mm, respectively. All resonance frequencies are normalized by that of the circular microstrip antenna.

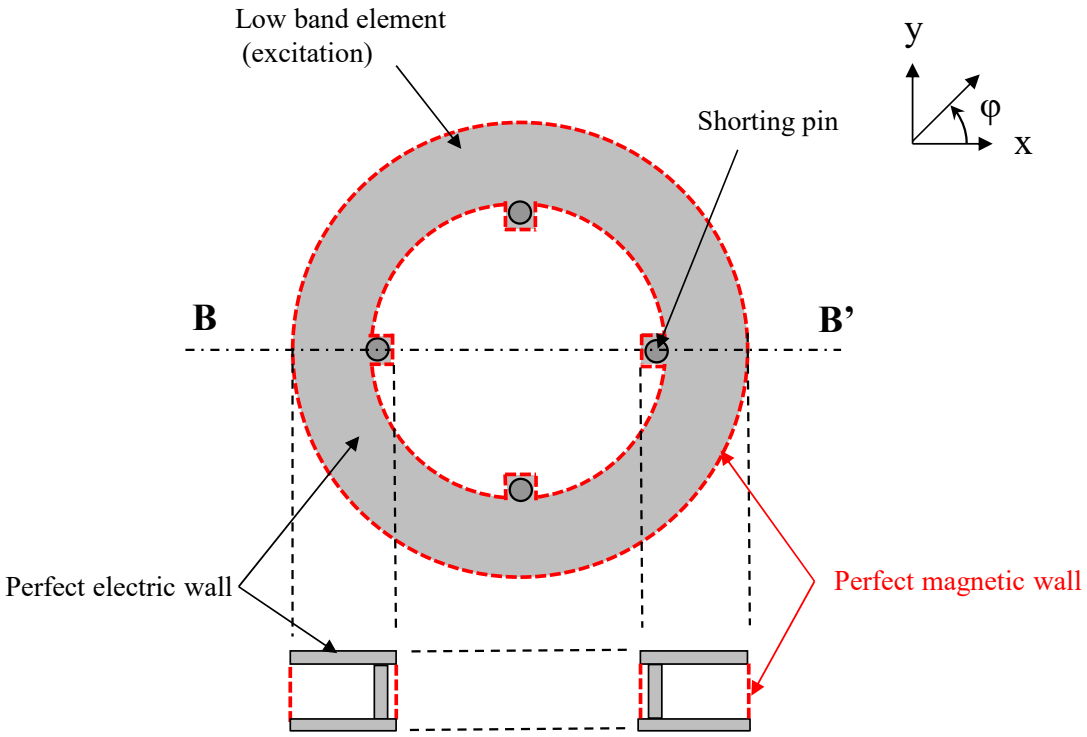

Fig. 4.2-3 Eigenvalue analysis model for the proposed antenna. (Top and cross-sectional views along the B-B' line)

	Ratio=0.2	Ratio=0.5	Ratio=0.8
Ring antenna grounded at the inner edge	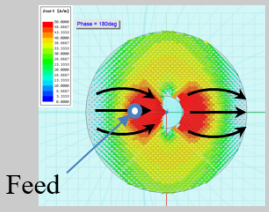	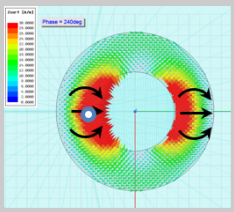	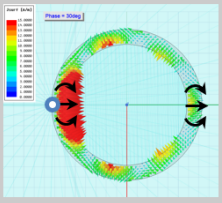
Ring antenna	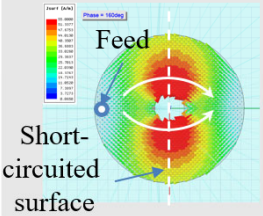	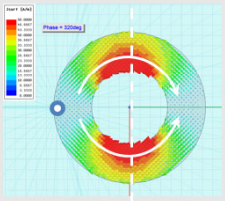	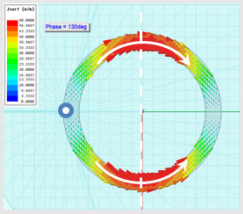
Proposed antenna	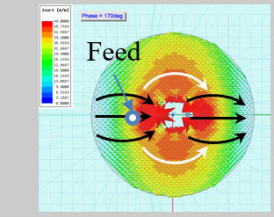	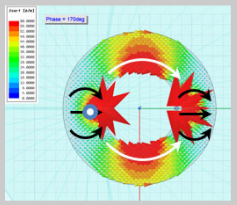	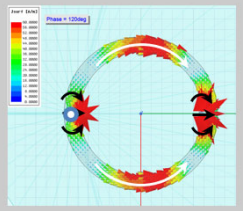

Fig. 4.2-4 Electromagnetic field analysis results for the surface current vectors of three types of antennas for various inner/outer diameter ratios: black lines indicate currents between the outer and inner circles, whereas white lines indicate currents along the radiating conductor.

C. Detailed analysis of the proposed antenna

The proposed antenna is flexible in terms of the number, installation angle, and diameter of the short-circuit pins. The installation angle is defined as the angle by which one shorting pin is rotated under the condition that two shorting pins are placed at opposite positions.

In this section, by adjusting these parameters, the condition that the resonance frequency becomes constant even under changes to the inner/outer diameter ratio is discussed.

1) Four shorting pins

Fig. 4.2-5 summarizes analytical results for the surface current magnitude of the proposed antenna, when the number of shorting pins is four and the inner/outer diameter ratio is 0.5.

(i) Adjustment by the installation angle of the shorting pins

In Case 1, the shorting pins are 90° apart, and the feeding point and shorting pin are placed close to one another. In Case 2, all the shorting pins are rotated by 45° from the Case-1 configuration. Both cases exhibit the same resonance frequency; this is because the resonant frequency of the microstrip antenna is specified by the shape of the radiation conductor. As shown in Case 3, changing the positions of the four shorting pins increases the resonance frequency. The current distribution in Fig. 4.2-5 shows that the current increased when the shorting pins were densely placed and a behavior is similar to that of a ring antenna grounded at the inner edge, as

shown in Fig. 4.2-4.

(ii) Adjustment of the shorting-pin diameter

The analytical results for the case with four shorting pins under variation of the pin diameter are discussed. In Case 4, the resonance frequency is the same as that of the circular microstrip antenna when the shorting-pin diameter changes from 4 mm to 0.7 mm. In Case 5, the diameter of the shorting pin is further reduced to 0.4 mm, which is lower than the resonance frequency of the circular microstrip antenna.

2) Two shorting pins

Fig. 4.2-6 summarizes the analytical results of the surface-current-magnitude results for the proposed antenna, when the number of shorting pins is two and the inner/outer diameter ratio is 0.5.

(i) Adjustment of the installation angle of shorting pins

First, the result when the two shorting pins are placed facing one another and rotated in the circumferential direction is discussed. In Cases 6 and 7, the shorting pins are set in the horizontal direction and at 45°, respectively. Both cases have the same resonance frequency, as with Cases 1 and 2. Although the direction of E-plane rotates according to the shorting-pin position, the desired polarization plane can be obtained by rotating the antenna itself.

Next, the analytical results under changes to the installation angle of the shorting pin are discussed. The position of the shorting pin near the feeding point is fixed, whereas the other shorting pin is rotated counterclockwise. As shown in Case 8, the

resonance frequency is the same as that of the circular microstrip antenna for an installation angle of 50°. When the installation angle is 90°, two modes are generated, as depicted in Case 9 and 9'. Herein, Fig. 4.2-7 shows the resonance frequency of each mode when the installation angle is changed. Only mode #1 is generated up to 75°, whereas mode #2 appears for larger installation angle. When the installation angle is set to 50° (85°), the resonance frequency is approximately the same as that of the circular microstrip antenna with respect to mode #1 (#2) even if the inner/outer diameter ratio is changed.

(ii) Adjustment by the shorting-pin diameter

As shown in Case 10 in Fig. 4.2-6, when the installation angle is 0° and the diameter of the shorting pin is gradually reduced from 2 mm, the resonance frequency becomes equivalent to the circular microstrip antenna of diameter 0.8 mm.

Finally, an analysis is performed when the inner/outer diameter ratio is changed from 0.2 to 0.8 for Cases 4, 8, and 10 with resonance frequencies being the same as that of the circular microstrip antenna. The resonance frequency difference between the proposed antennas listed in Table 4.2-1 and the circular microstrip antenna is less than 6%. Therefore, even if the inner/outer diameter ratio changes, the resonance frequency of the proposed antenna remains constant for Cases 4, 8, and 10.

Based on these analyses, it is found that the resonance frequency of the proposed antenna can be controlled by changing the installation angle and diameter of the shorting pins. This offers us a DOF for improving the frequency operation of ring microctrip antennas.

	Case 1	Case 2	Case 3	Case 4	Case 5
Surface current	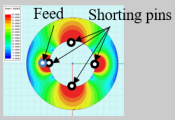	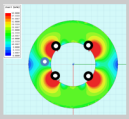	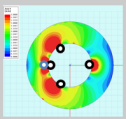	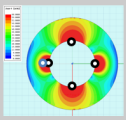	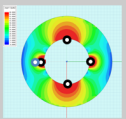
Number of shorting pins	4	4	4	4	4
Diameter of shorting pins	2mm	2mm	2mm	0.7mm	0.4mm
Normalized resonance frequency	1.09	1.09	1.20	1.00	0.98

Fig. 4.2-5 The analytical results of the surface current magnitude of the proposed antenna. The number of shorting pins is four, and the inner/outer diameter ratio is 0.5. All resonance frequencies are normalized by the resonance frequency of the circular microstrip antenna.

	Case 6	Case 7	Case 8	Case9	Case9'	Case10
Surface current	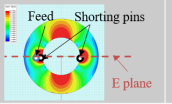	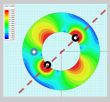			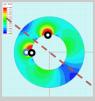	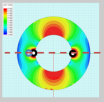
Number of shorting pins	2	2	2	2	2	2
Diameter of shorting pins	2mm	2mm	2mm	2mm	2mm	0.8mm
Installation angle	0deg.	0deg.	50deg.	90deg.	90deg.	0deg.
Normalized resonance frequency	1.09	1.09	1.00	0.90	1.02	1.00

Fig. 4.2-6 The analytical surface-current-magnitude results for the proposed antenna. The number of shorting pins is two, and the inner/outer diameter ratio is 0.5. All resonance frequencies are normalized by the resonance frequency of the circular microstrip antenna.

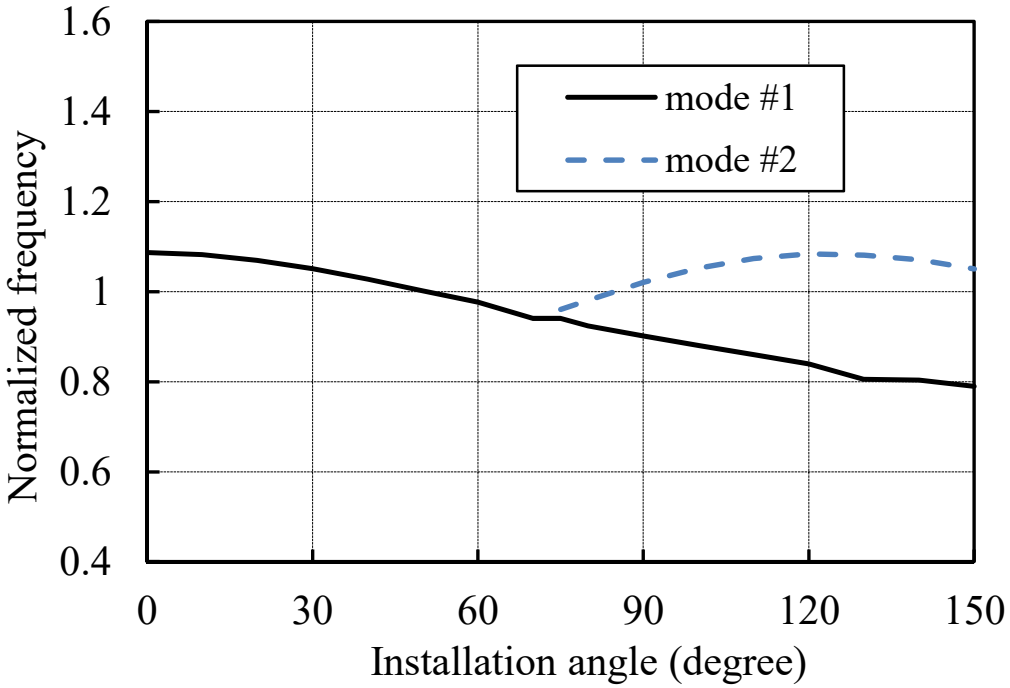

Fig. 4.2-7 Simulated resonance frequency of Case 9 and 9' in Fig. 4.2-6 : the number of shorting pins is two, the inner/outer diameter ratio is 0.5, and the installation angle of shorting pins is 50°. All resonance frequencies are normalized by the resonance frequency of the circular microstrip antenna.

Table 4.2-1 Normalized resonance frequencies with respect to the inner/outer diameter ratio in the proposed antenna. The numbers of cases correspond to those in Fig. 4.2-5 and Fig. 4.2-6.

Inner/outer diameter ratio	Case 4	Case 8	Case 10
0.2	1.01	1.02	1.01
0.5	1.00	1.00	1.00
0.8	1.05	0.94	1.05

4.3. Dual-band circularly polarized antenna

In this section, the design procedure and designed/ measurement results of the dual-band circularly polarized antenna using the proposed antenna are shown. The operating frequencies are L5 (1176.45 ± 13 MHz), L2 (1227.60 ± 16 MHz), L6 (1278.75 ± 21 MHz), and L1 (1575.42 ± 16 MHz), as used in the Japanese satellite positioning system Quasi-Zenith Satellite System (QZSS) [63]. Herein, a dual-band antenna with L5, L2, and L6 as the low band and L1 as the high band is designed.

A. Geometry

The geometrical configuration of the dual-band circularly polarized antenna is shown in Fig. 4.3-1 [56][58], in which the proposed antenna as a low band element encloses the high band element.

In Section 4.2, it is found that the resonance frequency can be controlled by the number, installation angle, and diameter of shorting pins. Herein, four pins are used from the viewpoint of symmetry. Further, the outer diameter of the shorting pins is chosen to be 4 mm from the viewpoint of manufacturability. A two-point feed microstrip antenna with a parasitic element is adopted, because the relative bandwidth of the low band is as wide as 11.1%. Two stubs are installed on the outer periphery of the low band element to cancel the reactance of the feeding pins[64][65].

Meanwhile, since the relative bandwidth of the high band is as narrow as 2.0%, the

high band element has only one feeding point and two notches, which are etched upon the outer edge to generate the orthogonal mode. A ring microstrip antenna is also adopted for the high band element to achieve miniaturization, and the open stub is attached to the inner edge for impedance matching [66]. The high band element is located between the first and the second layer of the low band element to extend the bandwidth of the high band element. Dielectric spacers support all the radiating conductors, as shown in Fig. 4.3-1.

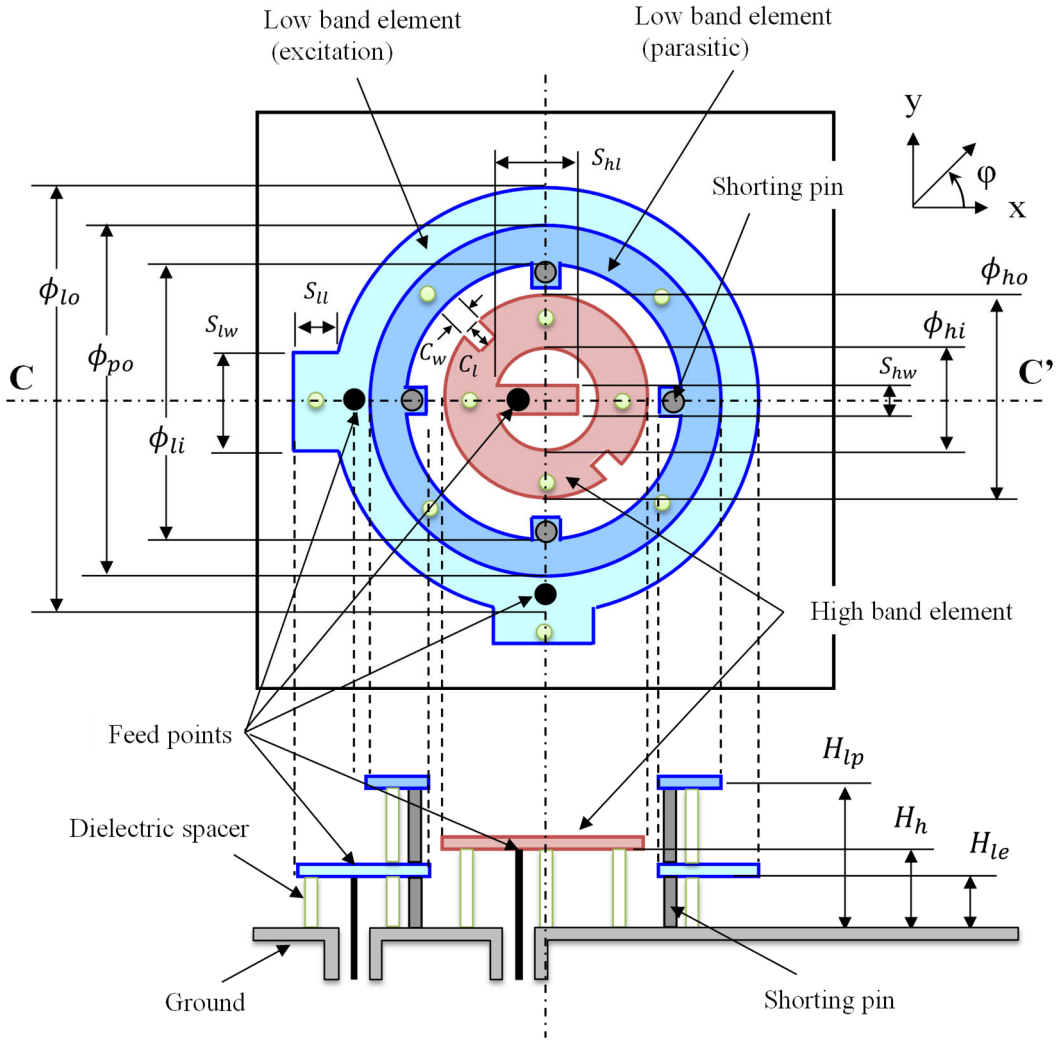

Fig. 4.3-1 A dual-band circular polarized antenna using the proposed antenna as a low-band element (top and cross-section view along C-C' line.

B. Design Procedure

Fig. 4.3-2 shows the design flow for a dual-band circularly polarized antenna using the proposed antenna as a low-band element. After the initial design is completed using eigenvalue analysis, a detailed design procedure is performed using full-wave analysis.

First, the design frequencies for the low band and high bands (F_l, F_h) are given and the heights of the excitation elements in these respective bands (H_l, H_h) are set. Thereafter, the number and diameter of the shorting pins (N_s, ϕ_s) are set provisionally. The inner and outer diameters of the low band excitation element and the high band (ϕ_{li}, ϕ_{lo}, ϕ_{hi}, ϕ_{ho}) are derived via eigenvalue analysis, such that the resonance frequencies are equal to F_l and F_h, respectively. If you find a combination of parameters for which the inner diameter of the low band is greater than the outer diameter of the high band ($\phi_{ho} < \phi_{li}$), full-wave analysis is then performed. Note that the diameters of these elements are restricted to avoid physical interference between them. For the low band element, the height (H_p) and inner/outer diameter ratio of the parasitic element (ϕ_{pi}, ϕ_{po}) were designed to achieve $S_{11} < -10\,\mathrm{dB}$, similar to what is found in an ordinary stacked microstrip antenna. Then, the capacitive stub (S_{ll}, S_{lw}) and the feeding pin position (D_l) are adjusted for impedance matching.

For the high band element, the length and width of the two notches on the outer edge (C_l, C_w) are selected to generate right-hand circularly polarization. For impedance matching purposes, the length and the width of the open stub (S_{hl}, S_{hw})

and the probe position of the feeding pin (D_h) are optimized.

If the low band element does not satisfy S_{11}<−10 dB, the eigenvalue analysis is conducted again with a lower inner/outer diameter ratio, so as to broaden the bandwidth of the low band element. As the inner circle of the low band becomes small, the inner/outer diameter ratio of the high band element must be increased to reduce the size of the high band element. By contrast, if the high band element does not satisfy requirements, the inner/outer diameter ratio of the high band element needs to be reduced to broaden the bandwidth. Because the outer circle of the high band element becomes larger, the number or diameter of the shorting pins and the inner/outer diameter ratio of the low band element must be adjusted to avoid a physical interference with the inner circle of the low band element. If the operating bandwidth still does not satisfy requirements, the design needs to be repeated from the beginning with the height of the low and/or high band element increased.

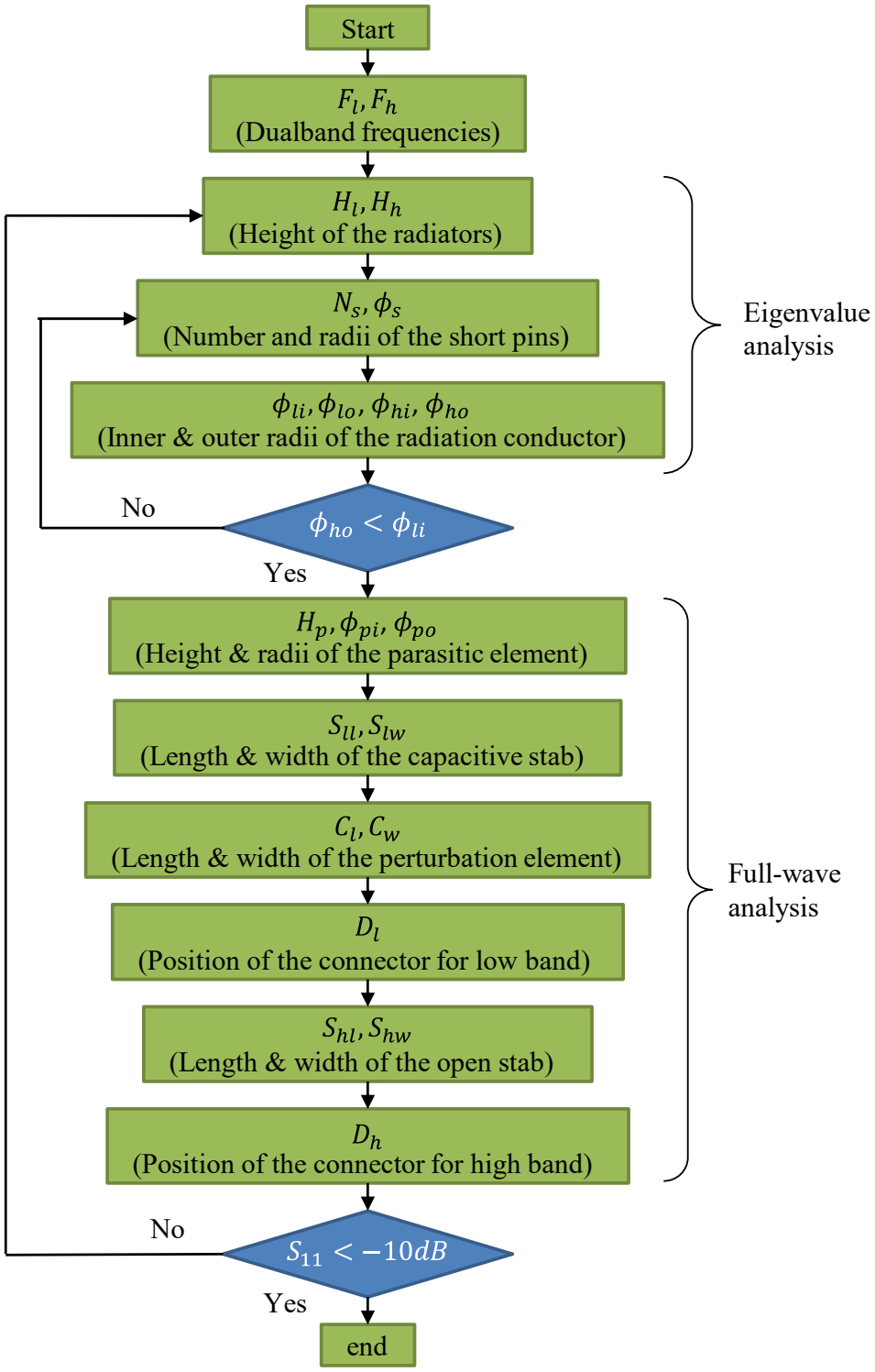

Fig. 4.3-2 Design flow for a dual-band circularly polarized antenna using the proposed antenna as a low-band element.

C. Designed and Measured Results

The designed and experimentally measured results of the proposed antenna element are now discussed. A prototypical picture of the proposed antenna is shown in Fig. 4.3-3. The radiating conductors of both frequency bands and the shorting pins are made of aluminum. The designed dimensions are as listed in Table 4.3-1. The relative permittivity and dielectric loss tangent of the dielectric spacer were 4.3 and 0.009, respectively, while the outer diameter of the dielectric spacer was 0.05λ_c. Note that the proposed antenna can be connected directly to a 50-Ω feed circuit without any impedance matching circuit, whereas the input impedance of the ring antenna with the same inner/outer diameter is around 800Ω, which requires an additional impedance matching circuit.

Fig. 4.3-4 shows the simulated and measured results of the reflection coefficient. The results were closely matched. The measured bandwidths with S11<−10 dB are 16.0% (15.0%, designed) and 8.4% (7.4%, designed) for the low and high band elements, respectively. The frequency characteristic of the measured result is slightly higher than that of the designed result because of the error due to the spacer's relative permittivity.

Fig. 4.3-5 and Fig. 4.3-6 show the simulated and measured results of the radiation pattern. The measured results for co-polarization and cross-polarization show good agreement with the design results. Because the outer diameter of the low band element was 0.69 λ_c, the magnetic current sources contributing to radiation were separated by more than half the wavelength, such that the pattern shape obtained was similar to that of a two-element array.

Fig. 4.3-7 shows that good correlation was found between the simulated and measured results for the axial ratios of both bands. The measured relative bandwidths for an axial ratio < 3 dB are 15.2% (16.7%, designed) and 1.6% (1.3%, designed) for the low band and high band elements, respectively. Fig. 4.3-8 shows the designed and measured results of the actual gain versus frequency. For both bands, the results obtained show good agreement with a difference of 0.5 dB or less. The above evaluation results confirm the validity of the design, as well as the effectiveness of the proposed antenna.

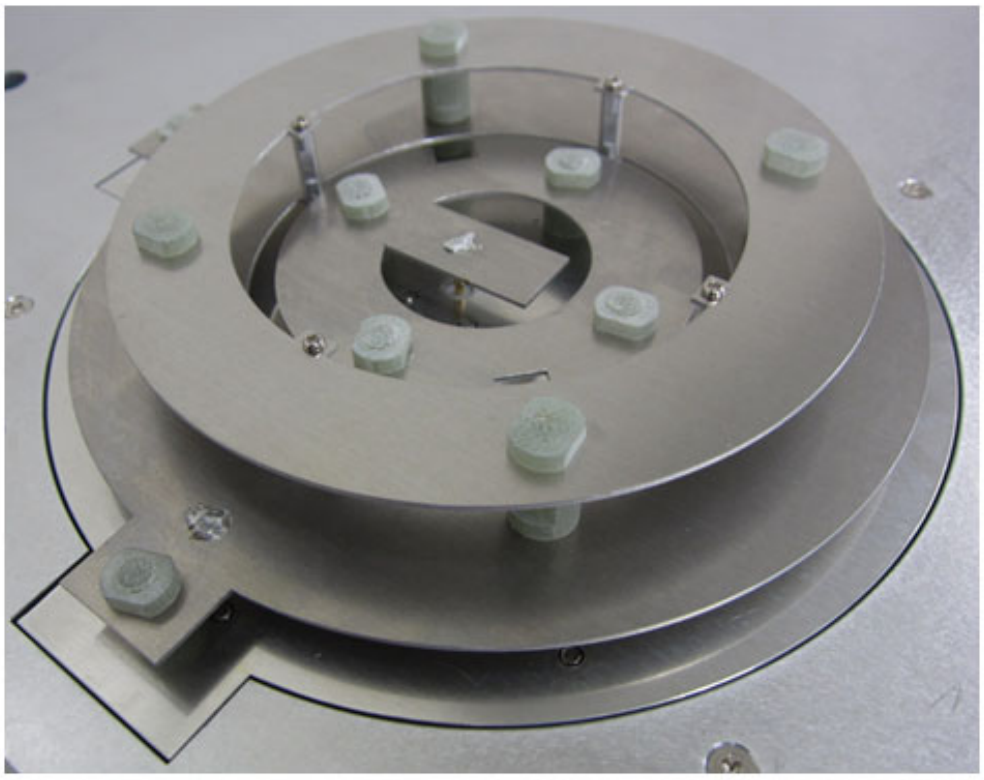

Fig. 4.3-3 Manufactured antenna element.

Table 4.3-1 Parameters normalized by the central-frequency wavelength of the whole band (1.377 GHz)

Category	Item	Value	Explanation
Low band excitation element	ϕ_{li}	0.40	Inner diameter
	ϕ_{lo}	0.69	Outer diameter
	$r_l = \phi_{li}/\phi_{lo}$	0.58	Inner/outer diameter ratio
	H_l	0.02	Height
	ϕ_s	0.02	Diameter of the shorting pins
Low band parasitic element	ϕ_{pi}	0.40	Inner diameter
	ϕ_{po}	0.59	Outer diameter
	H_p	0.06	Height
High band element	ϕ_{hi}	0.18	Inner diameter
	ϕ_{ho}	0.35	Outer diameter
	$r_h = \phi_{hi}/\phi_{ho}$	0.50	Inner/outer diameter ratio
	H_h	0.05	Height

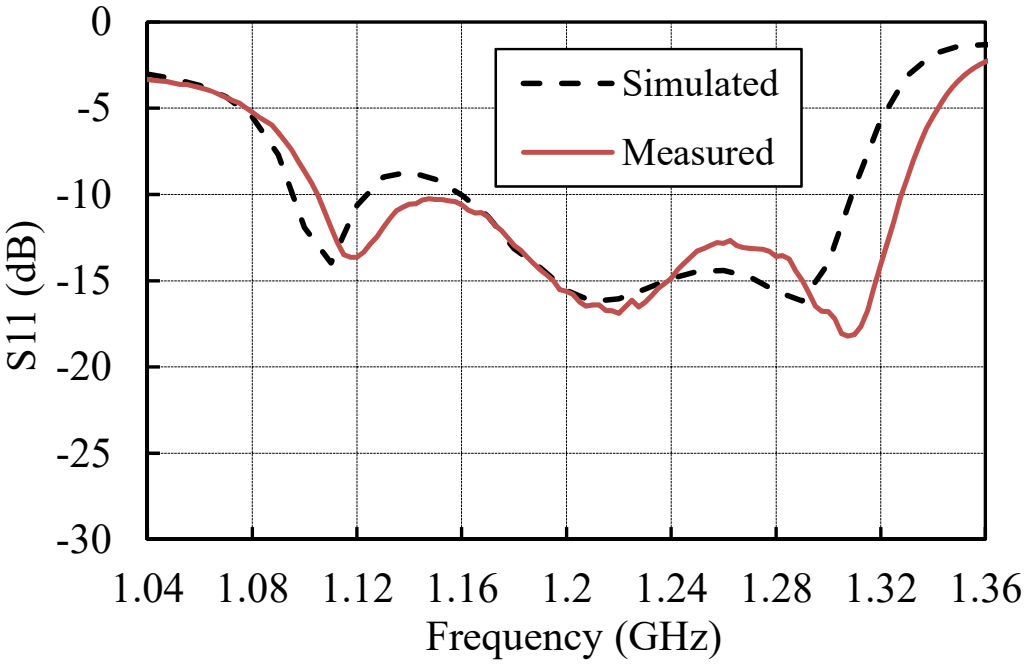

(a)

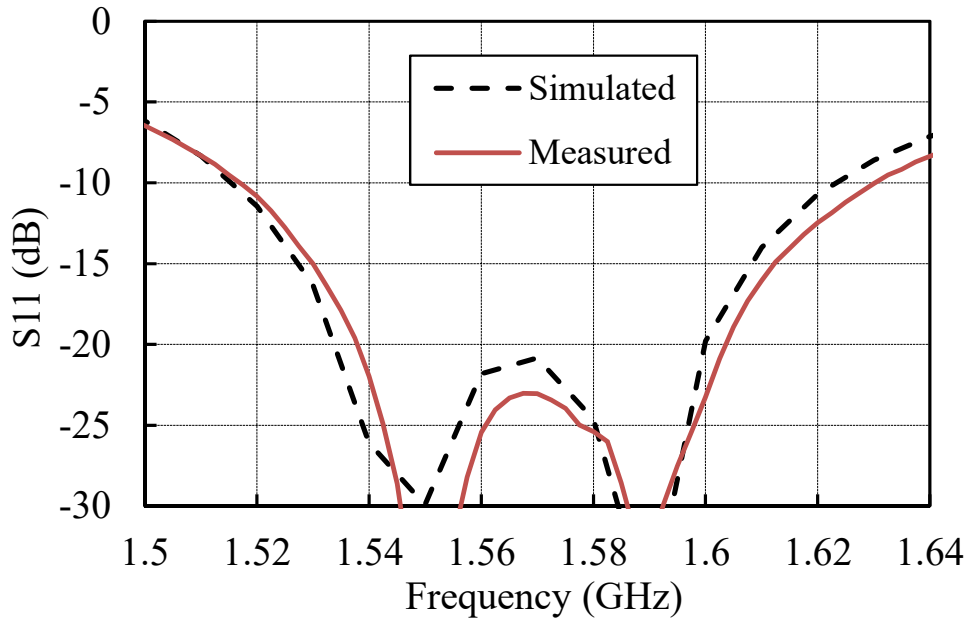

(b)

Fig. 4.3-4. Simulated and measurement reflection coefficient:

(a) low band and (b) high band.

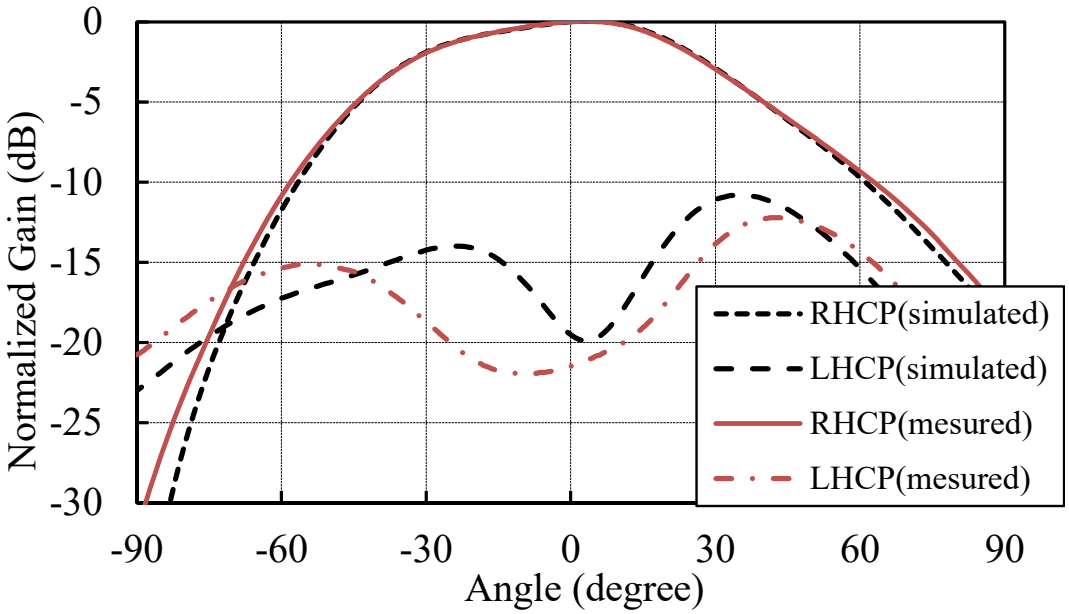

(a)

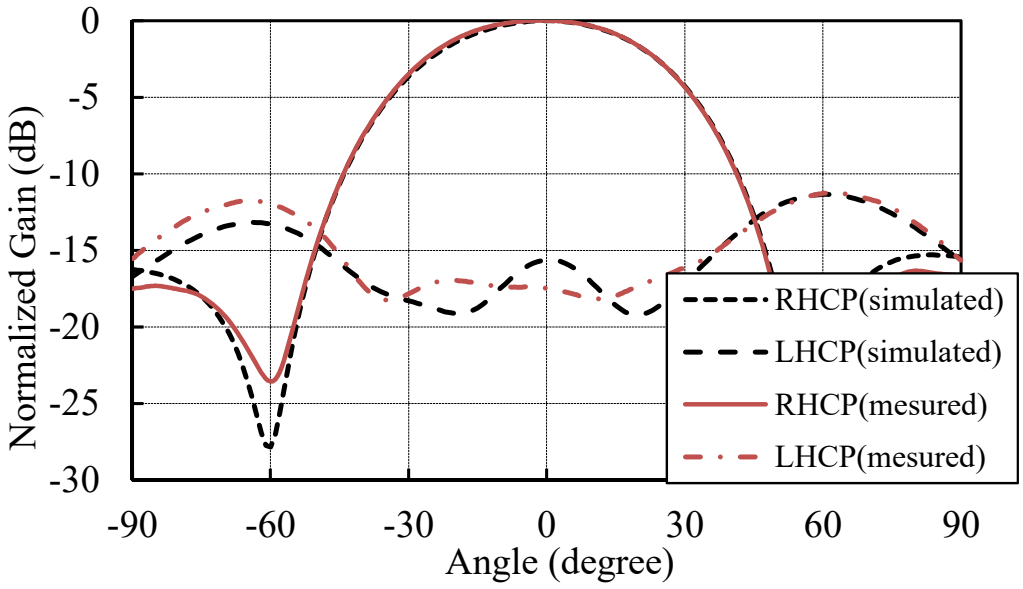

(d)

Fig. 4.3-5 Element pattern in the xz cut plane at the center frequency of (a) L5 (b) L2

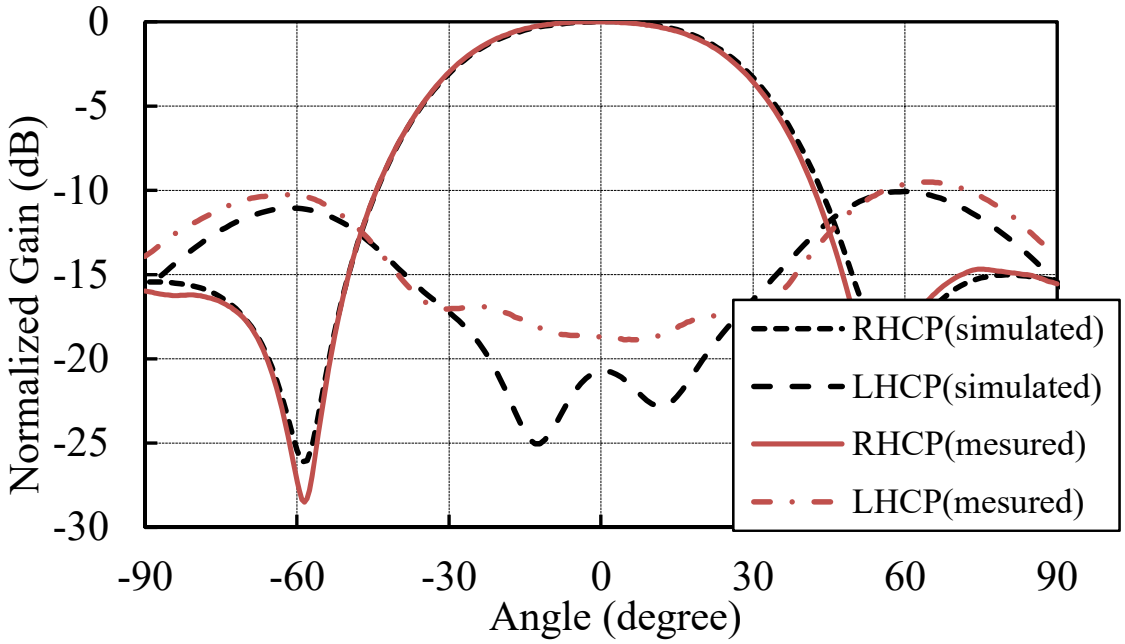

(a)

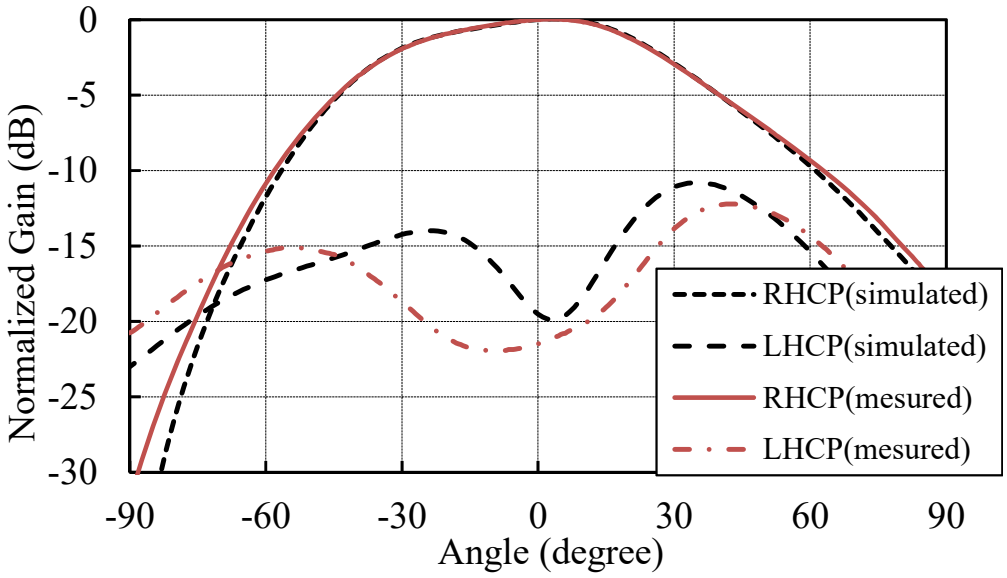

(b)

Fig. 4.3-6 Element pattern in the xz cut plane at the center frequency of (a) L6 (b) L1.

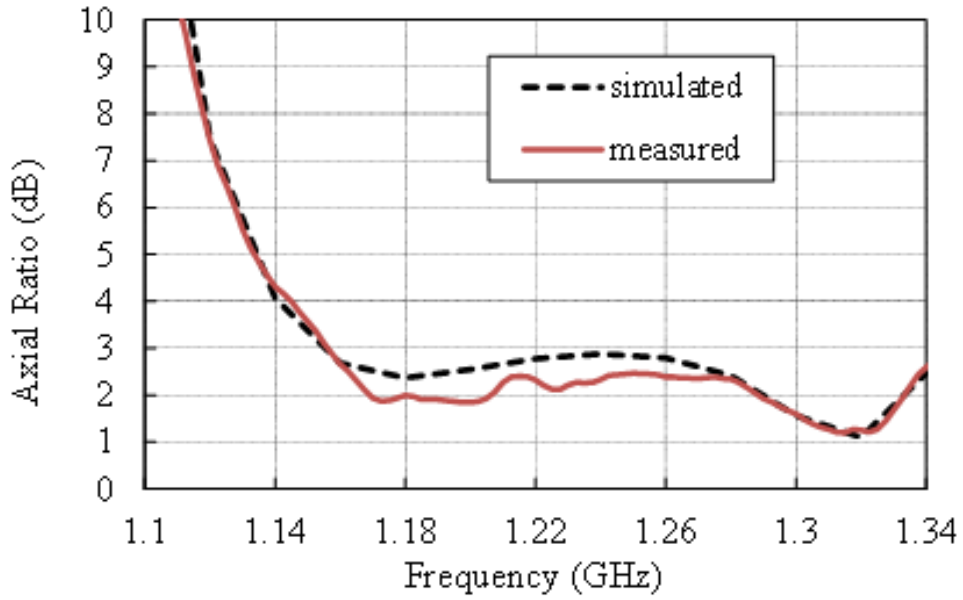

(a)

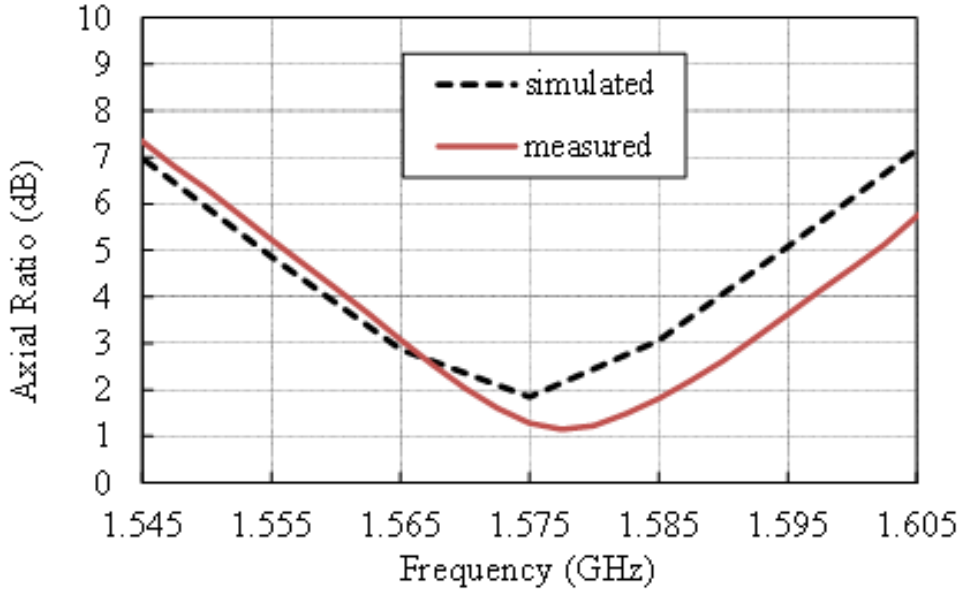

(b)

Fig. 4.3-7 Axial ratio versus frequency: (a) low band and (b) high band.

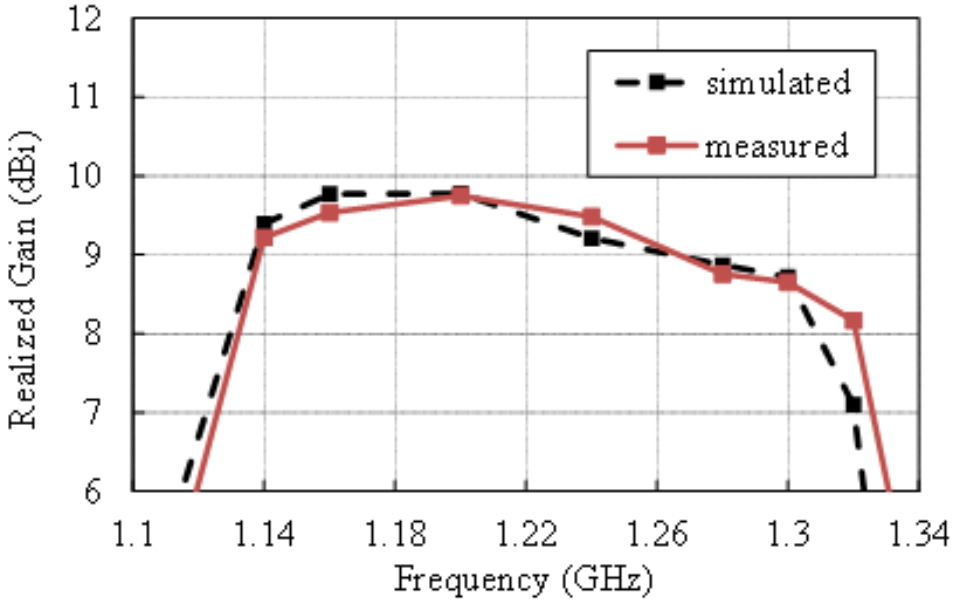

(a)

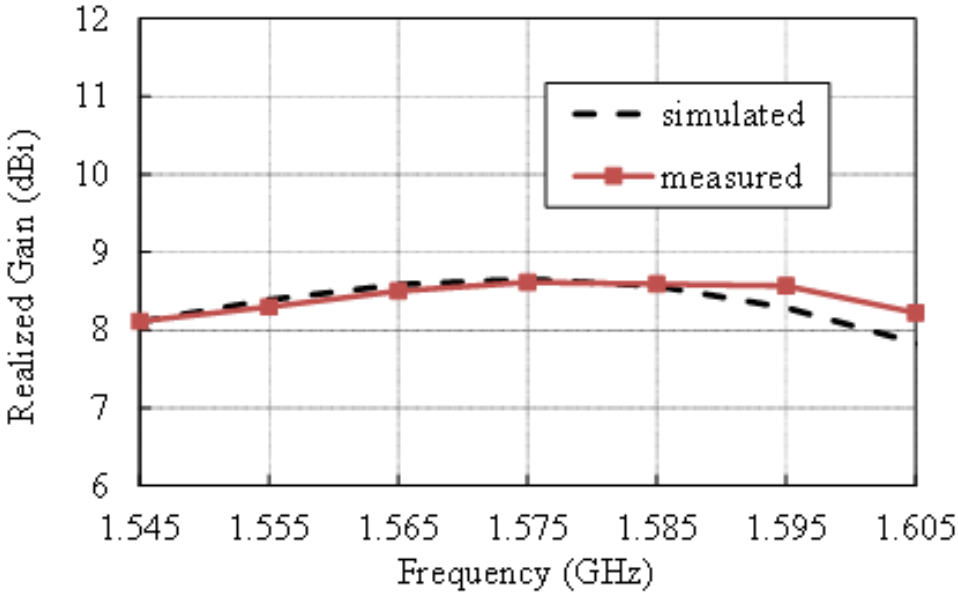

(b)

Fig. 4.3-8 Actual gain versus frequency: (a) low band (b) high band.

Table 4.3-2 shows the benchmark of dual band microstrip antennas. It was confirmed that the footprint of the proposed antenna is smaller than that of other methods. The low-band bandwidth is wider due to the parasitic element.

Table 4.3-2 Benchmark of dual band microstrip antennas

Ref.	Footprint λ_L^2	Dielectric constant	Band width (%)(*) (low and high band)	Antenna gains (dBi) (low and high band)
[68]	0.57x0.57	4.5	2.0, 2.0	6, 7
[69]	0.62x0.62	1.0	3.2, 3.1	8, 7.5
Proposed	0.56x0.56	1.0	13.9, 1.6	8.7, 8.4

* BWs are overlapped bandwidths for 3 dB axial ratio and -10 dB of reflection coefficient.

4.4. The test results of the array

In this section, the test results of the proto flight model of the satellite positioning system QZSS are presented[58].

4.4.1. Aperture design

A mask pattern for uniform irradiation within the global viewing angle is defined for the satellite used in this system.

Assuming a rectangular beam that satisfies the mask pattern, the ideal excitation distribution is calculated. Considering that the flat-top pattern is generated by a two-dimensional array, the ideal excitation distribution f(r) is expressed as the following equation.

$$f(r) = 2\frac{J_1(u)}{u} \tag{4.4.1-1}$$

$$u = kr\sin\theta_h \tag{4.4.1-2}$$

where r is the distance from the center, k is the wave number, θ_h is the beam width.

The initial excitation distribution determined on the conditions;

- ✓ Distances between the innermost elements should be set as more than half of wavelength so that the antennas can be placed.
- ✓ The position of the elements should be the same in all bands.

- ✓ The number of elements is set to be a multiple of four so that the feed circuit has a symmetrical shape.
- ✓ The amplitude density ratio was made as uniform as possible between the high and low bands.

The excitation distribution and element positions are designed using a nonlinear optimization method with gain in the mask as the constraint.

An amplitude distribution is formed by the unequal divided power feeding network using a layout in which concentric circular elements are arranged to obtain a convex radiation pattern with small variations for each cut plane. An accurate radiation pattern can be made using a 20-element array that is fed by two independent beam-forming networks whose excitation coefficients are designed for each band as shown in Table 4.4.1-1 and Table 4.4.1-2.

As shown in Fig. 4.4.1-4, the array antenna consists of three rings. Four elements are placed at ϕ=240mm, eight elements at ϕ=600 mm, and eight elements at ϕ=1200 mm. The beam-forming network is made of a hollow rectangular coaxial line that is small and lightweight and having low loss. Owing to the low-profile antenna and the beam-forming network, thin RF front ends in which the whole thickness of the radiating part and the feeding part is approximately 350 mm are realized.

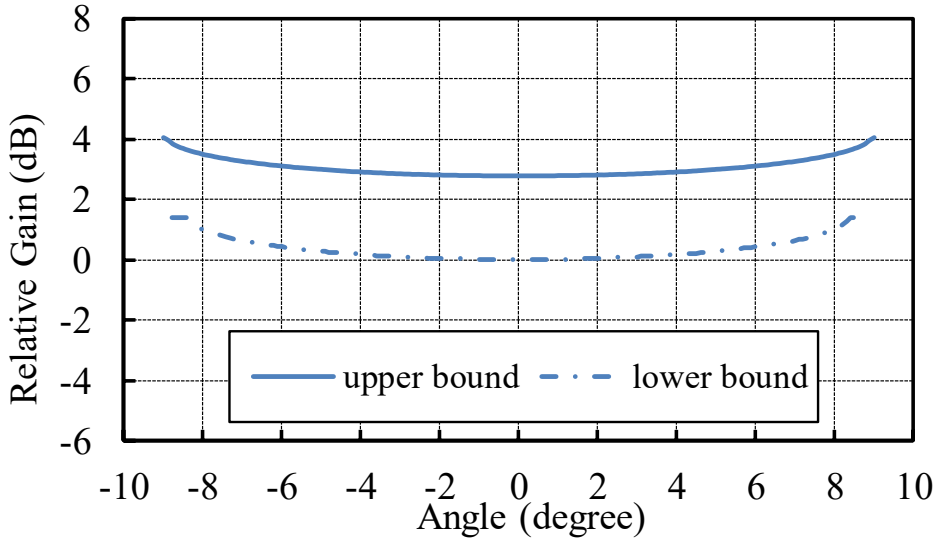

Fig. 4.4.1-1 Mask pattern

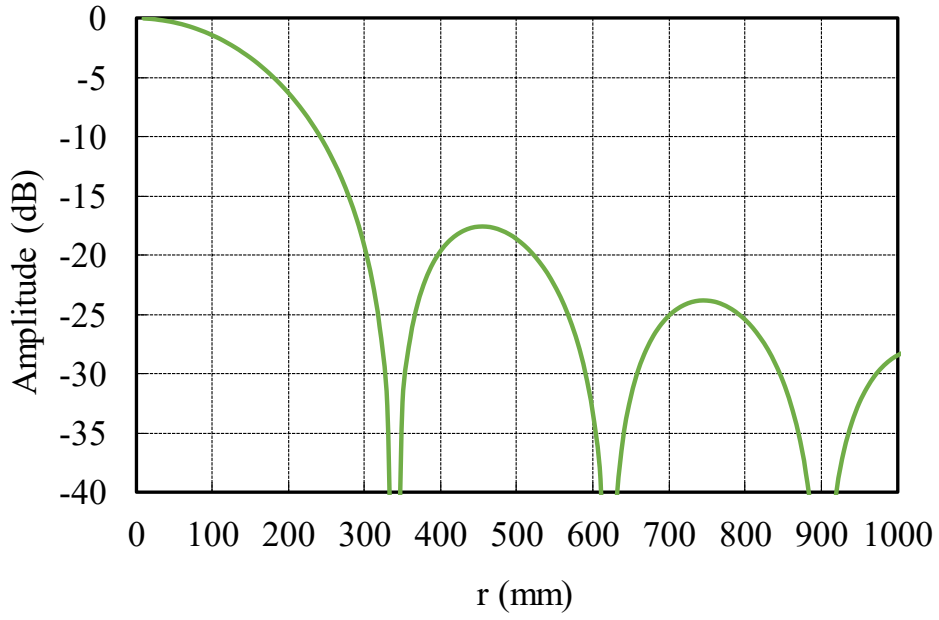

Fig. 4.4.1-2 Excitation distribution required for rectangular beam

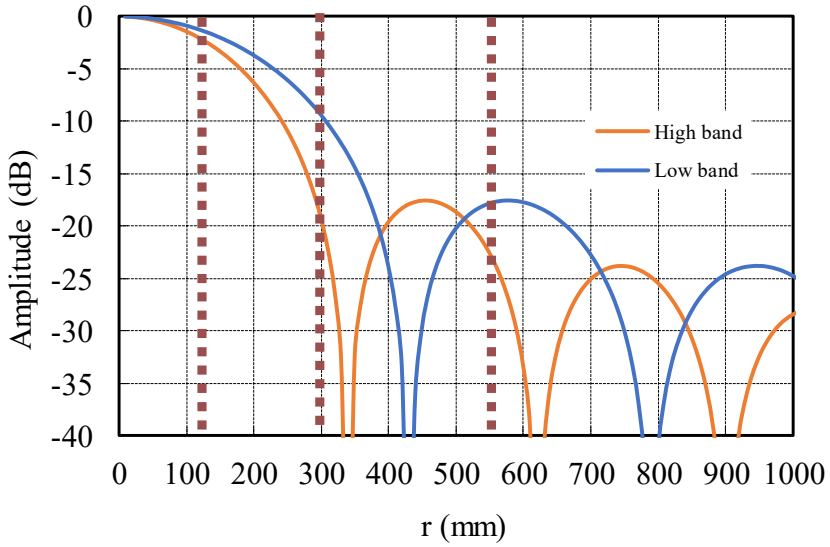

Fig. 4.4.1-3 Initial excitation distribution

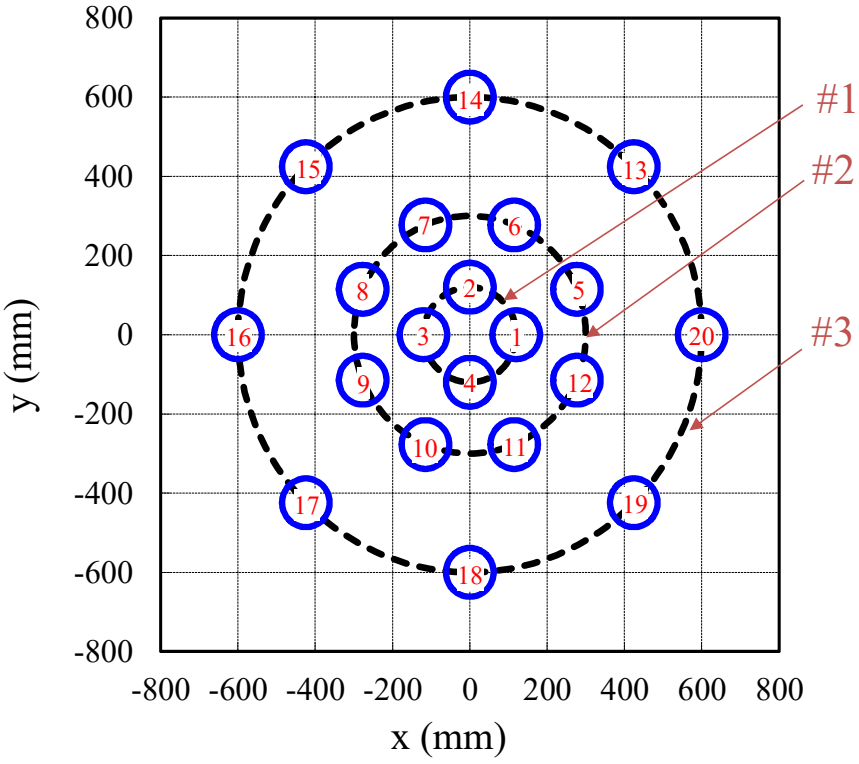

Fig. 4.4.1-4 Array arrangement

Table 4.4.1-1 Ideal excitation distribution for the low band

Circular Number	Amplitude (dB)	Phase (deg.)
#1	0	0
#2	-4	0
#3	-13	180

Table 4.4.1-2 Ideal excitation distribution for the high band

Circular Number	Amplitude (dB)	Phase (deg.)
#1	0	0
#2	-6	0
#3	-11	180

4.4.2. Proto flight model test results

The proto flight model unit is illustrated in Fig. 4.4.2-1. The reflection characteristics including the beam-forming network are shown in Fig. 4.4.2-2 and Fig. 4.4.2-3. Although the measured results slightly shifted toward the higher frequency, they have good agreement with the simulated results. As shown in Fig. 4.4.2-4 and Fig. 4.4.2-5, there is a high degree of agreement between the designed and measured radiation pattern results. Beams suitable for the coverage which the upper and lower bounds are close can be formed, and they satisfy the requirement in all frequency bands. The simulated and measured results corresponded well in each frequency band, indicating that the proposed design is adequate. The efficiencies of the antenna containing the feeding circuit in L5, L2, L6, and L1 are 73.1% (design value: 72.1%), 82.0% (design value: 83.8%), 78.3% (design value: 77.1%), and 85.5% (design value: 82.8%), respectively.

A Quasi-Zenith Satellite Unit 3 equipped with this antenna array was successfully launched and was put in the geostationary orbit [63]. A centimeter level augmentation service using QZSS was surveying, intelligent construction, and e-agriculture.

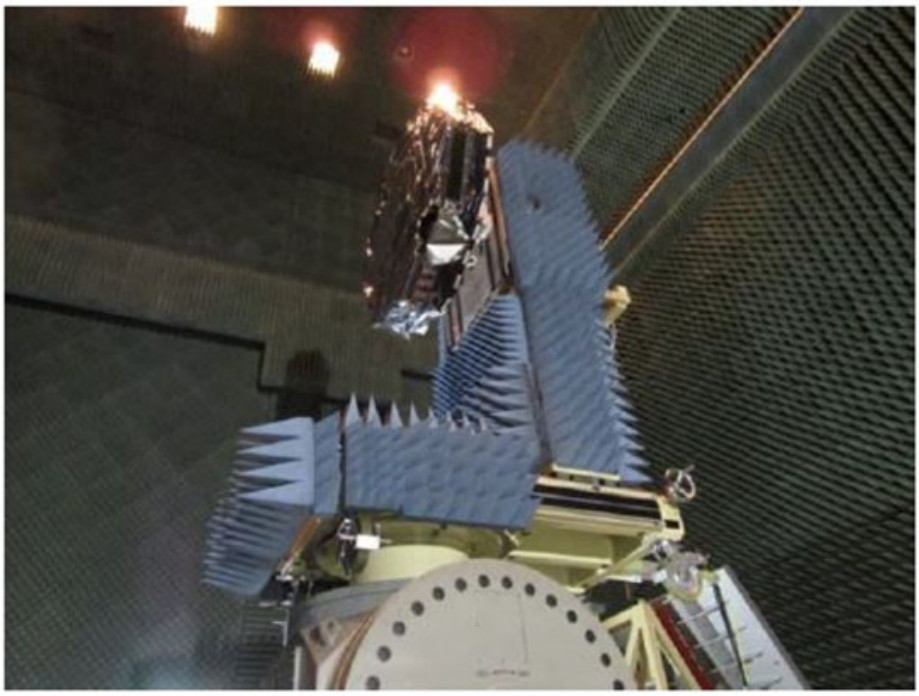

Fig. 4.4.2-1 Measurement setup for proto flight model test.

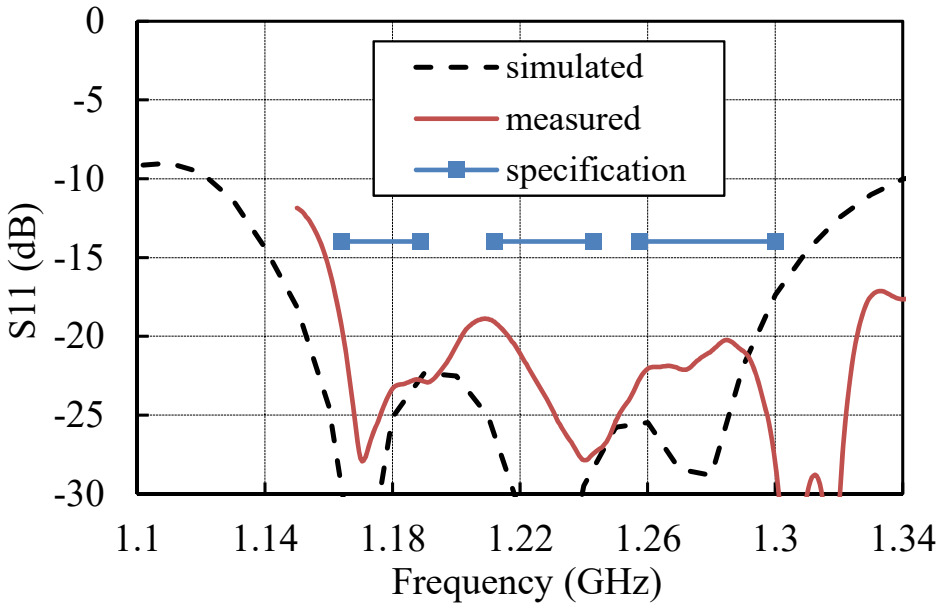

Fig. 4.4.2-2 Simulated and measured reflection coefficients in low band.

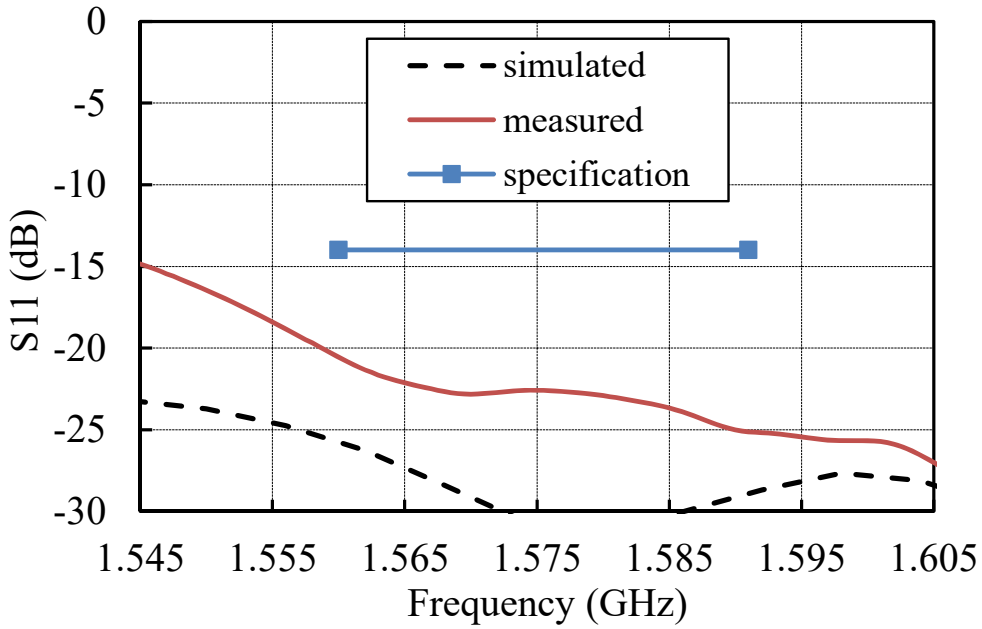

Fig. 4.4.2-3 Simulated and measured reflection coefficients in high band.

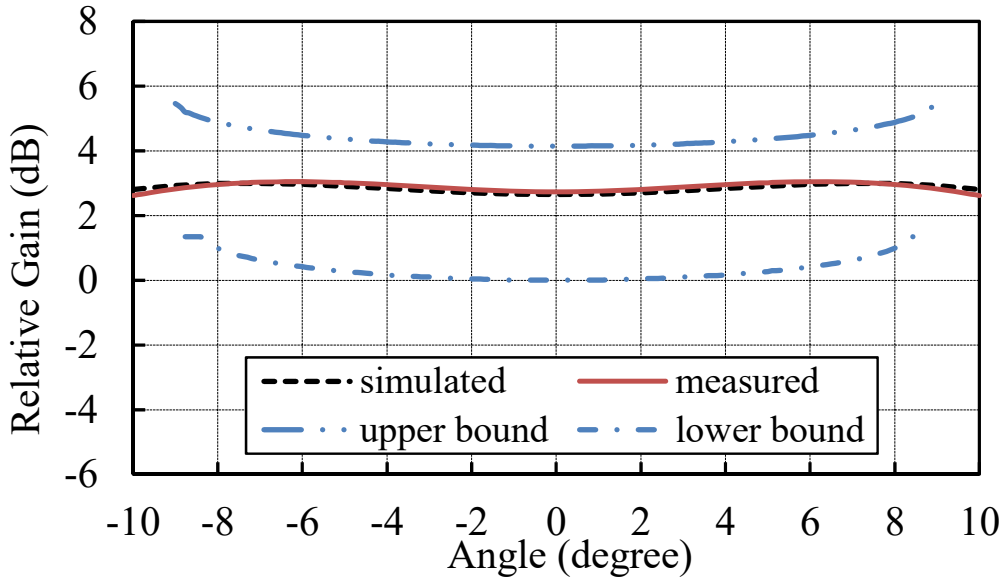

(a)

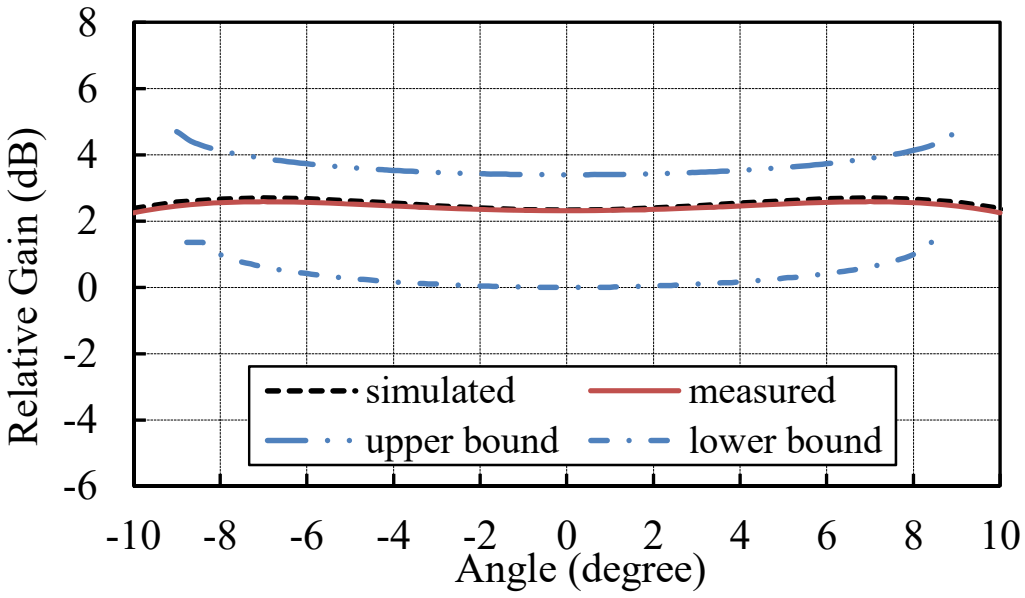

(b)

Fig. 4.4.2-4 Relative radiation patterns in the azimuth cut plane at the center frequency of (a) L5 (b) L2

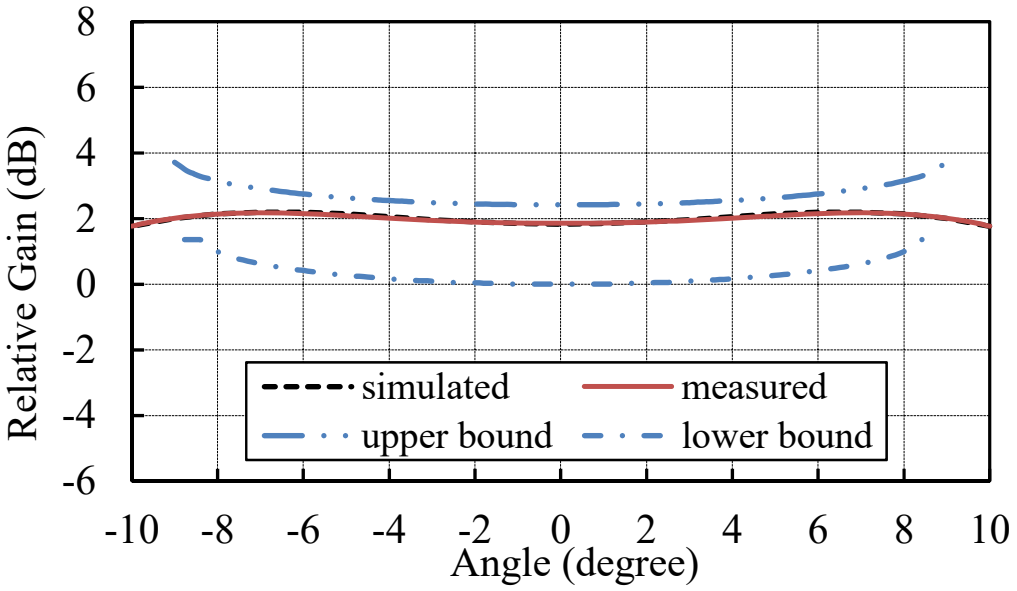

(a)

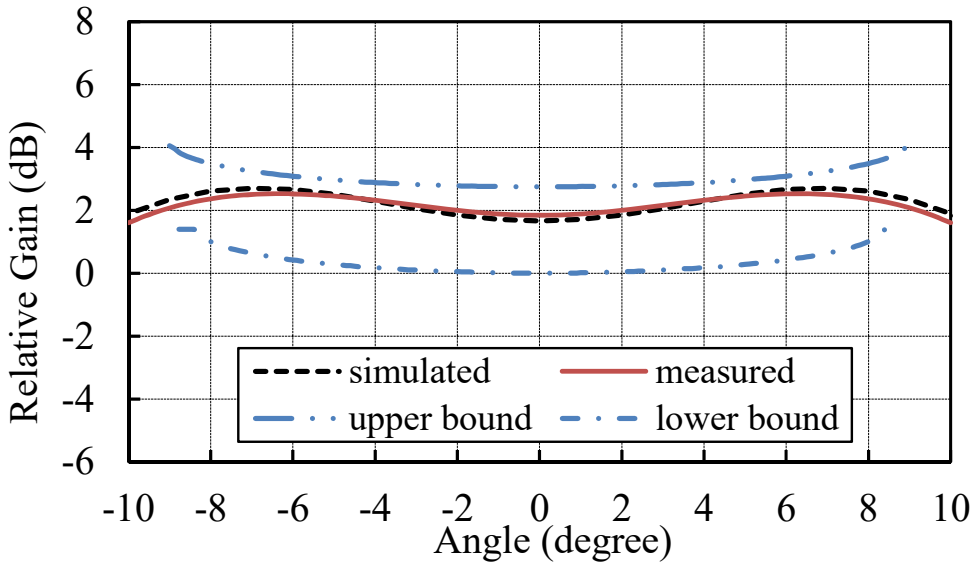

(b)

Fig. 4.4.2-5 Relative radiation patterns in the azimuth cut plane at the center frequency of (a) L6 (b) L1.

4.5. Versatility

Finally, the versatility of the proposed antenna is demonstrated. The antennas shown so far have been designed in the L band. Here, the characteristics of the design at C band, Ku band are shown.

Fig. 4.5-1-Fig. 4.5-3 show the simulated reflection coefficient, element pattern in the xz cut plane, and axial ratio versus frequency, respectively. The same performance can be obtained even if the frequency band changes. Table 4.5-1 and Table 4.5-2 shows that the realized gain hardly changes even if the frequency changes, because the proposed antenna does not use a dielectric substrate and is basically composed of metal.

From the above, it was found that this antenna and the design method operate effectively even if the frequency changes.

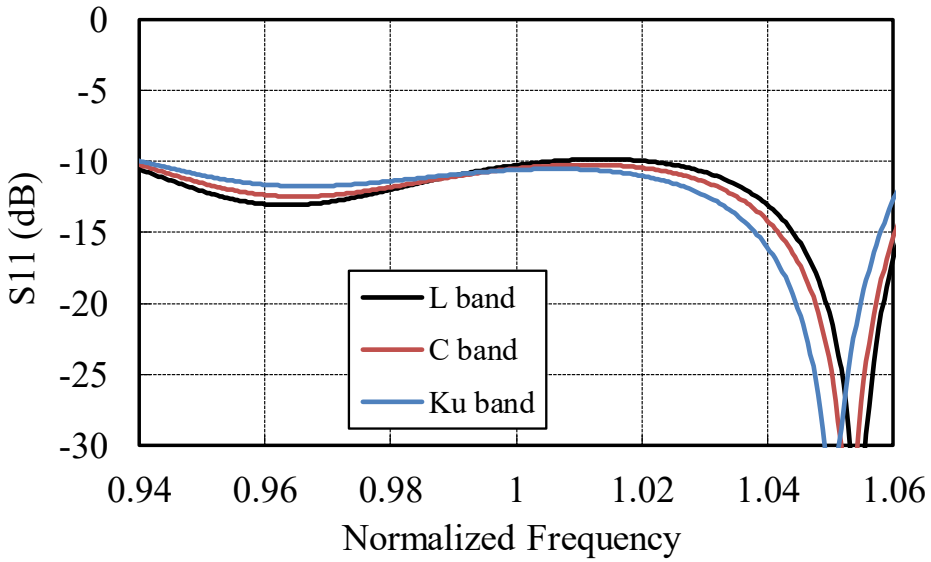

(a)

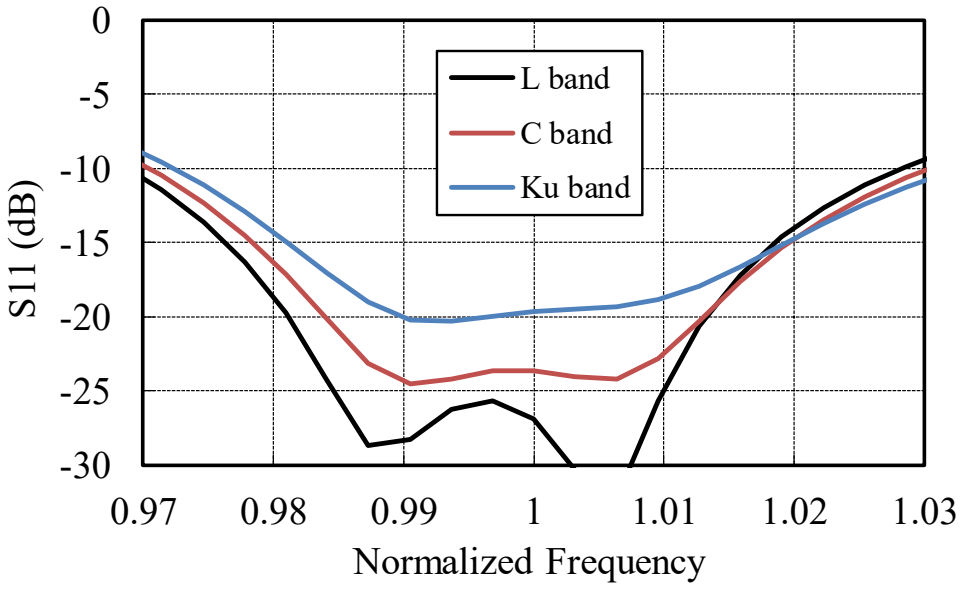

(b)

Fig. 4.5-1. Simulated reflection coefficient in each band:

(a) low band and (b) high band.

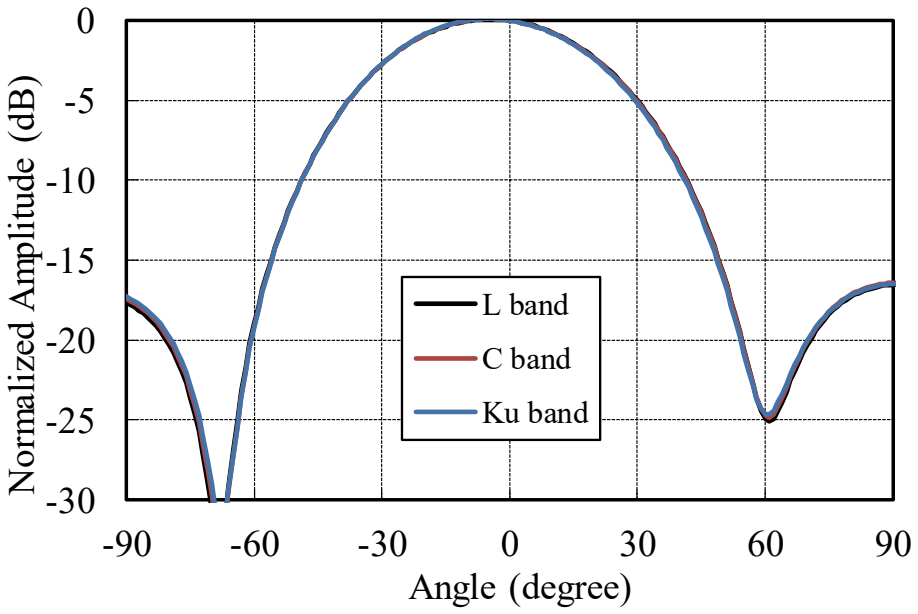

(a)

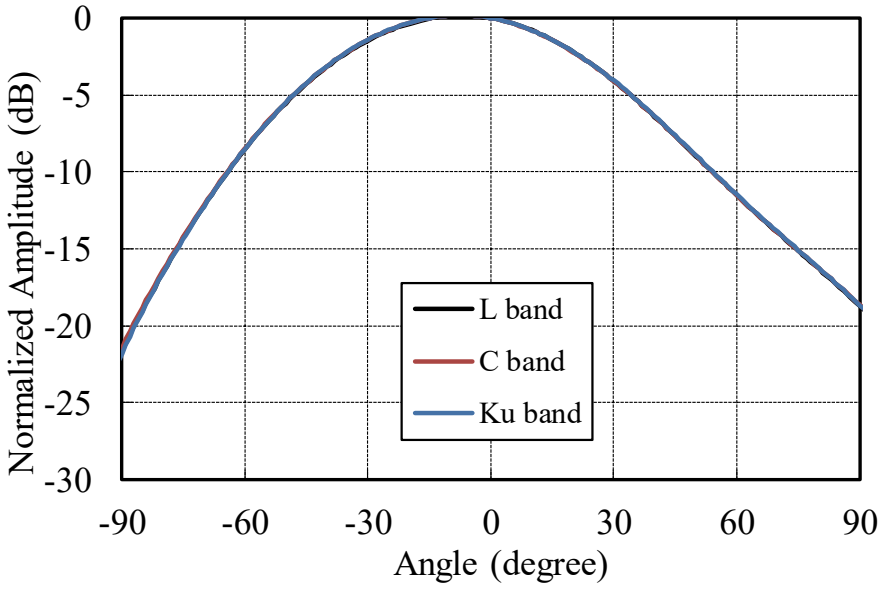

(b)

Fig. 4.5-2. Element pattern in the xz cut plane at the center frequency: (a) low band and (b) high band.

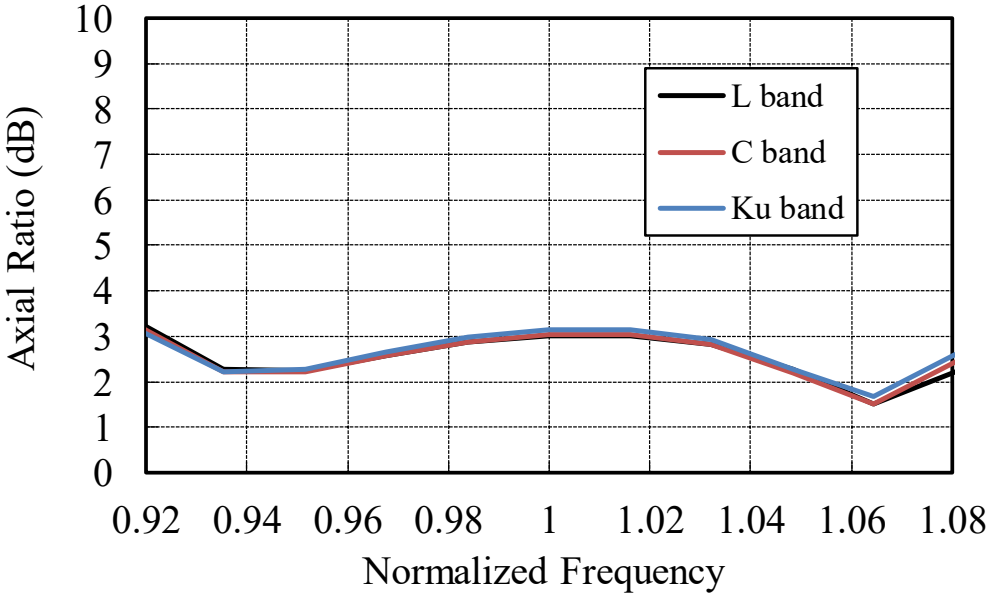

(a)

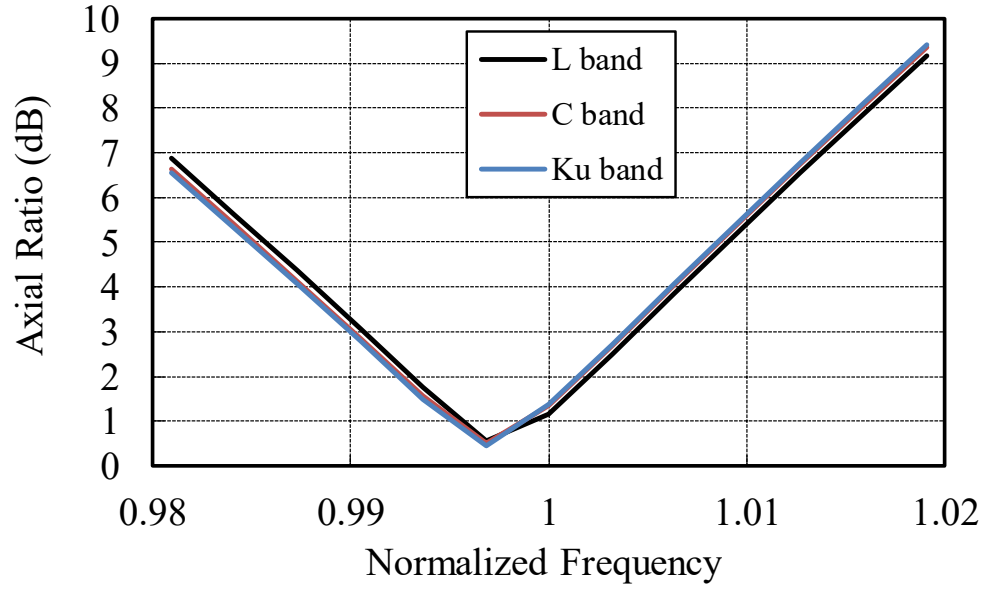

(b)

Fig. 4.5-3 Axial ratio versus frequency: (a) low band and (b) high band.

Table 4.5-1 Comparison of gains and losses for each antenna for low band

	L band (1.1-1.6 GHz)	C band (5.5-8.0 GHz)	Ku band (11-16 GHz)
Realized Gain (dBi)	9.6	9.6	9.4
Dielectric Loss (dB)	0.1	0.1	0.2
Conductor Loss (dB)	0.1	0.1	0.1

Table 4.5-2 Comparison of gains and losses for each antenna for high band

	L band (1.1-1.6 GHz)	C band (5.5-8.0 GHz)	Ku band (11-16 GHz)
Realized Gain (dBi)	8.9	8.8	8.7
Dielectric Loss (dB)	0.2	0.2	0.3
Conductor Loss (dB)	0.1	0.1	0.1

4.6. Summary

In this chapter, a circularly polarized ring microstrip antenna with shorting pins was demonstrated. The number and/or diameter of shorting pins can be used to control the operating frequency. Even under increase of the inner diameter, the resonance frequency remains constant for a fixed outer diameter, making the proposed antenna applicable to various systems. As an example of a use for the proposed antenna, a dual band antenna is designed and measured. Furthermore, the electrical performance for a proto flight model of a satellite positioning system using the proposed antenna is demonstrated. The measurement and designed results agreed well, which proves that the antenna can be put into practical use.

4.7. References

[47] J. Mink, "Circular ring microstrip antenna elements," in Proc. of Antennas and Propag. Society Int. Symp., Quebec, Canada, 1980, vol. 18, pp. 605-608.

[48] H. Chen, and K. Wong, "On the circular polarization operation of annular-ring microstrip antennas," *IEEE Trans. Antennas and Propag.*, vol. 47, no, 8, pp. 1289-1292, Aug. 1999.

[49] M. Bilgic and K. Yegin, "Modified annular ring antenna for GPS and SDARS automotive applications," *IEEE Trans. Antennas Wireless Propag. Lett.*, vol. 15, pp. 1442-1445, Dec. 2015.

[50] S. Lin and K. Huang, "A compact microstrip antenna for GPS and DCS application," *IEEE Trans. on Antennas and Propagat.*, vol. 53, no. 3, pp. 1227-1229, March 2005.

[51] N. Goto, and K. Kaneta, "Ring patch antennas for dual frequency use," in Proc. of Antennas and Propag. Society Int. Symp., Blackburg, VA, USA, 1987, vol.1, pp.338-341.

[52] H. Arai, K. Kaneta, and N. Goto, "Input impedance characteristics of ring patch antenna," *IEICE Technical Report*. AP88-80, pp. 49-54, Oct. 1988.

[53] W. Chujo, M. Fujise, H. Arai, and N. Goto, "Improvement of the isolation characteristics of a two-layer self-diplexing array antenna using a circularly polarized ring patch antenna," *IEICE Trans. Commun.,* vol. E76-B, no.7, pp.755-758, July 1993.

[54] S. Kumagai, Y. Kazama, and N. Goto, "Dual-frequency ring patch antennas for GPS," in *Proc. of Int. Symposium on Wireless Comm. Systems*, Siena, Italy, 2005,

pp. 601-605.

[55] A. Montesano, C. Montesano, R. Caballero, M. Naranjo, F. Monjas, L. E. Cuesta, P. Zorrilla, and L. Martinez, "Galileo system navigation antenna for global positioning," in *Proc. 2nd Eur. Conf. Antennas Propag. (EUCAP)*, Edinburgh, UK, 2007, pp.1-6.

[56] J. Goto, A. Hirota, K. Mochizuki, Satoshi Yamaguchi, Kazunari Kihira, Toru Takahashi, H. Sumiyoshi, M. Otsuka, N.Yoneda, and J. Hirokawa, "Design of the Circularly Polarized Ring Microstrip Antenna with Shorting Pins," *IEICE Trans. Commun*, submitted.

[57] J. Goto, S. Yamaguchi, K. Kihira, T. Takahashi, and H. Miyashita, "Dual frequency patch antenna using partially shorted annular ring patch antenna," in *Proc. of Antennas and Propag. Society Int. Symp.*, Memphis, TN, USA, 2014, pp.1-2.

[58] K. Mochizuki, K. Miura, H. Sumiyoshi, H. Ishida, A. Aikawa, T. Nishino, and A. Matsumoto, "Test result of L-band Antenna Assy for QZS-3 PFT," in *Proc. 60th Space Sciences and Technology Conf. 3K14,JSASS-2016-4530*, Hokkaido, Japan, 2016, pp.1-6. (in Japanese)

[59] Y. Lin and L. Shafai, "Characteristics of concentrically shorted circular patch microstrip antennas," IEE proc. vol. 137, no.1, Feb. 1990.

[60] D. Sengupta and L. Martins-camelo, "Theory of dielectric-filled edge-slot antennas," IEEE Trans. Antennas Propag., vol.AP-28, no.4, pp.481-490, July 1980.

[61] K. Carver, and J. Mink, "Microstrip antenna technology," *IEEE Trans. Antennas and Propag.*, vol. 29, iss. 1, pp. 2-24, Jan. 1981.

[62] L. Shen, S. Long, M. Allerding, and M. Walton, "Resonant frequency of a circular disc, printed-circuit antenna," *IEEE Trans. Antennas and Propag.*, vol. 25, iss. 4,

pp. 595-596, July 1977.

[63] http://qzss.go.jp/en/overview/services/sv06_clas.html

[64] M. Plessis, and J.H. Cloete, "Tuning stubs for microstrip patch antennas," in *Proc. of Antennas and Propag. Society Int. Symp.*, Ann Arbor, MI, USA, 1993, pp. 964-967.

[65] I. Park, R. Mittra, and I. Aksun, "Analysis of microstrip patch antennas with tuning stubs using the closed-form Green's function," in *Proc. of Antennas and Propag. Society Int. Symp.*, Ann Arbor, MI, USA, 1993, pp. 1442-1445.

[66] W. M. Merrill, "Coax transition to annular ring for reduced input impedance at 2.4 GHz and 5.8 GHz," in *Proc. of Antennas and Propag. Society Int. Symp.*, Waltham, MA, USA, 2000, vol. 3, pp.1440-1443.

[67] W. Stutzman, G. Thiele, Antenna theory and design, 3rd Edition, 2012.

[68] X. Sun, Z. Zhang, and Z. Feng, "Dual-band circularly polarized stacked annular-ring patch antenna for GPS application," *IEEE Trans. Antennas Wireless Propag. Lett.*, vol. 10, pp. 49-52, March 2011.

[69] Y. Cai, K. Li, Y. Yin, and X. Ren, "Dual-band circularly polarized antenna combining slot and microstrip modes for GPS with HIS ground plane," *IEEE Trans. Antennas Wireless Propag. Lett.*, vol. 10, pp. 49-52, March 2015.

5. Two-Dimensional Injection-Molded Horn Array Antenna for Millimeter-Wave Active Phased Array Antenna

5.1. Introductory remarks

In recent years, the use of millimeter-wave bands has attracted attention from the viewpoint of high-speed communication and securing of frequency bands. In order to use the millimeter-wave band for wireless communication of high-speed moving objects such as aircraft, high performances of the system are required; improvement of antenna performance that realize long-distance millimeter-wave band communication, reduction of the size and weight of equipment, high-speed beam control performance to follow the attitude of aircraft. A large-capacity wireless communication system for aircraft capable of transmitting 100 Mbps using the 40 GHz band has been developed, and 100 Mbps bidirectional communication between an aircraft flying at an altitude of 8,000 m and the ground using this system has been successful [70].

However, they aimed at communication between the aircraft and the ground and applied mechanical control to the direction of flight of the aircraft and electronic control to the left and right directions where the attitude change is fast. Accordingly, it was difficult to apply it to communication between high-speed moving objects that required high-speed beam scanning in two dimensions. Therefore, the development of an active phased array antenna (APAA) capable of two-dimensional electron beam

scanning is desired.

The candidate of antennas used in the millimeter-wave band include hollow waveguide array antennas [71]. This type of antenna has the advantage of low loss but has problems such as high cost and large weight. In addition, wide-angle beam scanning is difficult because the element spacing cannot be reduced. For this reason, they adopted a resin waveguide horn array antenna as a compact and highly manufacturable antenna even in the millimeter-wave band [72]. This array antenna can be integrally molded with the radiating part and the feeding part by injection molding and metal coating, and has the features of low cost, excellent productivity, and less occurrence of grating lobes even during wide-angle beam scanning. However, the input impedance was designed in the front direction, and there was a problem that the axial ratio characteristics deteriorated during wide-angle beam scanning [73].

In this chapter, a design method to obtain low axial ratio characteristics even in wide-angle beam scanning in a two-dimensional electronically controlled two-dimensional active phased array antenna is shown [74]. In addition, an array antenna and APAA are built in the millimeter wave 46GHz band, and the validity of the above design method is confirmed by measurement.

Section 5.2 gives an overview of APAA. Section 5.3 describes the design method and simulation results of the radiation part of APAA. Finally, Section 5.4 describes the antenna measurement results and the APAA prototype measurement results.

5.2. APAA system overview

5.2.1. Configuration of APAA

Fig. 5.2.1-1 shows an overview of APAA. This APAA is composed of an 8 × 8 element radiating part, the feed part, the radio frequency (RF) module, the control unit, the power supply unit, the local oscillator, and the cooling mechanism. The transmitting and receiving antennas are provided separately. Each volume is about 11 liters, but the size will be reduced to about 7 liter by reducing the fan by improving heat radiation. The antenna part consisting of the radiation part and the feed part is integrally formed by injection molding a cycloolefin polymer (COP, relative dielectric permittivity: 2.3, dielectric loss tangent: 0.0005) and coating the surface with conductors. The antenna type is a circular waveguide horn.

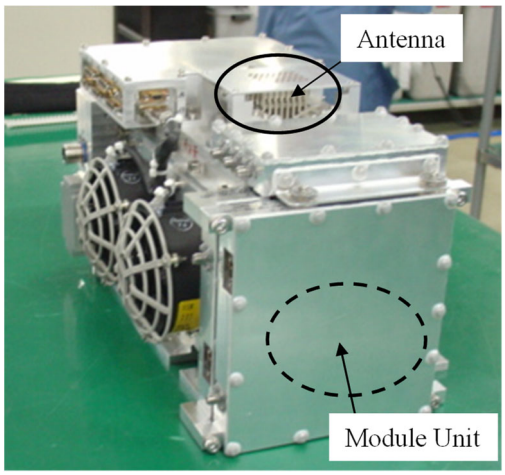

(a) APAA (bird's eye view)

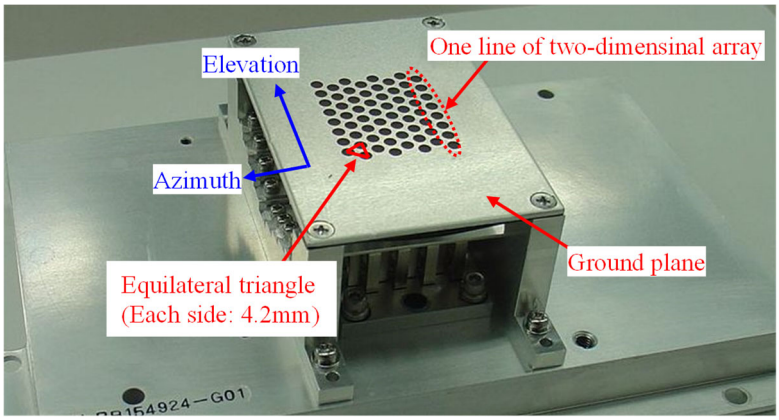

(b) Antenna including the hollow waveguide adapter for measurements

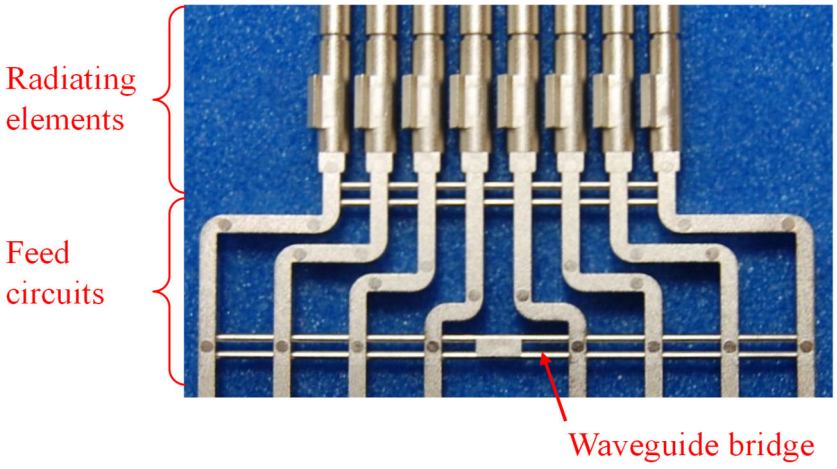

(c) One line of two-dimensional array

Fig. 5.2.1-1 Photos of the prototype APAA

5.2.2. Configuration of radiating part

Fig. 5.2.2-1 shows the detailed configuration of the antenna unit. An equilateral triangular array with a side of 4.2 mm is adopted, and the ground plane is arranged on the same plane as the opening end of the radiation part. The radiating part and the feed part are integrally formed, but in a two-dimensional array antenna the feed part is divided into multiple sections and difficult to assemble. Therefore, by installing a waveguide bridge between adjacent resin waveguides in the same row, it is possible to integrally mold [75]. Since the diameter of this waveguide bridge is sufficiently small with respect to the wavelength of the operating frequency, there is almost no leakage between adjacent resin waveguides.

The left-hand figure in Fig. 5.2.2-2 shows the element antenna that consists of a circular horn, an iris for impedance matching, a polarizer, a circle-to-rectangle converter, and a rectangular waveguide. Here, the aforementioned problems are depicted in Fig. 5.2.2-2. The polarization is assumed to be right-handed circular polarization (RHCP). The linearly polarized electromagnetic field input from the rectangular waveguide is converted to a circularly polarized wave (RHCP, in this case) by a polarizer, as shown in Fig. 5.2.2-2 (a). Part of this is reflected at the edge of the aperture and is also reflected by coupling from surrounding elements. The main polarization component passes through the polarizer again, becomes linear polarization, returns to the input port, and becomes a reflection loss of the antenna (Fig. 5.2.2-2 (b)). Besides, the reverse polarization component of the reflected wave from the aperture is reflected again by the circle-to-rectangle converter (Fig. 5.2.2-2

(c)), is radiated to space as the reverse polarization, and causes deterioration of the axial ratio characteristics (Fig. 5.2.2-2 (d)).

The next section shows an array antenna design method that cope with this problem. The electromagnetic field simulator HFSS is used for the design. For design efficiency, a periodic boundary condition is applied to assume an infinite array.

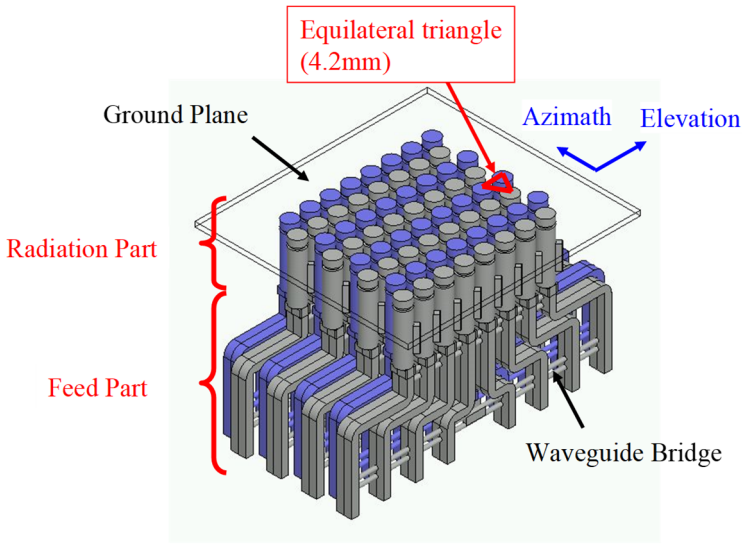

Fig. 5.2.2-1 Two dimensional circular polarized horn array antenna

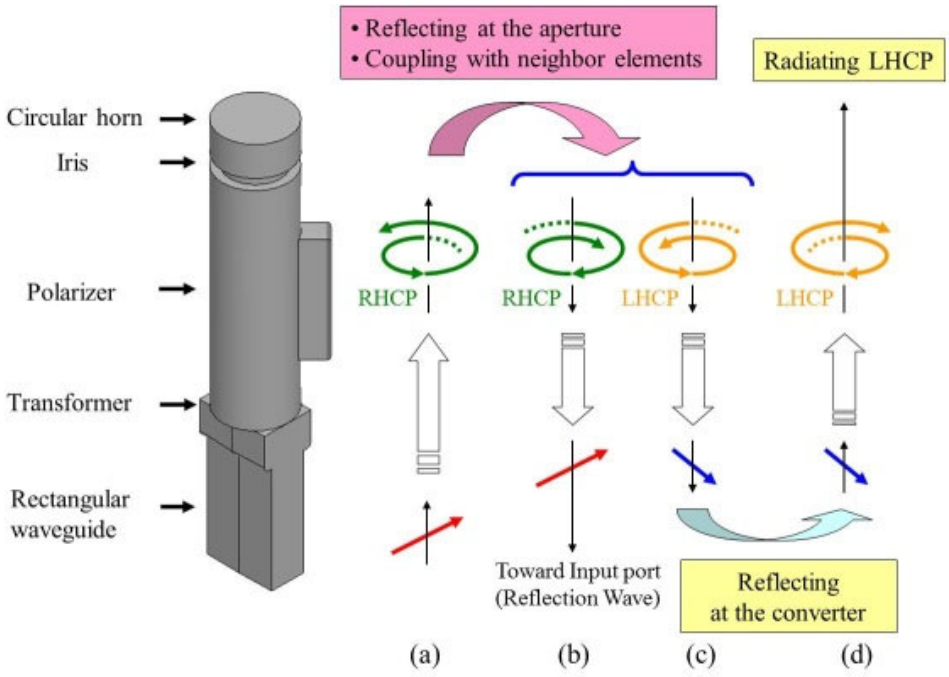

Fig. 5.2.2-2 Principle of the inverse polarized wave radiations

5.3. Design of radiating part

This section describes the design method of the radiation part of the proposed antenna. Here, a receiving antenna that operates at 46.8 GHz and possesses RHCP is assumed. The transmission antenna can be designed in the same manner on the bases of the reciprocity theorem.

5.3.1. Principle

In the radiating part, the iris is the only component that can suppress the reverse polarization component shown in the previous section. Since the polarizer is originally designed to emit low-axis ratio circularly polarized waves, the dimension should not be changed. In addition, the circle-to-rectangle converter cannot control the inverse polarization component. Therefore, only the iris can improve the axial ratio.

Fig. 5.3.1-1 shows the iris design model. This model can be represented as a two-port equivalent circuit shown in Fig. 5.3.1-2. V_i and H_i are the vertical and horizontal polarization components of the incident wave, and S_{VV} and S_{HH} are reflection coefficients of the vertical and horizontal polarized waves, respectively. Also, S_{VH} and S_{HV} are the active reflection coefficients between orthogonal modes. Here, the following equation holds.

$$\begin{bmatrix} V_r \\ H_r \end{bmatrix} = \begin{bmatrix} S_{VV} & S_{VH} \\ S_{HV} & S_{HH} \end{bmatrix} \quad (5.3.1\text{-}1)$$

$$\begin{bmatrix} V_i \\ H_i \end{bmatrix} = \begin{bmatrix} 1/\sqrt{2} \\ -j/\sqrt{2} \end{bmatrix} \quad (5.3.1\text{-}2)$$

When these are converted into circularly polarized waves, the principally polarized wave component (RHCP) and the inversely polarized wave component (LHCP) of the reflected wave are expressed by the following equations, respectively.

$$S_{RHCP} = (V_r - jH_r)/\sqrt{2} \quad (5.3.1\text{-}3)$$

$$S_{LHCP} = (V_r + jH_r)/\sqrt{2} \quad (5.3.1\text{-}4)$$

From these equations, in order to obtain low axial ratio characteristics, the position and depth of the iris should be adjusted so that the inverse polarization component is small. Therefore, the iris can be defined as matching structure between antenna and space.

The design is performed in the following steps. First, the inversely polarized component of the reflected wave of the antenna without the iris is observed with a Smith chart. Next, the phase reference plane is moved to the conductance circle that passes through the center of the Smith chart. The iris that operates as a series inductor is provided at this position, and the depth of the iris is adjusted so as to move the locus of the reflection coefficient to the center on the Smith chart. Fig. 5.3.1-3 shows the equivalent circuit model of the iris. $\overline{Z_L}$ represents the normalized impedance of the load, whereas S represents the normalized admittance at the voltage-minimum point. Herein, the position and the depth of the iris can be designed using following equations [76]:

$$d_0 = \pm\frac{\lambda}{2} + \frac{\lambda}{4\pi}\cos^{-1}\frac{S-1}{S+1} \tag{5.3.1-5}$$

$$l_0 = \frac{\lambda}{2\pi}\tan^{-1}\frac{1-S}{\sqrt{S}} \tag{5.3.1-6}$$

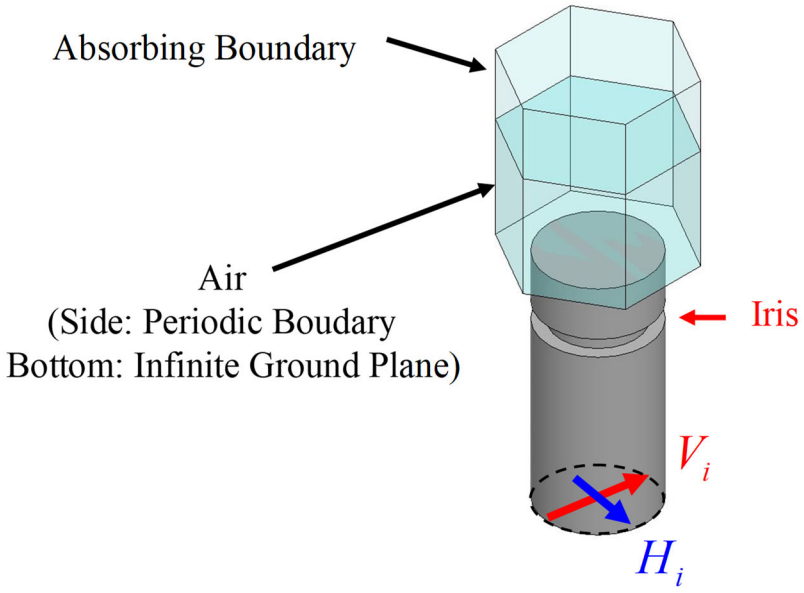

Fig. 5.3.1-1 Iris design model

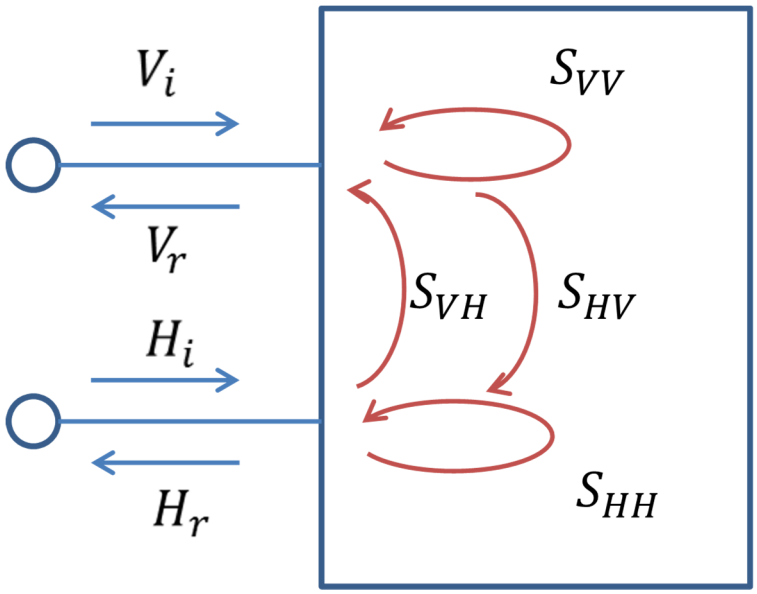

Fig. 5.3.1-2 Equivalent circuit model of Fig. 5.3.1-1

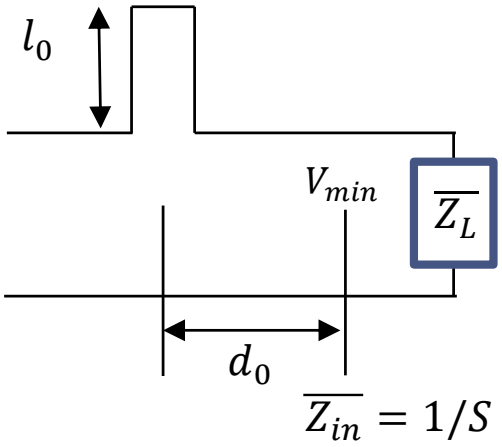

Fig. 5.3.1-3 Equivalent circuit model of the iris.

5.3.2. Design procedure

The design procedure of this antenna is described.

Fig. 5.3.2-1 shows the linear polarization component of the reflected wave during beam scanning without an iris. The characteristics when the beam is scanned in the direction of 0°, 10°, 20°, 30°, 40°, 45° from the boresight on the azimuth (AZ) cut plane are calculated. The reflected wave is converted into a circularly polarized wave component as shown in Eq. (4) to clarify the inversely polarized wave component (Fig. 5.3.2-2). The reverse polarization component without the iris is high as -6.4dB.

Next, the iris is designed so that the average value of S_{LHCP} becomes lower within the beam scanning range of 0° to 45° (Fig. 5.3.2-3). First, the phase reference plane is moved 1.65 mm from the aperture, and the locus on the Smith chart is moved to the vicinity of the equal conductance circle. Since the iris behaves as a series inductor, the locus moves to the center of the Smith chart as shown in Fig. 5.3.2-3 (a) by setting the iris depth to 0.35mm.

Here, the design results by the conventional method are also shown in the same figure. The conventional method is slightly better in the case of beam scanning in the front direction than in the proposed method. However, the value of the axial ratio increases significantly in the case of beam scanning in the wide-angle direction.

Finally, in order to verify the effectiveness of the proposed method, the whole antenna using the iris designed above is analyzed. Fig. 5.3.2-4 shows the analysis model, and Fig. 5.3.2-6 shows the beam scanning characteristics of the axial ratio. By installing the iris, the worst axial ratio within ±45° is reduced from 10.0dB to

6.6dB. As shown in Fig. 5.3.2-5, it is confirmed that the active reflection coefficient corresponds to the right-handed polarization characteristics without the polarizer shown in Fig. 5.3.2-3.

As described above, the method proposed in this dissertation guarantees the characteristics of beam scanning in the wide-angle direction by clarifying the inverse polarization component that degrades the axial ratio. The proposed method enables deterministic and efficient design, which was not possible with the conventional method under the same degree of freedom.

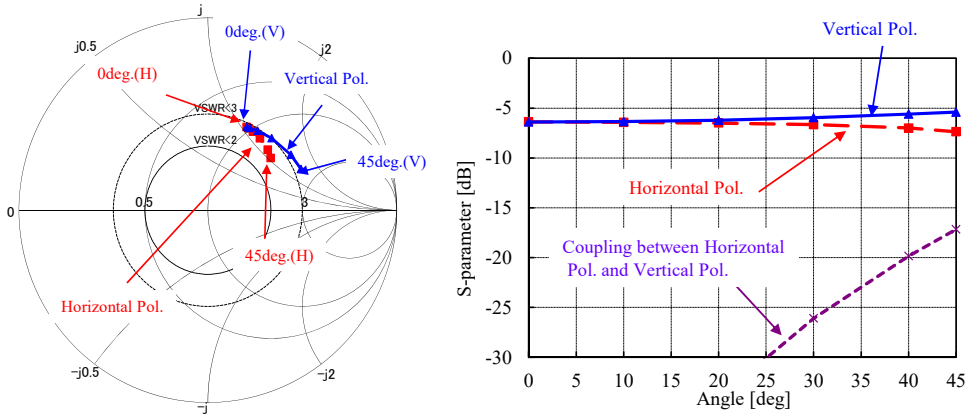

(a) Smith Chart (b) Rectangular Plot

Fig. 5.3.2-1 Reflection Properties without the iris with respect to the component of the linear polarization on azimuth cut plane

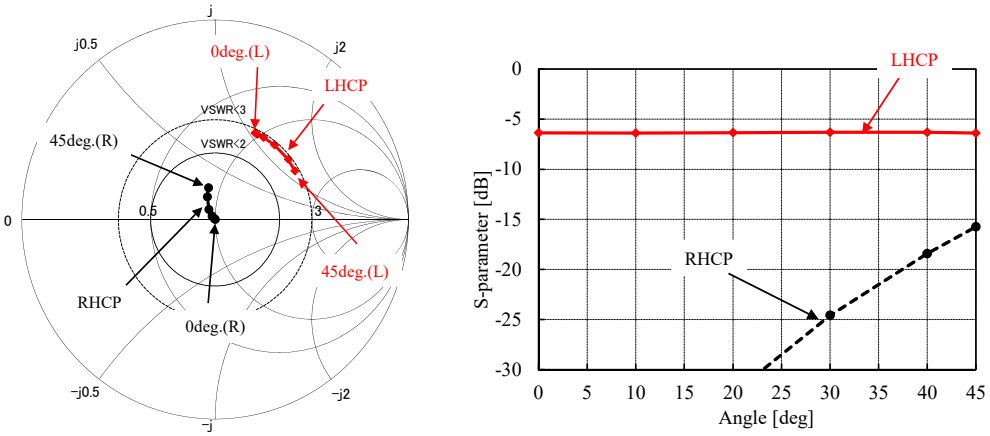

(a) Smith Chart (b) Rectangular Plot

Fig. 5.3.2-2 Reflection properties without the iris with respect to the component of the circular polarization on azimuth cut plane

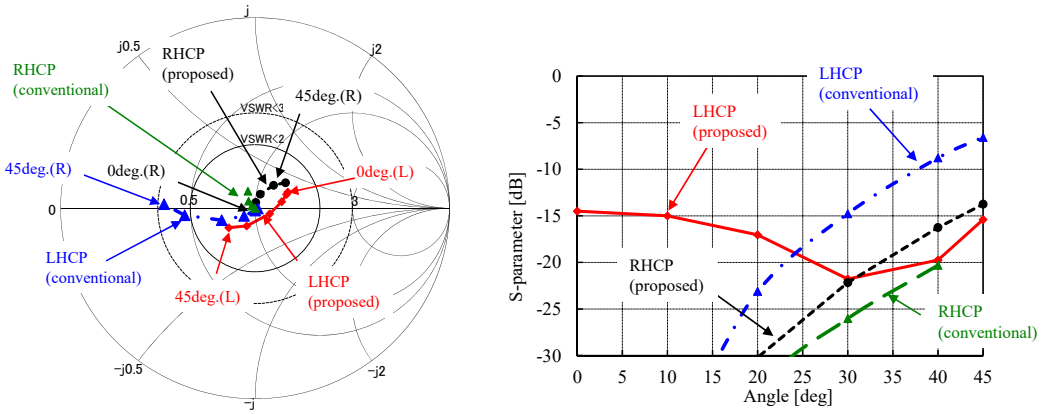

(a) Smith Chart (b) Rectangular Plot

Fig. 5.3.2-3 Reflection properties with the iris with respect to the component of the circular polarization on azimuth cut plane

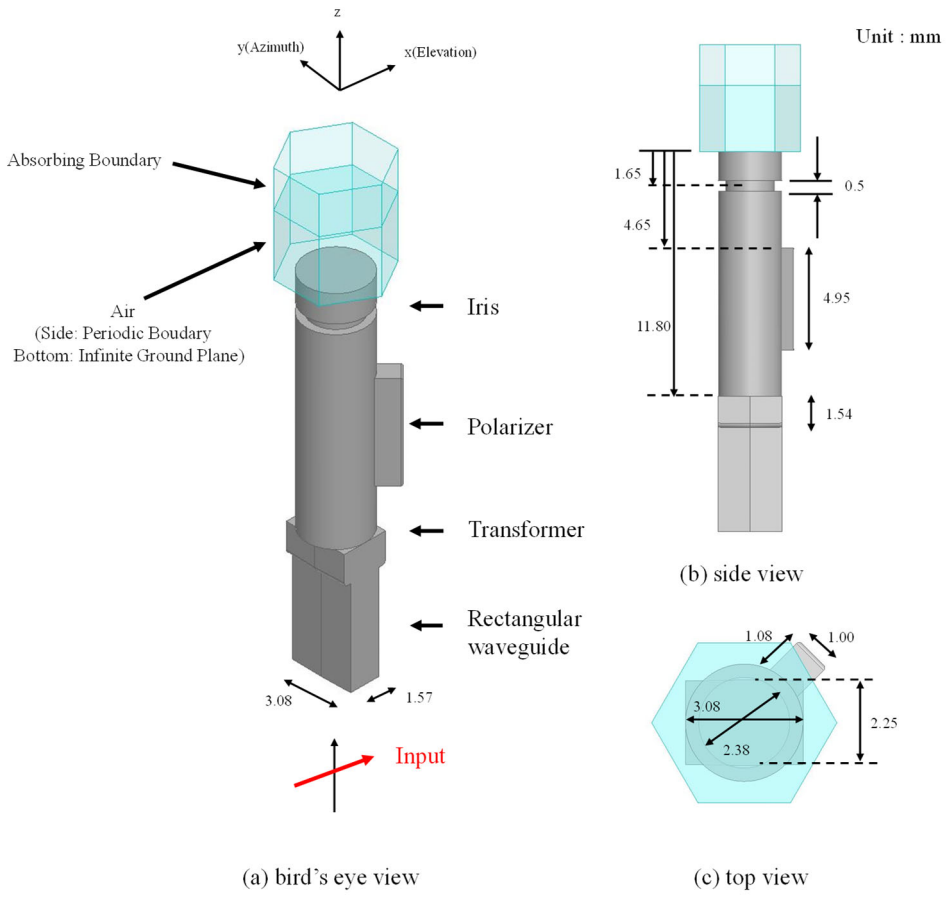

Fig. 5.3.2-4 Unit cell model (proposed method)

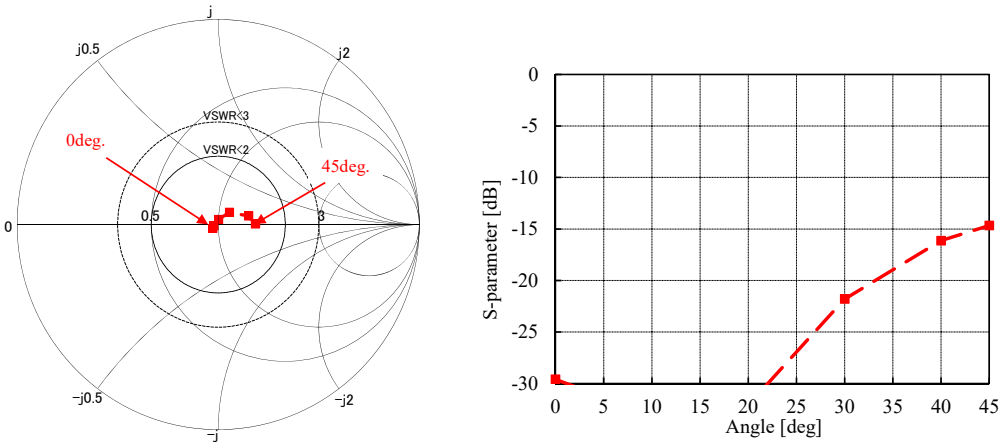

Fig. 5.3.2-5 Active reflection characteristic on azimuth cut plane

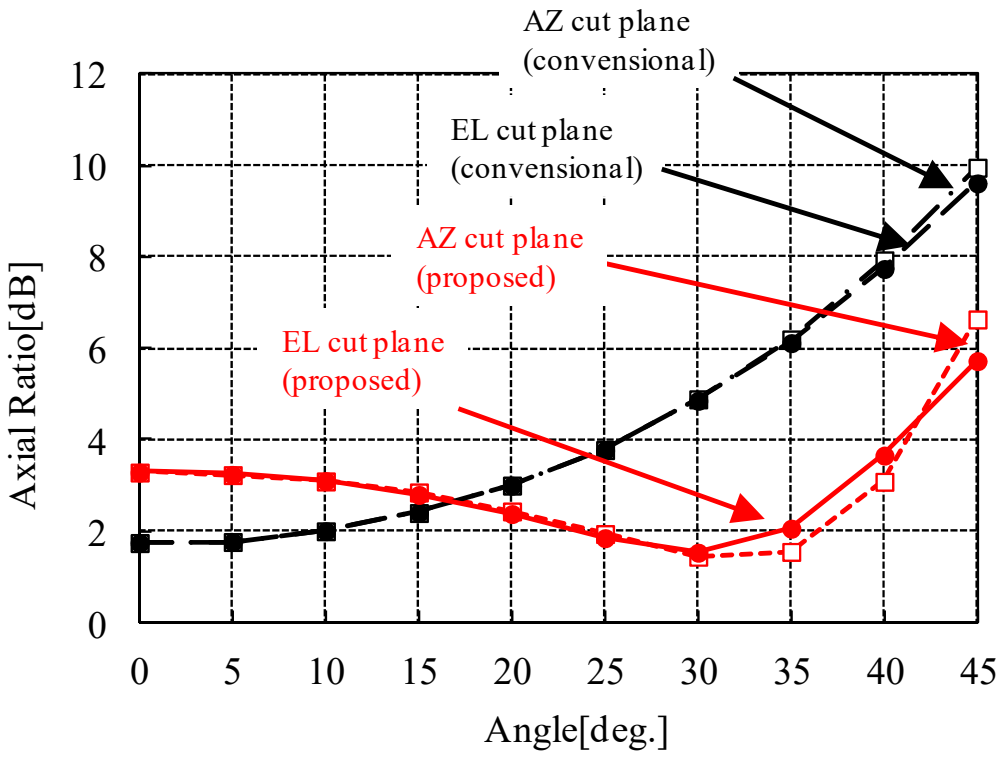

Fig. 5.3.2-6 Axial ratio with respect to the component of the RHCP on azimuth cut plane

5.4. Measurement results

In this section, measurement results to evaluate the validity of the design method shown in the previous section are presented.

5.4.1. Antenna measurement

First, the antenna measurement results are shown. Fig. 5.4.1-1 shows the configuration of the measurement system. The standard gain horn antenna for the transmission was set in the far field region, and the electromagnetic wave from it was received by the proposed array antenna.

Fig. 5.4.1-2 shows the averaged array element pattern. Note that the radiation patterns obtained by exciting the central 16 elements of the 64-element array were averaged. The measured values and the design values correspond well for both polarization components. The measured value of the power supply circuit loss is 0.27dB (design value 0.26dB).

Fig. 5.4.1-3 shows the axial ratio pattern. The worst axial ratio of 5.0dB within ±45° has been achieved. From the above, the validity of the design method is confirmed by measurement.

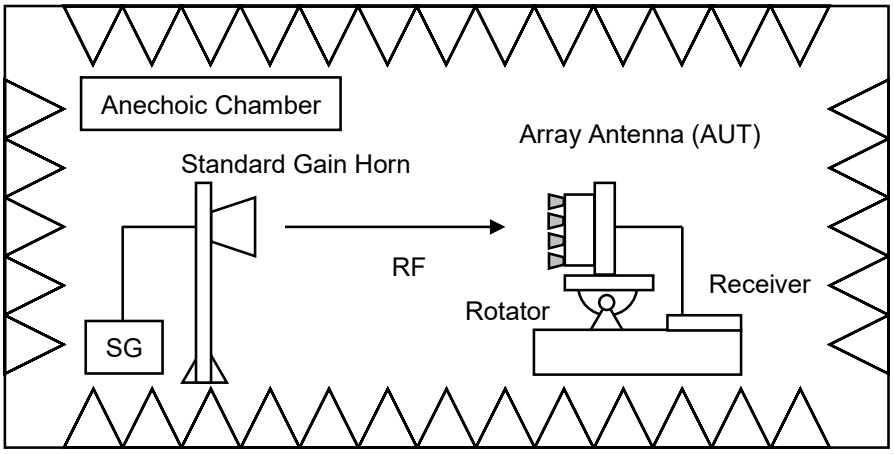

Fig. 5.4.1-1 Measurement configurations for array antenna

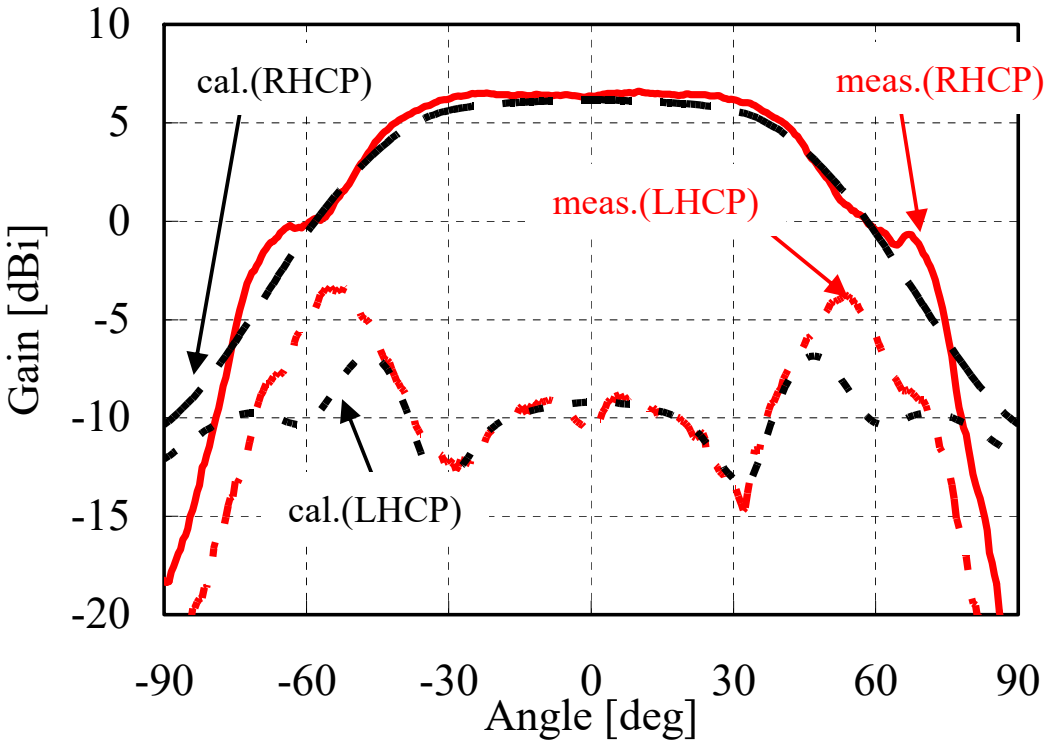

Fig. 5.4.1-2 Average array element pattern (azimuth cut plane)

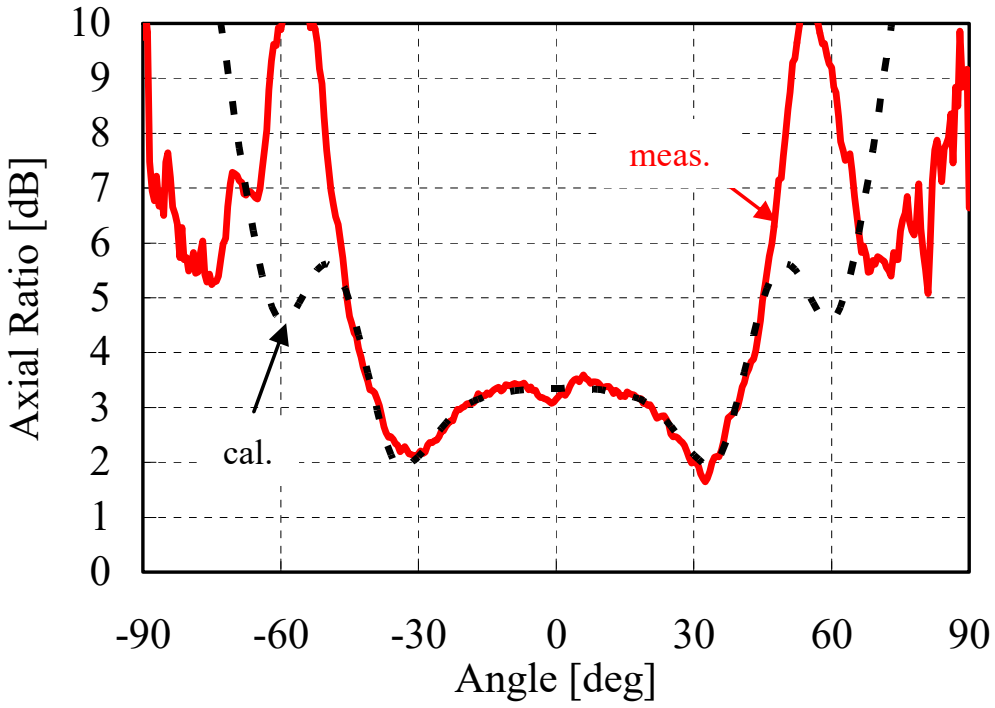

Fig. 5.4.1-3 Axial ratio pattern (azimuth cut plane)

5.4.2. APAA measurement results

Finally, the APAA measurement results are shown. Fig. 5.4.2-1 shows the configuration of the transmission APAA and reception APAA measurement systems. In the case of transmitting APAA, electromagnetic waves transmit from a specimen loaded with an RF module and a power supply unit were received by an opposing antenna in the far field. In the case of receiving APAA, the electromagnetic waves from the standard gain horn antenna transmit to the APAA.

Fig. 5.4.2-2 and Fig. 5.4.2-3 show the radiation patterns when the beam is scanned to the front direction and the edge of the coverage area in the azimuth cut plane, respectively. Fig. 5.4.2-4 shows the axial ratio pattern. Although these results include errors such as RF modules, it was confirmed that the measured values corresponded well with the design values as in the antenna measurement. Here, an error analysis of the RF module was performed to evaluate the validity of the measurement results, where the amplitude error was 1.7 dB rms, the phase error was 8°rms, and the number of trials was 300. As shown in Table 5.4.2-1, the measured values of the sidelobe levels were within the prediction level.

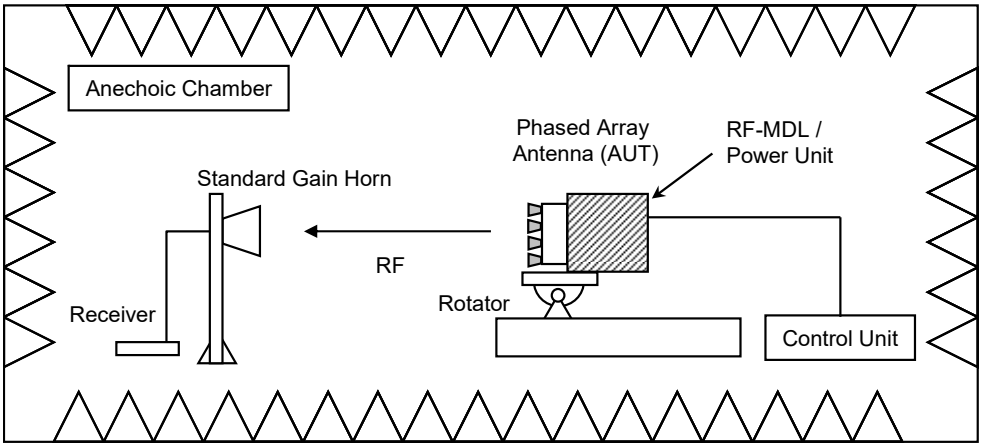

(a) Tx APAA

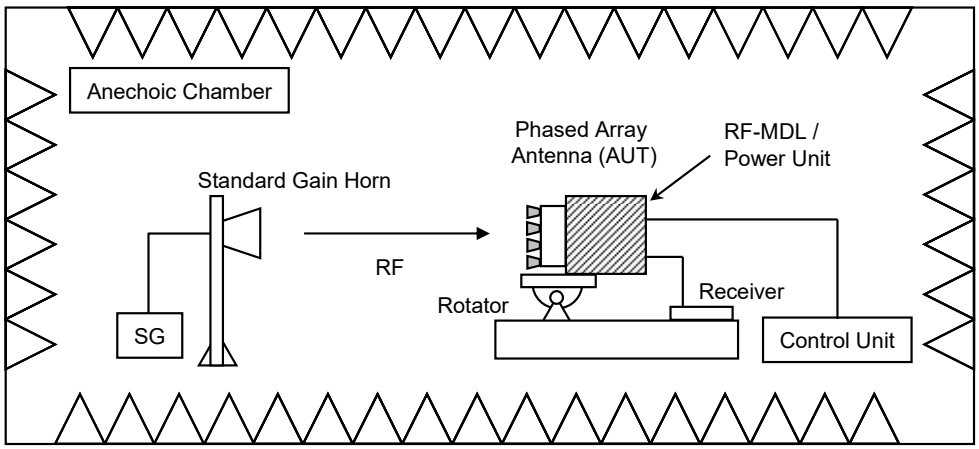

(b) Rx APAA

Fig. 5.4.2-1 Measurement configurations for APAA

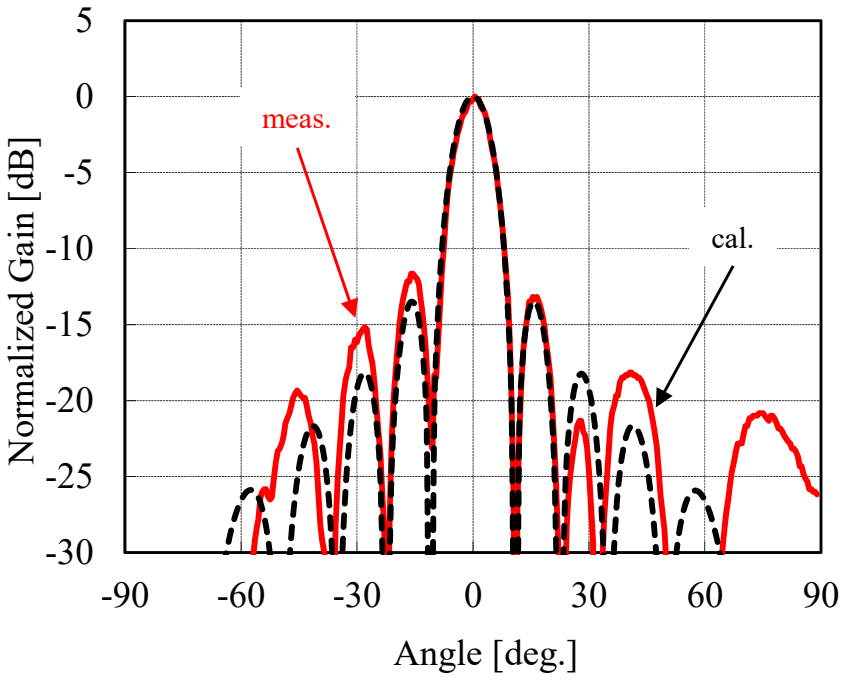

Fig. 5.4.2-2 Elevation radiation pattern (broadside beam)

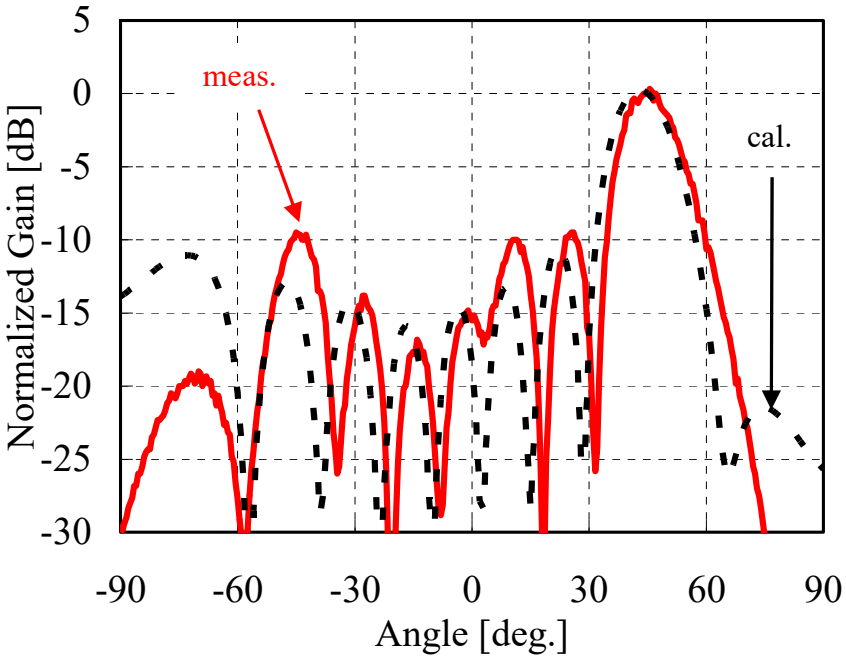

Fig. 5.4.2-3 Azimuth radiation pattern at the edge of coverage

Table 5.4.2-1 Error analysis with respect to the sidelobe level

Items		Boresight scanning	45-degree scanning
Simulation	Average	-13.5dB	-10.4dB
	Max.	-11.3dB	-8.8dB
	Min.	-15.3dB	-11.2dB
Measurement		-11.7dB	-9.5dB

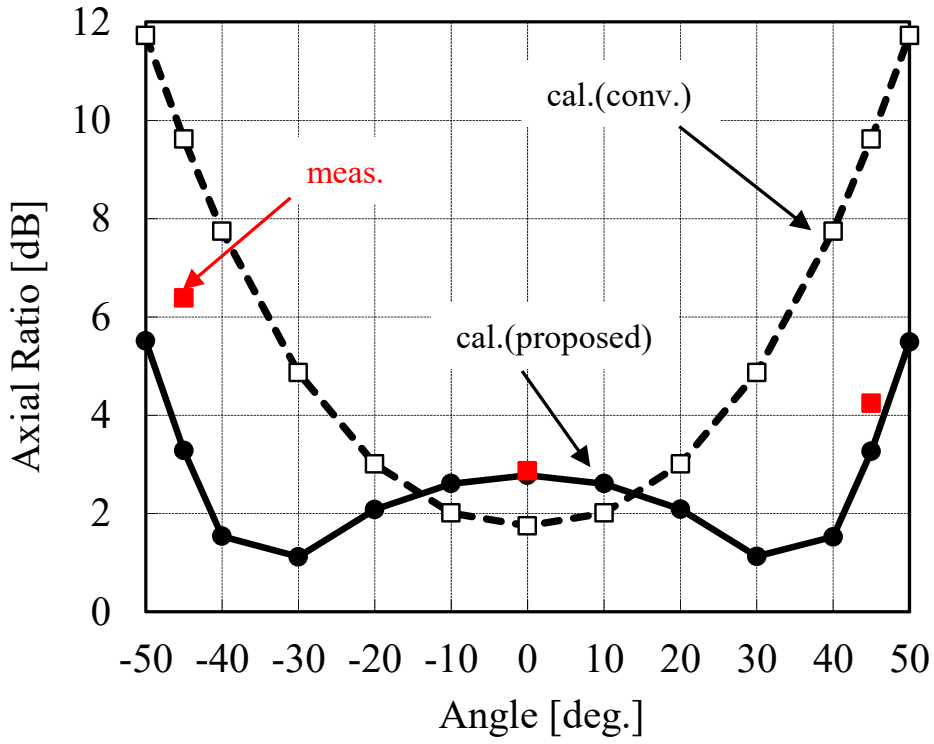

Fig. 5.4.2-4 Elevation axis ratio

Table 5.4.2-2 shows the benchmark of horn array antennas. It was confirmed that the proposed horn antenna has a wider coverage area than the other methods.

Table 5.4.2-2 Benchmark of horn array antennas

Ref.	Coverage area	tan δ	Polarization	Band width (%) (*)
[77]	0 degree	- (metal)	Linear polarization only	8
[78]	0 degree	0.0009	Linear polarization only	10
[72]	< 30 degrees	0.0005	Circular polarization	10
Proposed	< 45 degrees	0.0005	Circular polarization	10

* BW is bandwidths for -10 dB of reflection coefficient.

5.5. Versatility

Finally, the versatility of the proposed antenna is demonstrated. The antennas shown so far have been designed in 48 GHz band.

Here, the characteristics of the design at 60 GHz, 90 GHz, and 120 GHz are shown. Fig. 5.5-1 and Fig. 5.5-2 show the axial ratio versus frequency and the reflection characteristics, respectively. The same performance can be obtained even if the frequency band changes. Table 5.5-1 shows that the realized gain decreases as the frequency increases, because of the increase of dielectric loss.

From the above, it was found that this antenna and the design method operate effectively even if the frequency changes.

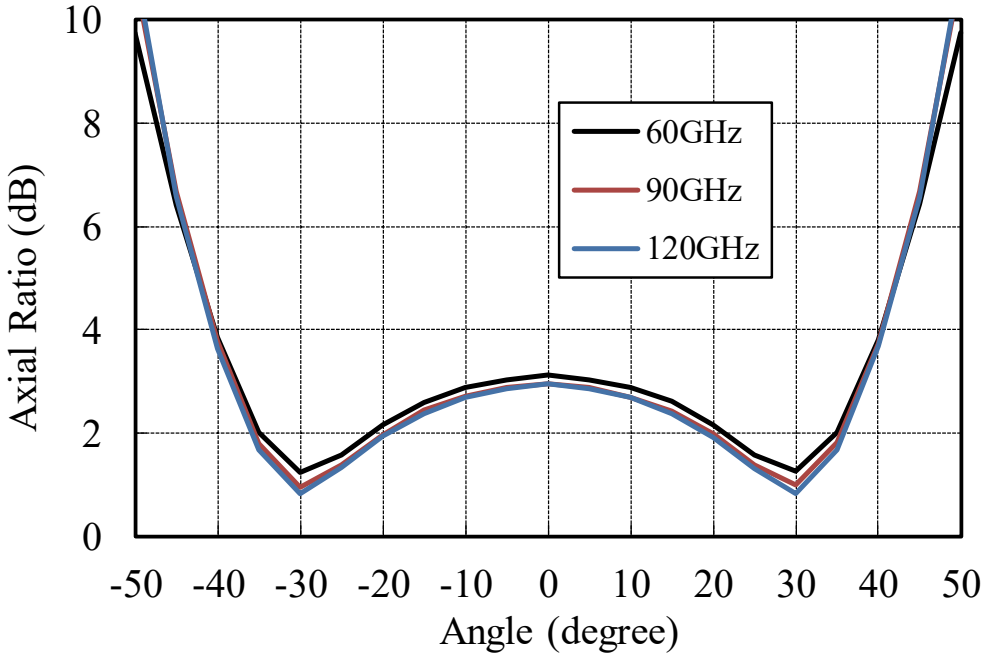

Fig. 5.5-1 Axial ratio versus frequency in each band

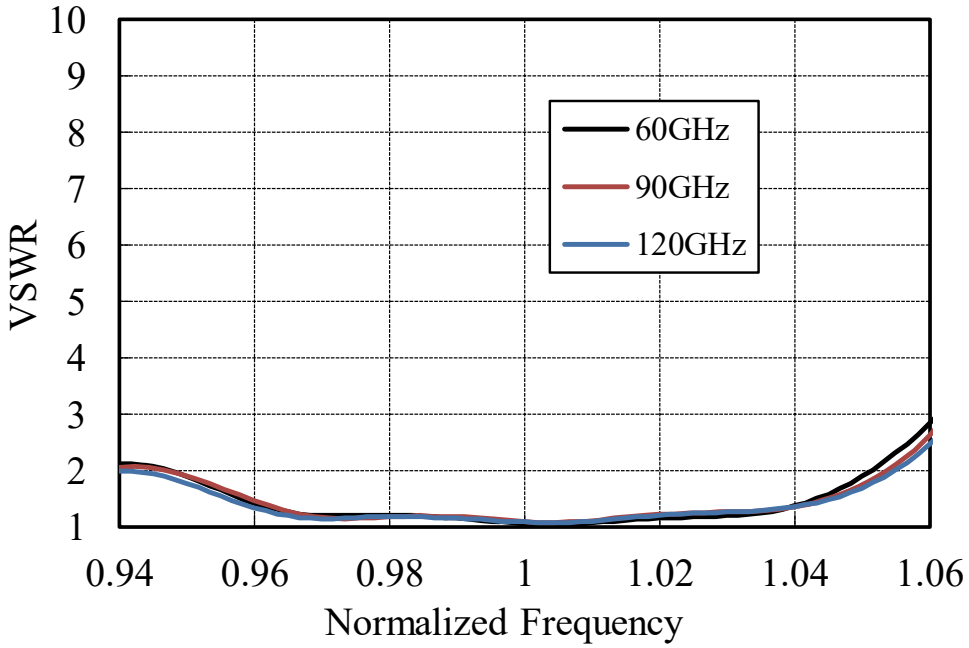

Fig. 5.5-2. Simulated reflection coefficient in each band.

Table 5.5-1 Comparison of gains and losses for each antenna

	60 GHz	90 GHz	120 GHz
Realized Gain (dBi)	5.7	5.5	4.8
Dielectric Loss (dB)	0.9	1.1	1.8
Conductor Loss (dB)	0.1	0.1	0.1

5.6. Summary

A design method to obtain low axial ratio even in wide-angle beam scanning for an injection-molded two-dimensional horn array antenna was studied. A prototype antenna has been fabricated in the millimeter-wave band, and the validity of the design method has been confirmed by measurement.

Acknowledgments: A part of the study in this chapter was the result of a research commissioned by the Ministry of Internal Affairs and Communications, "Research & Development on Millimeter-wave High-speed Mobile Communication System Technology."

5.7. References

[70] http://www.nict.go.jp/press/2010/06/23-1.html

[71] G. Strauss and K. Breitsameter, "A circular polarized TEM horn antenna array with large scanning angle," in *Proc. of IEEE Radio and Wireless Symposium*, Phoenix, AZ, USA, Jan 2011, pp. 98-101.

[72] Y. Aramaki, H. Uchida, T. Nishino, N. Yoneda, I. Naito, H. Miyashita, Y. Konishi, "Molded dielectric waveguide horn array antenna," *Technical Report of IEICE*, AP2008-178, pp.163-167, Jun. 2009.

[73] Y. Aramaki, H. Uchida, T. Nishino, N. Yoneda, I. Naito, H. Miyashita, M. Miyazaki, "Improvement of array element pattern of molded dielectric waveguide horn array antenna," *Proc. of the 2008 Communication Society Conf. of IEICE,* B-1-113, 2008.

[74] J. Goto, S. Yamaguchi, M. Tanaka, M. Otsuka, and H. Miyashita, "Design of 2 dimensional injection-molded horn array antenna for mm-wave APAA," *IEICE Trans. Commun.*, vol. J100-B, no.3, pp. 253–260, 2017.

[75] A. Yamamoto, H. Yukawa, N. Yoneda, "Improvement of assembling resin-made waveguide array antennas for millimeter-wave applications," *Proc. of the 2011 General Conf.*, C-2-60, Mar. 2011.

[76] R. Collin, *Foundations for microwave engineering*, 2nd edition, pp. 311-312, 2001.

[77] R. Shen, X. Ye, J. Xie, Z. Chen and C. Jin, "A W-band circular box-horn antenna array radiating sum and difference beams with suppressed sidelobe," *IEEE trans. and propagat.* vol. 67, iss. 9, Sept. 2019.

[78] Y. Cai, Y. Zhang, L. Yang, Y. Cao, and Z. Qian, "Design of low-profile metamaterial-

loaded substrate integrated waveguide horn antenna and its array applications," *IEEE Trans. on Antennas and Propagat.*, vol. 65, no. 7, pp. 3732-3737, July 2017.

[79] T. Cameron, and G. Eleftheriades, "Analysis and characterization of a wide-angle impedance matching metasurface for dipole phased arrays," *IEEE Trans. Antennas Propag.*, vol.63, no.9, pp.3928-3938, Sept. 2015.

6. Conclusions

6.1. Summary

The target of the study in this dissertation is the realization of miniaturization and high functionalization of radiating elements for array antennas on moving platforms. There are three issues in these antennas: first, miniaturizing antennas reduces their degree of freedom and increases the input impedance, which makes it difficult to obtain the impedance matching; second, since array antenna performances are often degraded when scanned to a wide angle, design technology to realized high performances over the wide coverage is required; third, because the size of wideband antennas tends to become large, the antenna type and the material used must be selected appropriately. In order to design antennas that suit for moving platforms, this dissertation deals with newly proposed design methods for three types of antennas, as shown below.

In Chapter 1, antennas on moving platforms and requirements to these antennas are introduced. Needs for small and high functional antennas are also discussed.

In Chapter 2, the issues in antennas on moving platforms are identified. The common technical issue discussed in this thesis is “impedance matching”. By observing the behavior and phenomena of each antenna and clarifying the problems and their causes, the novel techniques are devised to solve the issues. Outline of the dissertation is also shown in this chapter.

Chapters 3-5 deal with newly proposed design methods for three types of antennas. In Chapter 3, a novel traveling-wave series-fed microstrip antenna array is discussed. A conventional series-fed microstrip antenna array is lack of the degree of freedom, and only way to control radiation power from each element is changing the width of each element. In addition, a meander line is used to compensate the phase distortion because the transmission phase varies with the radiation power from each element. Although the length of the meander line can be arbitrarily selected and makes array design easy, the meander line increases insertion loss and spurious radiation. In the proposed antenna, additional slits placed on the output side of the antenna element are introduced as a new degree of freedom to control the radiation power from each element. Also, the unequal element spacing is applied to compensate passing phases of each antenna element; meander lines that would increase the insertion loss and spurious radiation are not used. Because the phase distribution is adjusted by the element position and the excitation amplitude distribution required to realize a desired radiation pattern changes according to the element position, the amplitude distribution is designed by using a genetic algorithm. A 9-element linear array is designed and tested, and the simulated and measured results agree, thus validating the proposed design.

In Chapter 4, a novel circularly polarized ring microstrip antenna and its design. A conventional ring microstrip antenna maintains good radiation characteristics with a smaller dimension than circular microstrip antennas. But, since the minimum input impedance of ring microstrip antennas quickly increases when the inner/outer diameter ratio increases, an additional matching circuit needs to be embedded, which prevents the inner area from being used for other purposes. In the proposed

antenna, the shorting pins, which are discretely disposed on the inner edge of the ring microstrip antenna, are introduced as a new degree of freedom to improve the resonance frequency control. The number and diameter of the shorting pins control the resonance frequency; the resonance frequency can be made almost constant with respect to the inner/outer diameter ratio, thereby expanding the use of the ring microstrip antenna. As an example of a use for the proposed antenna, a dual-band antenna where the proposed antenna includes another ring microstrip antenna is designed and measured, and these results agree well with measurement. Furthermore, the electrical performance for a proto flight model of a satellite positioning system using the proposed antenna is demonstrated. The measurement and designed results agreed well, which proves that the antenna can be put into practical use.

In Chapter 5, a light-weight horn antenna that covers up to 45 degrees is proposed. A conventional metal horn array antenna is low loss but has large weight as well as large element spacing, which prevents wide-angle beam scanning. To solve this problem, an injection-molded horn array antenna, which is compact, low-loss and highly manufacturable, has been proposed. However, the axial ratio was deteriorated during wide-angle beam scanning, because the antenna was designed to be impedance-matched in the front direction, without considering the axial ratio at all. In this dissertation, the mechanism that the axial ratio degrades in the injection-molded horn array antenna is clarified. Besides, the reflection wave that degrades the axial ratio is extracted by converting the expression of the reflection wave from the liner polarization to the circular one. The circular component of the reflection wave can be controlled by the position and depth of the iris placed near the horn

array antenna's aperture. By suppressing this component over the wide coverage, the beam scanning characteristics are guaranteed. The proposed method enables a definitive and efficient design of the injection-molded horn array antenna, by utilizing the same degree of freedom as conventional one. A prototype antenna has been fabricated in the millimeter-wave band, and the validity of the design method has been confirmed by measurement.

6.2. Future works

Lastly, future works regarding this thesis are described.

For the microstrip array discussed in Chapter 3, the design method was based on the genetic algorithm (GA) but it is desired to develop a GA-independent design method. If the antennas can be placed at equal intervals, the canonical excitation distribution can be used. The unequal spacing is due to the phase delay at the radiating element. In microstrip antennas, it is known that the "radiation phase" can be controlled by the length of the antenna. Therefore, it may be possible to compensate for the passing phase by changing the "radiation phase" by changing the length of each element.

For the dual-frequency aperture shared antenna in Chapter 4, the design procedure was based on electromagnetic field simulation. It is necessary to develop a method to theoretically analyze a microstrip antenna with shorting pins for efficient design. Many theoretical expressions have already been reported in numerous papers and the impedance of a shorting pin can also be expressed using the Bessel and Neumann

functions. In the future, the proposed antenna will be analyzed theoretically by combining these equations.

For the injection-molded horn array dealt with in Chapter 5, it may be difficult to enlarge the coverage up to 60 degrees with the existing parameters. In this case, creation of new degree of freedom is needed. Because the axis ratio deteriorates when the reflection performance is poor, additional impedance matching structure will enlarge the coverage. Herein, a technique has been proposed that can improve the reflection of the antenna in the wide-angle direction by placing a dielectric substrate with a specific conductor pattern, which will improve the performance of the proposed horn array antenna.

The antennas and design methods developed in this dissertation contribute to the realization of miniaturization and high functionalization of radiating elements for array antennas on moving platforms and are considered to have wide applicability. There will be increasing demands for larger capacity for communication systems and higher resolution for radar systems. Therefore, higher frequency bands such as THz band are expected to be utilized. The antennas proposed in the thesis, which have versatility and low loss properties, will satisfy such requirements in the future.

Publication list

Refereed journals

Chapter 3

1. J. Goto, M. Matsuki, T. Maruyama, T. Fukasawa, N. Yoneda, and J. Hirokawa, “Design of the traveling-wave series-fed microstrip antenna array with power control slits of unequal inter-element spacing," *IEICE Trans. Commun*, vol. E104-B, no.6, Jun. 2021.

Chapter 4

2. J. Goto, A. Hirota, K. Mochizuki, Satoshi Yamaguchi, Kazunari Kihira, Toru Takahashi, H. Sumiyoshi, M. Otsuka, N.Yoneda, and J. Hirokawa, “Design of the Circularly Polarized Ring Microstrip Antenna with Shorting Pins,” *IEICE Trans. Commun*, submitted.

Chapter 5

3. J. Goto, S. Yamaguchi, M. Tanaka, M. Otsuka, and H. Miyashita, “Design of 2 dimensional injection-molded horn array antenna for mm-wave APAA,” *IEICE Trans. Commun.,* vol. J100-B, no.3, pp. 253−260, 2017.

Other studies

4. J. Goto, K. Kihira, T. Takahashi, M. Otsuka, and H. Miyashita, “A study on modulation method for transmission system using phased array antennas," *IEICE Trans. Commun*, vol. J101-B, no.2, pp.187−193, 2018.

5. S. Yamaguchi, J. Goto, T. Takahashi, M. Otsuka, and Y. Konishi, “Post-wall slotted waveguide array antennas with tilted beam radiation patterns for a broadband communication system in 60 GHz band," *IEICE Trans. Commun*, vol. J94-B, no.11, pp.1498−1502, 2011.

International conferences

Chapter 4

1. J. Goto, S. Yamaguchi, K. Kihira, T. Takahashi, and H. Miyashita, “Dual frequency patch antenna using partially shorted annular ring patch antenna,” in *Proc. of Antennas and Propag. Society Int. Memphis*, TN, USA, 2014, pp.1-2.

Chapter 5

2. J. Goto, S. Yamaguchi, M. Tanaka, T. Takahashi, and Y. Konishi, “An injection-molded circular polarized horn array antenna with low axial ratio,” in *Proc. 7th Eur. Conf. Antennas Propag. (EUCAP)*, Gothenburg, Sweden, 2013, pp.1590-1594.

Other studies

3. J. Goto, T. Shijo, and M. Ando, “Method of moment for local correction of physical optics,” in *Proc. of Int. Symp. of Antennas and Propag.*, Sendai, Japan, 2004, 2E2-2, pp.565-568.
4. J. Goto, T. Shijo, and M. Ando, “Method of moment for local correction of physical optics to eliminate fictitious penetrating rays,” in *Proc. of Int. Symp. of Antennas and Propag.*, Seoul, Korea, 2005, TC1-2, vol.2, pp.395-398,

5. J. Goto, S. Yamaguchi, T. Takahashi, and Y. Konishi, “A novel approach of singularity extraction in the hybrid FEM/MoM for slotted waveguide antennas,” in *Proc. of Int. Symp. of Antennas and Propag.*, Seoul, Korea, 2011, ThF1, pp.1-4.
6. J. Goto, M. Ohtsuka, and H. Miyashita, “A study on modulation method for transmission system using phased array antennas,” in *Proc. 10th Eur. Conf. Antennas Propag. (EUCAP)*, Davos, Switzerland, 2016, pp.1-2.
7. J. Goto, T. Fukasawa，M. Otsuka，and N. Yoneda, “Design and measurements of a tapered slot antenna array with suspended stripline probe feed,” in *Proc. 13th Eur. Conf. Antennas Propag. (EUCAP)*, Krakow, Poland, 2019, pp.1-3.

Domestic conferences and technical reports in Japan

Chapter 3

1. J. Goto, T. Maruyama, S. Yamaguchi, T. Fukasawa, and N. Yoneda, “Design of a travelling-wave series-fed microstrip array antenna”, *Proc. of the 2018 General Conf.*, B-1-60, March 2018.
2. J. Goto, M. Matsuki, T. Maruyama, S. Yamaguchi, T. Fukasawa, and N. Yoneda, “Design of the travelling-wave series-fed microstrip array antenna”, *Technical Report of IEICE*, AP2018-1, pp.1-6, Apr. 2018.
3. J. Goto, M. Matsuki, T. Maruyama, S. Yamaguchi, T. Fukasawa, and N. Yoneda, “Experimental evaluation of a travelling-wave series-fed microstrip array antenna”, *Proc. of the 2018 Communication Society Conf. of IEICE,* B-1-104, Sept. 2018.

Chapter 4

4. J. Goto, S. Yamaguchi, T. Takahashi, T. Nishino, and Y. Konishi, “Partially shorted ring patch antenna,” *Proc. of the 2010 Communication Society Conf. of IEICE,* B-1-76, Sept. 2010.
5. J. Goto, S. Yamaguchi, T. Takahashi, and Y. Konishi, “A single layer dual-frequency patch antenna including the partially shorted annular ring patch antenna”, *Proc. of the 2012 General Conf.*, B-1-133, March 2012.

6. J. Goto, S. Yamaguchi, T. Takahashi, and Y. Konishi, “Design of A double-layer dual-frequency patch antenna including the partially shorted annular ring patch antenna”, *Proc. of the 2012 Communication Society Conf. of IEICE,* B-1-159, Sept. 2012.
7. J. Goto, S. Yamaguchi, T. Takahashi, and Y. Konishi, “Evaluation of dual frequency patch antenna using partially shorted annular ring patch antenna”, *Proc. of the 2012 Communication Society Conf. of IEICE,* B-1-117, Dec. 2012.
8. J. Goto, S. Yamaguchi, T. Takahashi, and Y. Konishi, “Evaluation of dual frequency patch antenna using partially shorted annular ring patch antenna”, *Proc. of the 2013 General Conf.*, B-1-123, March 2013.

Chapter 5

9. J. Goto, S. Yamaguchi, T. Takahashi, and Y. Konishi, “Design of the circular polarized waveguide array antenna”, *Proc. of the 2011 General Conf.*, B-1-172, March 2011.
10. J. Goto, S. Yamaguchi, T. Takahashi, and Y. Konishi, “Experimental validation of the design method for the circular polarized horn array antenna”, *Proc. of the 2011 Communication Society Conf. of IEICE,* B-1-154, Sept. 2011.
11. J. Goto, S. Yamaguchi, T. Takahashi, and Y. Konishi, “The design method for the two-dimensional circular polarized horn array antenna”, *Technical Report of IEICE*, AP2012-183, pp.209-214, Jan. 2012.

Other studies

12. J. Goto, T. Shijo, M. Ando, J. Hirokawa, “Analytical discussion of penetrating rays in PO in terms of stationary phase method,” *Proc. of the 2003 Communication Society Conf. of IEICE,* C-1-5, Sept. 2003.
13. J. Goto, S. Yamaguchi, K. Kakizaki, K. Hirata, M. Otsuka, H. Miyashita, and S. Makino, “A waveguide crossed-slot antenna with cross-polarization on a single aperture,” *Proc. of the 2007 General Conf.*, B-1-102, March 2007.
14. J. Goto, S. Yamaguchi, T. Takahashi, M. Otsuka, and Y. Konishi, “Unwanted radiation suppression of a printed dipole with a ground plane,” *Proc. of the 2009 General Conf.*, B-1-119, March 2009.
15. J. Goto, S. Yamaguchi, T. Takahashi, T. Nishino, M. Otsuka, and Y. Konishi, “Evaluation of the unwanted radiation suppression technique for printed dipole array antennas with a ground plane,” *Technical Report of IEICE*, AP2009-48, pp.23-27, July 2009.
16. J. Goto, S. Yamaguchi, T. Takahashi, T. Nishino, M. Otsuka, and Y. Konishi, “Evaluation of the unwanted radiation suppression technique for printed dipole array antennas with a ground plane,” *Proc. of the 2009 Communication Society Conf. of IEICE,* B-1-111, Sept. 2009.
17. J. Goto, S. Yamaguchi, T. Takahashi, T. Nishino, and Y. Konishi, “Singularity extraction in slotted waveguide analysis by FEM/MoM,” *Proc. of the 2010 General Conf.*, B-1-178, March 2010.
18. J. Goto, S. Yamaguchi, T. Takahashi, and Y. Konishi, “A high accuracy analysis for slotted waveguide by FEM/MoM,” *Technical Report of IEICE*, AP2010-176, pp.13-17, March 2011.

19. J. Goto, K. Kihira, T. Takahashi, and H. Miyashita, “A study on modulation method for transmission system using phased array antennas,” *Proc. of the 2013 Communication Society Conf. of IEICE,* B-1-215, Sept. 2013.
20. J. Goto, K. Kihira, T. Takahashi, and H. Miyashita, “A study on modulation method for transmission system using phased array antennas,” *Technical Report of IEICE*, AP2013-10, pp.47-50, Oct. 2013.
21. J. Goto, K. Kihira, T. Takahashi, and H. Miyashita, “Experimental evaluation of modulation method for transmission system using phased array antennas,” *Proc. of the 2014 General Conf.*, B-1-184, March 2014.
22. J. Goto, K. Kihira, M. Otsuka, and H. Miyashita, “Experimental evaluation of the excitation distribution robustness on the system modulated by phased array Antennas,” *Proc. of the 2014 Communication Society Conf. of IEICE,* B-1-163, Sept. 2014.
23. J. Goto, S. Yamaguchi, T. Fukasawa, and H. Miyashita, “Design of the taper slot antenna fed by the suspended strip lines,” *Proc. of the 2016 Communication Society Conf. of IEICE,* B-1-87, Sept. 2016.
24. J. Goto, S. Yamaguchi, T. Fukasawa, and H. Miyashita, “Experimental evaluation of the taper slot antenna fed by the suspended strip lines,” *Proc. of the 2017 General Conf.*, B-1-100, March 2017.
25. J. Goto, T. Maruyama, S. Udagawa, T. Fukasawa, and N. Yoneda, “Design of a traveling-wave series-fed dipole array antenna,” *Proc. of the 2019 General Conf.*, B-1-73, March 2019.
26. J. Goto, T. Maruyama, S. Udagawa, T. Fukasawa, and N. Yoneda, “Experimental evaluation of a traveling-wave series-fed dipole array antenna,” *Proc. of the 2019 Communication Society Conf. of IEICE,* B-1-78, Sept. 2019.

27. J. Goto, T. Fukasawa, and N. Yoneda, “A study of sidelobe suppression on a superdirective array antenna,” *Proc. of the 2020 General Conf.*, B-1-55, March 2020.
28. J. Goto, T. Fukasawa, and Y. Inasawa, “Experimental study on excitation error tolerance of low sidelobe level superdirective antenna,” *Proc. of the 2020 Communication Society Conf. of IEICE,* B-1-41, Sept. 2020.